

AD621678

EVALUATION OF FACTORS AFFECTING THE CALIBRATION ACCURACY OF AIRCRAFT STATIC PRESSURE SYSTEMS

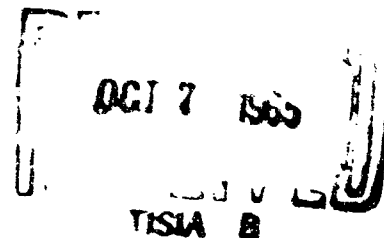
RICHARD V. DALEO
FLOYD W. HAGEN
ROBERT R. KOOIMAN
DONALD I. THOMPSON

ROSEMOUNT ENGINEERING COMPANY

TECHNICAL REPORT SEG-TR-65-35

CLEARINGHOUSE FOR FEDERAL SCIENTIFIC AND TECHNICAL INFORMATION	Microcopy	1.00	133	pp. 00
	4.00			
ARCHIVE COPY				

JULY 1965



SYSTEMS ENGINEERING GROUP
RESEARCH AND TECHNOLOGY DIVISION
AIR FORCE SYSTEMS COMMAND
WRIGHT-PATTERSON AIR FORCE BASE, OHIO

NOTICES

When Government drawings, specifications, or other data are used for any purpose other than in connection with a definitely related Government procurement operation, the United States Government thereby incurs no responsibility nor any obligation whatsoever; and the fact that the Government may have formulated, furnished, or in any way supplied the said drawings, specifications, or other data, is not to be regarded by implication or otherwise as in any manner licensing the holder or any other person or corporation, or conveying any rights or permission to manufacture, use, or sell any patented invention that may in any way be related thereto

Copies of this report should not be returned to the Research and Technology Division unless return is required by security considerations, contractual obligations, or notice on a specific document.

**EVALUATION OF FACTORS AFFECTING THE
CALIBRATION ACCURACY OF AIRCRAFT STATIC
PRESSURE SYSTEMS**

*RICHARD V. DeLEO
FLOYD W. HAGEN
ROBERT R. KOOIMAN
DONALD I. THOMPSON*

FOREWORD

The research and development work, upon which this report is based, was accomplished by the Department of Aeronautical Research of the Rosemount Engineering Company, under USAF Contract Number AF 33(600)-42754. The program was conceived and initiated by Mr. C.J. Jolley of the Aeronautical Systems Division, Directorate of Operational Support Engineering. The contract was initiated under Project 8201, Task No. 820112. The contractor's report number is REC 66227. The task engineer was Lt. William Imfeld of the Flight Vehicle Division, Flight Control Branch, ASNPFC.

Acknowledgement is made for the assistance and advice of Mr. C.J. Jolley of the Flight Control Branch, and for the technical advice of Dr. Frank D. Werner of the Rosemount Engineering Company, Minneapolis, Minnesota.

This report was submitted by the authors June 1962.

This technical report has been reviewed and approved.

DAVID V. STOCKMAN
Chief, Instruments Division
Directorate of Airframe Subsystems Engineering

ABSTRACT

Several factors affecting the calibration accuracy of flight vehicle static pressure systems have been considered in some detail. The standard atmospheres used within the past 40 years are tabulated and compared. Altimeter calibration techniques and standards are discussed. The influence of pressure system leakage has been evaluated both analytically and experimentally. The influence of skin irregularities in the vicinity of fuselage static pressure ports has been calculated from linearized theory and the results presented in graphical form. Fuselage irregularities were measured on 18 military transport type aircraft. The predicted static pressure errors as a function of Mach number compare reasonably well with flight test results from a NASA program.

A few revisions are suggested to the USAF document governing the design of flight vehicle static and total pressure systems, MIL-P-26292.

TABLE OF CONTENTS

	<u>Page</u>
FOREWORD	ii
ABSTRACT	iii
LIST OF TABLES	vi
LIST OF APPENDICES	vi
LIST OF ILLUSTRATIONS	vii

<u>Section</u>	<u>Page</u>
1. INTRODUCTION	1
2. STANDARD ATMOSPHERES	3
2.1 Introduction	3
2.2 Comparison of Standard Atmospheres	4
2.3 Summary of Standard Atmospheres Used for Altimeter Calibration	8
3. PRESENT ALTIMETER CALIBRATION STANDARDS, TECHNIQUES AND PROCEDURES	10
3.1 Synopsis of Visitation	10
3.2 Discussion of Present Altimeter Calibration Standards and Techniques with Recommendations for Immediate Improvement	14
3.3 Discussion of Altimeter Calibration Procedures	22
4. FUTURE ALTIMETER CALIBRATION STANDARDS, TECHNIQUES AND PROCEDURES	36
4.1 Altimeter Calibration Standards Presently Available	36
4.2 Additional Altimeter Calibration Standards and Techniques	38
4.3 Procedural Developments	41
5. INFLUENCE OF PRESSURE SYSTEM LEAKAGE AND PRESSURE LAG ON AIRCRAFT STATIC PRESSURE MEASUREMENTS	43
5.1 Pressure Lag	43
5.2 Pressure Errors Caused by Flow Through Static Pressure Orifices	49

TABLE OF CONTENTS (CONT'D)

<u>Section</u>		<u>Page</u>
6.	PRESSURE ERRORS CAUSED BY DIMENSIONAL VARIATIONS AND IRREGULARITIES OF STATIC PRESSURE PORTS ON PITOT-STATIC TUBES	58
6.1	Testing Procedure	59
6.2	Presentation of Data	59
6.3	External Burrs in the Immediate Vicinity of the Static Ports	64
6.4	Conclusions	66
7.	FUSELAGE SKIN IRREGULARITIES IN THE VICINITY OF FUSELAGE STATIC PRESSURE PORTS AND FUSELAGE MOUNTED AERODYNAMICALLY COMPENSATED PITOT-STATIC TUBES	68
7.1	Fuselage Static Pressure Ports	68
7.2	Fuselage-Mounted Aerodynamically Compensated Pitot-Static Tubes	72
8.	AIRCRAFT SKIN CONTOUR MEASUREMENTS ADJACENT TO FLUSH STATIC PORTS ON MILITARY TRANSPORT TYPE AIRCRAFT	75
8.1	Introduction	75
8.2	Aircraft Skin Contour Measurements Adjacent to Flush Mounted Static Port Assemblies	75
8.3	Altitude Position Errors Due to Skin Irregularities in the Vicinity of Fuselage Static Pressure Ports.	90
8.4	Summary	93
9.	FLIGHT TEST METHODS FOR THE CALIBRATION OF AIRCRAFT STATIC PRESSURE SYSTEMS	98
9.1	Introduction	98
9.2	The Tower Fly-By Method	99
10.	REFERENCES	113

LIST OF TABLES

<u>Table</u>		<u>Page</u>
I	Comparison of Various Standard Atmospheres	6
II	Calculated Negative Systematic Altitude Error	18
III	Calculated Positive Systematic Altitude Error	20
IV	Estimated Altimeter Accuracies Using Mercurial Altitude Test Barometer, Type A-1	21
V	Hysteresis and Drift Figures for Nominal Value of 20 Ft. at 17,000 Ft.	27
VI	Hysteresis Results	31
VII	Classification I (Reference Standards)	37
VIII	Classification II (Working Standards)	37
IX	Angular Displacement of Forward Static Ports	58
X	Altitude Error Variation With Standard Atmosphere Temperature Changes	60
XI	Comparison of Altimeter Scale Error Tolerances With the Errors Introduced by Static Pressure Port Angularity Variations	63
XII	ΔH_{gl} for Burrs	66
XIII	Calibration Accuracy at Altitude for Low Speed Aircraft ($M = 0.7$) at Constant Angle of Attack	100
XIV	Maximum Effect of Compressibility Between $M = 0$ and $M = 0.7$ for Fuselage Mounted Static Ports	101

LIST OF TABLES (CONT'D)

<u>Table</u>		<u>Page</u>
XV	Tower Fly-By Predictions Used at Altitude - Variation of Angle of Attack Effect for Nose Boom Configurations Only .	103
XVI	Calibration Accuracies of Two Methods of Calibration at Altitude for Fuselage Static Ports: $M \leq 0.7$	105
XVII	Atmospheric Survey Following Tower Fly-By and Subsequent Calibration at Altitude Using Ground Tracking .	109

LIST OF APPENDICES

Appendix

A	Suggested Changes to MIL-P-26292 (USAF) Pitot and Static Pressure Systems, Installation and Inspection of	115
---	---	-----

LIST OF ILLUSTRATIONS

<u>Figure</u>		<u>Page</u>
1	Pressure Altitude Differences Between ARDC Model Atmosphere and NACA Standard Atmospheres	9
2	Graphical Representation of Inelastic Errors Obtained Under Cyclic Conditions	25
3	Graphical Representation Showing Inelastic Error Zone for Up-Scale Traversing	25
4	Mechanical Model and Dynamic Behavior of Standard Linear Solid	25
5	Hysteresis for 1,000 - 22,700 Ft. Range for Four Test Altimeters	30
6	Hysteresis for 1,000 - 50,000 Ft. Range for Four Test Altimeters	30
7	Experimental Determination of Drift After 100 Hours at 800 Feet for Four Representative Test Altimeters	32
8	Experimental Determination of Drift After 24 Hours at 22,700 Feet for Four Representative Test Altimeters	32
9	Experimental Determination of Drift After 22 Hours at 50,000 Feet for Four Representative Test Altimeters	32
10	Response of Standard Linear Solid Model to Successive Force Cycling	34
11	Equivalent Altitude Deviation for Fixed Error and for Error Proportional to Pressure	39
12	Equivalent Altitude Error at Major Transducer for Maximum Allowable Static Pressure System Lag as Shown on Figure 4 of MIL-P-26292 for an Altitude of 50,000 Feet.	45

LIST OF ILLUSTRATIONS (CONT'D)

<u>Figure</u>		<u>Page</u>
13	Equivalent Altitude Error at Instrument Panel for Maximum Allowable Static Pressure System Lag as Shown on Figure 4 of MIL-P-26292 for an Altitude of 50,000 Feet.	45
14	Viscosity Ratio for Air as a Function of Temperature . . .	47
15	Altitude Error Equivalence of Viscous Lag Error	47
16	Sketch Showing Mass-Flow and Pressure-Measuring Setup for Testing MA-1 Pitot-Static Tube.	50
17	Variations of Static Pressure Error of MA-1 Pitot-Static Tube with Mass Flow Parameter	50
18	Pressure Drop Across Static Orifices of MA-1 Pitot-Static Tube as a Function of Velocity of Air Through the Orifices .	50
19	Variation of Change of Static Pressure Error Caused by Disturbance of the External Flow with Rate of Change of Mass-Flow Coefficient.	50
20	Influence of Leakage for a Typical Aircraft Pitot-Static Tube Installation	50
21	Pressure - Altitude Errors Caused by Angular Displacement Variation of Static Pressure Ports on REC Model 852A Pitot-Static Tubes.	60
22	Pressure - Altitude Errors Caused by Angular Displacement Variation of Static Pressure Ports on REC Model 852A Pitot-Static Tube, #3.	60
23	Typical Aircraft Flight Envelope	60
24	Photograph of Burrs on Static Ports of REC Model 852A Pitot-Static Tube Number 2.	65

LIST OF ILLUSTRATIONS (CONT'D)

<u>Figure</u>		<u>Page</u>
25	Photograph of Burrs on Static Ports of REC Model 852A Pitot-Static Tube Number 3	65
26	Notation Used for 360° Cosine Wave Fuselage Skin Deformations	69
27	Allowable Wave Depth for an Equivalent Altitude Error at Sea Level of ± 50 Ft. as a Function of Z.	69
28	Allowable Wave Depth for an Equivalent Altitude Error at Sea Level of ± 100 Ft. as a Function of L.	71
29	Allowable Wave Depth for an Equivalent Altitude Error at Sea Level of ± 10 Ft. as a Function of L.	71
30	Allowable Wave Depth for an Equivalent Altitude Error at Sea Level of ± 50 Ft. as a Function of L.	71
31	Allowable Wave Depth for an Equivalent Altitude Error at Sea Level of ± 50 Ft. Static Ports Located at Bottom of Deflection at $L_1 = -0.5$	71
32	Static Ports are Located at Center of 360° Cosine Wave Skin Deformation, at $L_1 = -0.5$	74
33	Static Ports are Located at Edge of 360° Cosine Wave Skin Deformation, at $L_1 = 0$	74
34	Static Ports are Located 1 Away from Edge of 360° Cosine Wave Skin Deformation, at $L_1 = 1$	74
35	Static Ports are Located 2 Away from Edge of 360° Cosine Wave Skin Deformation, at $L_1 = 2$	74
36	The Assembly Used to Measure Skin Deformations on the Type A and B Aircraft.	77
37	The Assembly Used to Measure Skin Deformations on the Type C Aircraft.	78

LIST OF ILLUSTRATIONS (CONT'D)

<u>Figure</u>		<u>Page</u>
38	Schematic Showing Area of Fuselage Skin Measurements on Aircrafts (B) and (C).	81
39	Variations in Skin Contour on the Type A Aircraft.	82
40	Y_{Mean} Values for Aircraft Types (B) and (C).	83
41	Variation from the Mean Skin Contour at the Centerline Location for the B Type Aircraft.	85
42	Variation from the Mean Skin Contour at the Centerline and $\pm 4''$ Location for the Type B Aircraft.	86
43	Variation from the Mean Skin Contour at the Centerline Location for the C Type Aircraft.	88
44	Variation from the Mean Skin Contour at the Centerline and $\pm 4''$ Location for the Type C Aircraft.	89
45	Variations in Altitude Position Errors Between Type B Aircraft.	95
46	Variations in Altitude Position Errors Between Type (C) Aircraft.	96
47	Comparison of the Copilot's Static-Pressure-System Error With the Manufacturer's Calibration for the Three Types of Aircraft	97

Appendix A

3	Pitot Tube and Flush Static Port System	120
---	---	-----

SECTION 1

INTRODUCTION

Measurements of altitude are required for maintaining vertical separation of aircraft during flight. The measuring scheme which has been universally accepted is based on the measurement of atmospheric pressure and its relation to a pressure-height variation of a standard atmosphere. Since the atmosphere will vary considerably from standard, depending on geographical location, meteorological conditions and season as well as altitude, the measurements based on the pressure-height relationship will ordinarily be in terms of relative altitude. In recent years, with increasing operating speed and altitudes of aircraft, the adequacy of measuring systems has become questionable. It generally follows that the individual errors which contribute to the over-all system error increase with both speed and altitude. Current Civil Air Regulations for altitudes up to 29,000 feet specify 1,000 ft. vertical separation intervals and 2,000 ft. intervals for altitudes above 29,000 ft. For a greater utilization of air space, it has been suggested that the accuracy of altimetry systems be improved to a degree that will allow 500 foot separations up to an altitude of 20,000 ft. and 1,000 ft. separation for altitudes of 20,000 to 100,000 feet. The maximum allowable error permissible for a static system is somewhat arbitrary. However, considering the existence of a flight technical error wherein the aircraft deviates from its prescribed flight and considering the size of the aircraft itself, it has been suggested that 1/2 of the vertical separation minimum should be considered as a zone of no entry. Thus, under present flight regulations, the zone of no entry will be ± 250 feet at altitudes up to 29,000 and ± 500 feet above 29,000 feet. However, if a greater utilization of air space plan is adapted, then the zone of no entry will be ± 125 feet up to 20,000 feet and ± 250 feet above 20,000 feet.

The USAF covers all phases of the necessary static pressure system calibrations in a multitude of military specifications and technical manuals. The most pertinent document with respect to the maintenance of aircraft static pressure systems is

Military Specification MIL-P-26292 "Pitot and Static Pressure Systems, Installation and Inspection of". This document covers the design and maintenance of aircraft and missiles static pressure systems. At present, the principle documents covering the calibration of altimeters are found in the individual military specifications for the laboratory working standards, individual military specifications for the altimeters themselves, and various technical manuals.

The work accomplished under this contract is supported by the Directorate of Operational Support Engineering, Flight Vehicle Division, Flight Control Branch of the Aeronautical Systems Division. The general items covered in the program were as follows:

1. Standard atmospheres used in the calibration of civil and military aircraft altimeters.
2. Types and maintenance of pressure standards for calibration of altimeters.
3. Altimeter calibration procedures and techniques.
4. Aircraft static pressure systems, in-flight calibration techniques.
5. The influence of pressure leakage on the accuracy of static pressure systems.

The program has resulted in specific recommendations to the USAF regarding establishment of procedures and techniques to insure adequate vertical separation of aircraft, for combined military and civilian airways.

SECTION 2

STANDARD ATMOSPHERES

2.1. INTRODUCTION.

A standard atmosphere represents an arbitrary relationship between static air pressure and altitude. Aircraft altimeters are actually absolute pressure gages calibrated to read in terms of feet of altitude through the standard atmosphere relationship. A standard atmosphere may be calculated if a standard value of sea level pressure is taken as well as a variation of temperature with geometric height. The hydro-static differential equation, (1), may be integrated by using the perfect gas equation, (2), into either of the forms shown as equations (3) or (4).

$$dP = -\rho g dZ \quad (1)$$

dP = pressure difference

dZ = height difference

ρ = density

g = acceleration due to the Earth's gravitation.

$$\rho = P/RT \quad (2)$$

R = gas constant

T = temperature

$$\int_{P_0}^P \frac{dP}{P} = - \frac{g_s}{R} \int_0^Z \frac{dZ}{T} \quad (3)$$

g_s = constant

$T = f_1(Z)$

$$\int_{P_0}^P \frac{dP}{P} = - \frac{1}{R} \int_0^Z \frac{g dZ}{T} \quad (4)$$

$$g = f_2(Z)$$

$$H = \frac{1}{g_s} \int_0^Z g dZ \quad (5)$$

The solution shown in integral form, in Equation 3, is one where the acceleration due to the Earth's gravitation is assumed constant, usually at a sea level value. Early standard atmospheres were derived using this expression, Reference 1 thru 3. A more correct integral form is shown in Equation 4, where g is actually a function of Z . The integral form of Equation 4, on the right side, offers considerable complexity for integration, Reference 8. Mathematical simplicity may be retained, however, without the invalid assumption of constant g by a transformation combining g and Z into a new altitude parameter called geopotential altitude, H , Equation 5. A newer standard atmosphere, References 6 to 9, are all basically geopotential standard atmospheres. The atmospheres for References 5, 6 and 9 give the pressure altitude relationship in terms of geopotential altitude. Standard atmospheres of References 7 and 8 give the pressure altitude relationship in terms of both geopotential and geometric altitude Z . The newer geopotential standard atmosphere, therefore, offers the advantage that a standard atmosphere tabulated in geopotential units will provide greater geometric altitude separation. For example, the 70,000 - 60,000 ft. geopotential height difference provides a geometric difference of 10,063 ft. A standard atmosphere calculated from Equation (4) would be exactly correct in geometric units but would have the effect of decreasing altitude separations.

2.2. COMPARISON OF STANDARD ATMOSPHERES.

Since 1925 up to the present time there have been only two basic standard atmospheres in use in the United States.

Group I: Standard Atmospheres - Geometric measure calculated using constant gravitational acceleration.

One of the early standard atmospheres is given in NACA Report Number 218, published in 1925. It is a geometric standard atmosphere calculated on the assumption of constant gravity equal to the value at sea level from sea level to 65,000 ft. Values of pressure at 5,000 ft. intervals are tabulated as Column 1 of Table I. Between 1925 and 1952 several other atmospheric tables were published, but these were identical to NACA No. 218 over the range from sea level to 65,000 ft. The purpose of NACA Tech Note No. 538, published in 1935, was to extend the range of altitude to 80,000 ft. The purpose of NACA Report No. 837, published in 1946, was to extend the atmosphere to 100,000 ft. A common fault of the first three standard atmospheres is that over part of the range of altitude, pressures were arbitrarily rounded off to the nearest hundredth of an inch of mercury. The Kollsman Instrument Corporation established a Kollsman standard atmosphere which is identical to the other three except that more significant figures had been carried in the calculation. The Kollsman standard atmosphere is shown as Column 4 of Table I.

TABLE I
COMPARISON OF VARIOUS STANDARD ATMOSPHERES

Z = Geometric Feet H = Geopotential Feet

Pressures Tabulated Are in Units of In. Hg. Abs.

	(1)	(2)	(3)	(4)	(5)	(6)	(7)	(7')	(8)	(9)
Z or H	NACA 218 1925 (Z)	NACA 538 1935 (Z)	NACA 837 1946 (Z)	Kollsman Std. (Z)	WADC 1952 (H)	NACA 1235 1955 (h)	ARDC 1956 (H)	ARDC 1956 (Z)	ARDC 1959 (Z)	NASA TN D-822 1961 (H)
0	29.92	29.921	29.92	29.9212	29.9213	29.9213	29.921	29.921	29.921	29.9213
5000	24.89		24.89		24.8959	24.8959	24.896	24.897	24.897	24.8959
10000	20.58	20.58	20.58	20.5736	20.5769	20.5769	20.577	20.5807	20.581	20.5769
15000	16.88		16.88		16.8857	16.8858	16.886	16.893	16.893	16.8858
20000	13.75	13.75	13.75	13.7453	13.7500	13.7501	13.750	13.761	13.761	13.7501
<hr/>										
25000	11.10	11.10*	11.10	11.0984	11.1035	11.1035	11.103	11.118	11.118	11.1035
30000	8.880	8.88	8.880	8.8803	8.8854	8.88541	8.8854	8.9028	8.9028	8.88541
35000	7.036	7.04*	7.036	7.0356	7.0406	7.04060	7.0406	7.0602	7.0602	7.04060
40000	5.541	5.54	5.544	5.5412	5.5380	5.53801	5.5380	5.5584	5.5584	5.53801
<hr/>										
45000	4.364	4.36*	4.365	4.3641	4.3550	4.35497	4.3549	4.3753	4.3753	4.35497
50000	3.436	3.436	3.438	3.4370	3.4246	3.42466	3.4246	3.4444	3.4444	3.42466
55000	2.707	2.707*	2.707	2.7069	2.6931	2.69308	2.6931	2.7119	2.7118	2.69308
60000	2.132	2.132	2.132	2.1319	2.1178	2.11778	2.1178	2.1354	2.1354	2.11778
<hr/>										
65000	1.680	1.679*	1.679	1.6790	1.6654	1.66538			1.6846	1.66538
70000		1.322	1.322	1.3223	1.3096		1.3096	1.3244	1.3244	1.3096
75000		1.042*	1.042	1.0414	1.0298				1.0432	1.0298
80000		.820	.8202	.8202	.8089		.80895	.82183	.82183	.80895
<hr/>										
85000			.6460		.6368				.64745	.63742
90000			.5086	.5087	.5098		.50997	.51312	.51313	.50998
95000			.4006		.3938				.40531	.40057
100000			.3156	.3156	.3097		.31951	.32640	.32640	.31951
<hr/>										
105000					.2435					.26208
110000					.1927		.20615	.21133		.21133
115000					.1542					.17111
120000					.1246		.13518	.13909		.13909
<hr/>										
125000					.1017				.11349	
130000					.0837		.088995	.092945	.092945	

* From Kollsman Comparison Table

Group II: Standard Atmospheres - Geopotential measure calculated using inverse square gravitational acceleration.

A later group of standard atmospheres have been tabulated, References 5 thru 9. In all cases these are basically geopotential atmospheres. Five atmospheres have been tabulated in Columns 5 thru 9 of Table I. In the case of the 1959 ARDC standard atmosphere, Reference 8, even values in terms of geopotential altitude H , are not tabulated. For comparison, the 1956 atmosphere, Reference 7, has been tabulated both in terms of geopotential altitude and geometric altitude Z . When the 1959 atmosphere is compared with 1956 atmospheres, Columns 7 and 8, on the basis of geometric altitude Z , it is seen that the comparison is identical.

The five geopotential standard atmospheres may be compared up to 60,000 ft. directly from Table I and it is obvious that all are identical to four significant figures. NACA 1235 standard atmosphere terminates at 65,000 ft. Comparing the other four standard atmospheres on to 80,000 ft., it is found that all four are identical to four decimal figures. In the range from 80,000 to 130,000, it is seen from Table I that the WADC 1952 atmosphere deviates from the three later standard atmospheres.

In summary then, standard atmospheres published in the United States within the last 35 years fall into two groups. One is a geometric standard atmosphere (reference 1 through 4, Table I) in which gravity is assumed constant, the other (reference 5 through 9, Table I) is a geopotential atmosphere which accounts for variable gravity effects. Within each of these two groups comparison between different published standard atmospheres show that they are actually, for all practical purposes, identical, e.g., at 40,000 ft. references 5 through 9, Table I, agree within $\pm .0001$ m Hg. The standard atmosphere given by NACA Report 837, has been chosen as a representative atmosphere of the geometric height group because it extends to 100,000 ft. The ARDC 1956 standard atmosphere has been chosen as a representative of the geopotential group. The differences in terms of feet of altitude between the 837 and 1956 ARDC atmosphere is shown graphically in Figure 1. Up to approximately 35,000 ft. of altitude, differences are less than

15 feet of altitude. Beyond 35,000 ft. of altitude to 80,000 ft. of altitude, the difference steadily increased reaching a maximum at 80,000 ft. of altitude. At 80,000 ft., the altitude indicated by an altimeter calibrated per standard atmosphere 837 will read 262 feet low as compared to an aircraft calibrated to a standard atmosphere per 1956 geopotential atmosphere.

2.3. SUMMARY OF STANDARD ATMOSPHERES USED FOR ALTIMETER CALIBRATION.

1. During the current investigation, many military specifications covering the manufacture of altimeters and overhaul manuals were reviewed. These are currently used by both military and civil agencies. Several instrument manufacturers were contacted. It has been concluded that standard atmospheres specified for altimeter calibration within the past 25 years follow either the Group I or Group II Standard Atmosphere. Both standard atmospheres are being used at the present time almost as if they were perfectly interchangeable.

2. The standard atmospheres of Group I and II are not interchangeable. Differences are less than 15 ft. of altitude up to an altitude of about 35,000 ft. Above 35,000 ft. differences become progressively larger reaching 262 ft. at an altitude of 80,000 ft.

3. It is recommended that the Group II standard atmosphere be adopted and all barometric scales standardized thereto.

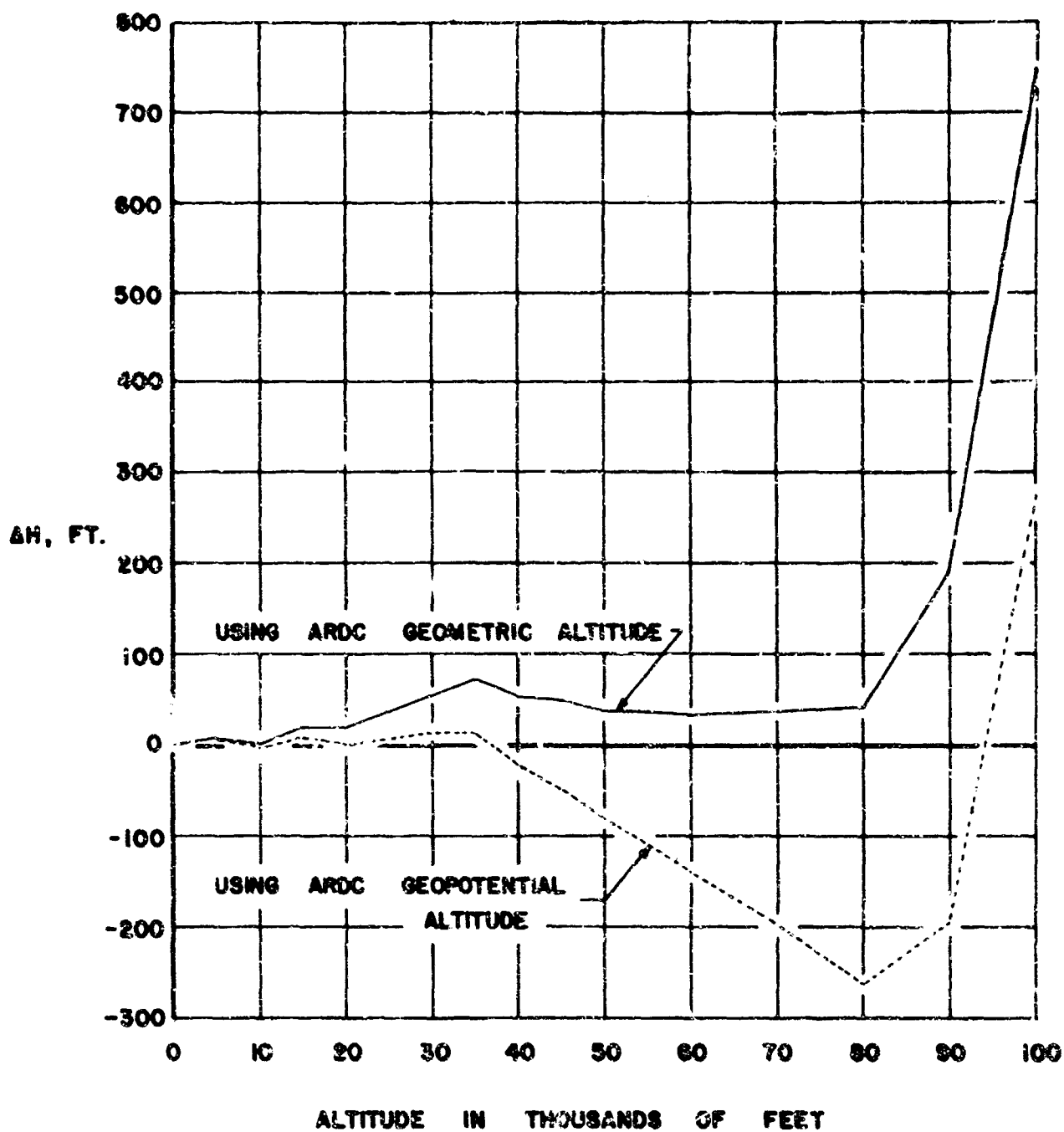


FIGURE 1
PRESSURE ALTITUDE DIFFERENCES BETWEEN ARDC
MODEL ATMOSPHERE (REFERENCE 7) AND NACA
STANDARD ATMOSPHERES (REFERENCES 1, 2, AND 3).

$$\Delta H = \frac{-\Delta P}{\rho} = \frac{-(P_{NACA} - P_{ARDC})}{\rho_{ARDC}}$$

SECTION 3

PRESENT ALTIMETER CALIBRATION STANDARDS, TECHNIQUES AND PROCEDURES

Within the scope of this phase of the study consideration has been given to various Air Force Facilities as well as other organizations concerned with the altimeter calibrations. Many of these facilities were visited and surveyed through the visitation as well as through a review of the documents governing the particular service facility.

3.1. SYNOPSIS OF VISITATION.

Visitations were made to five Air Force bases, two Naval bases, three commercial airlines, three instrument manufacturers, two airframe manufacturers and several other organizations which have either direct or indirect influence on pressure altimeter calibrations and accuracies.

3.1.1. Category 1, Air Force Bases; Olmsted, Wright-Patterson, Gentile, McClellan, Norton.

The calibration facilities and general procedures used at these bases are generally as prescribed through TO 33K6 and MIL-B-4308B. The A-1 fixed cistern type barometer represents both the plant standard and working standard at some establishments and is used as a direct readout device, i. e., the mercury column and scale are sighted by the operator through a magnifying lens. At other facilities, equipment capable of considerably higher accuracy is maintained as plant standards. The reference vacuum is maintained through a mercury sealed valve. Scales are calibrated generally in millimeters of mercury (fore-shortened for cistern effects) and in one of the two standard atmospheres. Mercury is not reused and is purchased from one of several sources. Temperature extremes in the altimeter calibration areas are estimated as high as $\pm 5^{\circ}\text{C}$. Calibration checks other than prescribed calibration which come at intervals of 180 days, generally consist of a cross check at the prevailing atmospheric pressure between at least two units. The reference vacuum is checked at various intervals by pressurizing the cistern and watching for air bubbles through the mercury seal (or by listening for a metallic clink) as the mercury column is pressurized against the valve

assembly. At one base the precision measurement equipment laboratory has set up a pressure maintenance survey team which has a responsibility of maintaining the working standards in operable condition. The team makes a daily check by performing atmospheric pressure checks between several units which agreement must be within $\pm .004''$ of mercury. The team also carries a vacuum pump and evacuates the mercury seal side of the A-1 barometers daily.

Calibration of altimeters is accomplished singly or in groups of from 2 to 28. Calibration after overhaul is frequently carried out under room temperature environment only.

3.1.2. Category 2, Naval Bases; Naval Air Development Center, Naval Western Primary Standards Laboratories.

Equipment used for calibration purposes at NADC consists of A-1 type manometry situated in temperature controlled cabinets. Semiautomatic (photo-scanner) type readout is used and the reference vacuum is maintained with mercury sealed valves.

The NWPSL maintains equipment capable of obtaining considerably higher accuracy than the A-1 type barometer. This equipment consists of higher caliber piston gages, a U-tube mercury manometer and a micrometer standard manometer which is a cistern type manometer fitted with a true length scale and facilities for measuring column heights in the cistern as well as the elongated tube.

3.1.3. Category 3, Commercial Airlines; American Airlines, United Airlines, Northwest Airlines.

The airlines also use fixed cistern type manometers for final calibrations. At one organization, temperature controlled cabinets are used and mercury sealed valves and photoscanner type readout is utilized. Another organization uses a vacuum pump and a thermocouple gage for maintaining and monitoring reference pressure and also uses photoscanner type readout.

Daily atmospheric checks are generally made between two manometers and also between the manometers and Fortin type barometers and the local Weather Bureau Station and also in one case against a precision aneroid station barometer.

The governing document for altimeter calibration is TS0C10A, although at least one airline is presently phasing in on the tighter tolerances recommended in ATA "Recommended Test Procedures for Altimeters", June 1961 (Reference 28).

Altimeter calibration is done generally at room temperature with an abbreviated check calibration at an elevated temperature. Altimeters are removed from the aircraft for recalibration and overhaul at periodic intervals based both on number of flying hours and chronological periods.

3.1.4. Category 4, Instrument Manufacturers: Kollsman, Eclipse-Pioneer, Pioneer-Central.

In all cases plant standards are maintained which are capable of substantially higher accuracies than the A-1 type barometer. Semiautomatic readout is generally used on the fixed cistern type barometer used for altimeter calibration and an active vacuum is maintained with vacuum pumps in all cases. Periodic calibrations are made against plant standards and daily checks include cross checks between barometers.

3.1.5. Category 5, Airframe Manufacturers: Lockheed, Douglas.

The A-1 type barometer is used also by the airframe manufacturers for altimeter calibration and these manometers are periodically overhauled and calibrated against plant standards. The plant standard used by one manufacturer is a piston gage; and a fixed cistern type manometer used with a vacuum pump and gage on the reference side and direct visual readout is used by the other.

3.1.6. Category 6.

This category includes additional organizations visited which are concerned with the problems associated with this phase of the contract, but which do not fall within the categories listed above.

3.1.6.1. National Bureau of Standards.

The National Bureau of Standards is responsible for maintaining pressure measuring capability of such a quality that all major corrections to the measurement can be made with a high degree of accuracy so that conventional working standards calibrations may be made traceable either directly or indirectly to N. B. S. This "Traceability" should not imply that conventional working standards may be "Certified".

However, for fixed cistern type barometers the scale may be certified and pressure calibration data may be obtained under a specified set of operating procedures. Fixed cistern type barometers are not generally calibrated by N. B. S. since the variable errors associated with normal usage are large compared to parameters which may be calibrated and/or certified. The normal procedure is for the barometer manufacturer to supply a calibration with the instrument, such calibration to be made against units which have in turn been calibrated by N. B. S. The role of the barometer operator is very critical in respect to these instruments and it has been emphasized by N. B. S. personnel that greater accuracies could be possible through use of transfer personnel and transfer standards. Transfer personnel who are highly skilled in calibration and maintenance techniques are most desirable; however, much could be gained through test problems circulated in the form of transfer standards to be calibrated at the different facilities.

3.1.6.2. U. S. Weather Bureau.

The Weather Bureau is responsible for securing hourly pressure measurements and for supplying these pressure measurements indirectly through control towers to a large number of aircraft under field conditions. This information is also supplied as in-flight information so that the reported pressures are very important, not only in regard to safety considerations during take-off and landing but also for vertical separation. The Fortin type barometers of 1/4 inch bore are generally relied upon for transfer standards and for calibration checks with aneroid type station barometers.

3.1.6.3. FAA.

Although the Weather Bureau is generally responsible for accurate station pressure readings, the Weather Bureau does not maintain offices at all locations in which case the FAA tower is responsible for supplying correct barometric information to aircraft. FAA station barometers are of the aneroid type and are checked at least once daily against Weather Bureau information wherever possible.

3.1.6.4. Hass Instrument Company.

Calibration of the A-1 type barometers is done in a room which is temperature controlled and is done against a similar type instrument which has been calibrated at

the Bureau of Standards. All calibrations are carried out with an active vacuum maintained on the reference side of the manometers which vacuum is monitored with a McLeod gage.

3.2. DISCUSSION OF PRESENT ALTIMETER CALIBRATION STANDARDS AND TECHNIQUES WITH RECOMMENDATIONS FOR IMMEDIATE IMPROVEMENT.

From practices observed at the various organizations covered by the visitation program, it may be concluded that the general class of instrumentation used for altimeter calibration is essentially identical at all the facilities. It may also be concluded, however, that the usage of such equipment is subject to considerable variation. The specific equipment used in all cases for altimeter calibration by the Air Force consists of the A-1 barometer. A error analysis based on manufacturing specifications as well as observations from the visitation program is given below:

3.2.1. Analysis of Errors for A-1 Barometer.

The Air Force mercurial, altitude test barometer, type A-1, Military Specification MIL-B-4308B (USAF) is the Air Force working standard for the calibration of altimeters and several hundred units are presently in service at approximately 180 Air Force bases. Errors assignable to the barometer may be segregated into three classifications:

1. Precision testing errors.
2. Repeatability testing errors.
3. Operating errors.

Errors falling within the categories 1 and 2 are, in general, random errors associated with the instrument due to its characteristics and construction. Operator errors are errors associated with the techniques of operating the barometer during altimeter calibration. For this error analysis, two sets of operator errors have been assigned. The first set is assigned in an attempt to be consistent with the operator errors as they may exist in the Air Force utilizing present day techniques. The second set is assigned with an attempt to be consistent with improved, suggested techniques. All quantitative values given are 3 sigma errors, i.e., the maximum statistical values which would occur in 99.7 percent of the measurements.

3.2.1.1. Precision Testing Errors of A-1 Barometers.

The precision testing errors refer to the dispersion of readings repeated under the same conditions and at approximately the same time. A quantitative value for this error has been taken from section 4.2.1.5 of MIL-B-4308B as ± 0.1 mm. Hg.

3.2.1.2. Repeatability Testing Errors of A-1 Barometers.

The repeatability errors refer to the dispersion of readings repeated under different conditions and at different times of testing. Errors have been assigned with primary reference to Air Force Technical Order Number 33A7-4-2-1. The various errors and the error assignments are as follows:

1. Temperature-Gravity Compensator = ± 0.1 mmHg.
2. Mercury meniscus uncertainty = ± 0.1 mmHg.
3. Zero setting = ± 0.05 mmHg.
4. Vernier accuracy = ± 0.025 mmHg.
5. Leveling error = ± 0.02 mmHg.
6. Temperature Error ($\pm 0.3^\circ$ C) = ± 0.04 mmHg at 760 mmHg.
7. Gravity uncertainty = ± 0.03 mmHg at 760 mmHg.

The errors listed as items 1 through 5 are purely random errors and essentially independent of pressure levels. Errors assignable under items 6 and 7 are errors which are proportional to pressure levels. If one adds all the errors listed in items 1 through 5, a maximum error of 0.295 mmHg may occur. However, since all errors are random, a much more representative over-all error would be the root-mean-square which results in an RMS of ± 0.15 mmHg. If items 6 and 7 are included, the result is an RMS value of ± 0.16 mmHg at 760 mmHg pressure.

3.2.1.3. Operator Errors Using Present Techniques.

Most of the errors assignable to the operator during altimeter calibration are of the random nature. In the following list, nine errors are listed, 1 - 6 and 9 being of a random nature and 7 and 8 being of a systematic nature. These errors with assignable values are as follows:

1. Neglection of scale correction chart reading. A correction chart is furnished and attached to each barometer listing the scale error as a function of pressure level. However, during altimeter calibration these are seldom, if ever, taken into account. The resulting error of ± 0.2 mm is given in Section 4.2.1.5 of MIL-B-4308B.

2. Use of altitude scale. In calibrations throughout the Air Force, it is common practice to use the altitude scale for altimeter calibrations. The altitude scale is primarily for convenience and not as accurate as the millimeter scale. Older barometers are inscribed with a pressure-altitude relationship corresponding to NACA TN 538. New barometers are inscribed with the pressure altitude scale corresponding to the ICAO Standard Atmosphere, which is given in NACA Report 1235, also ARDC Model Atmospheres. During the recent field surveys, both types of barometers were found to be in service in the Air Force. The altitude scale is not cut with the same precision as the millimeter scale and in addition, a correction chart for the altitude scale is not provided with the barometer. The use of the altitude scale gives an additional random error of ± 0.15 mmHg.

3. Mercury hysteresis and capillary depression, ± 0.1 mmHg. For most altimeter calibrations it was found from field trips that very few of the operators take precaution against minimizing mercury hysteresis. Although Technical Order Number 33A7-4-2-1, in paragraph 4-13, item C, instructs "rap the table to adjust the meniscus," a far more satisfactory method of reducing hysteresis would be to rap the cistern and specify exactly the method by which the rapping should occur. This is extremely important with the fixed cistern instrument, since the height of the mercury column in the cistern is assumed and not measured. Mercury hysteresis and capillary depressions have the effect of increasing this uncertainty. An error of ± 0.1 mmHg has been

assigned to this effect under repeatability errors and is considered to be that value obtained when necessary precautions are used. Accordingly, the additional error of ± 0.1 mmHg is assigned under operator errors.

4. Accuracy of setting sighting ring, ± 0.05 mmHg. The above assumption is based on the fact that the best the operator will be able to set a pressure or level is to $1/2$ of the smallest vernier reading. Since the smallest vernier reading is 0.1 mm (although it is 0.05 mm on later model barometers, many of the 0.1 mm verniers are still in service), this accuracy is estimated at 0.05 mmHg.

5. Temperature uncertainty, $\pm 0.5^\circ$ C. The half degree assumed error is compatible with good temperature controlled rooms when the operator takes precautions and watches for temperature changes as the calibration proceeds. Fortunately, even a $1/2^\circ$ C error (0.06 mm at 760 mmHg) will not cause sufficient altitude error to warrant taking into consideration at this point.

6. Elevation correction, gas head. This is the correction based on the altitude difference between the instrument to be calibrated and the cistern of the barometer. In almost all calibration facilities this pressure differential is only on the order of 1 or 2 feet and, hence, not worth taking into account in an error analysis where other errors are considerably larger.

7. Error due to the use of the mercury sealed valve. The Air Force type A-1 barometer is furnished with a mercury sealed valve for maintaining vacuum on the reference side of the barometer. In most cases, the valves probably do provide an adequate seal. However, during altimeter calibration where the pressure range from sea level to 80,000 feet is traversed, mercury will tend to pick up air bubbles and these air bubbles are easily transmitted to the reference vacuum chamber at the mercury sealed valve. To eliminate the possibility of vacuum deterioration with time and usage, it is recommended that the mercury sealed valve be replaced with a continuous vacuum pumping system. At the present time, the errors caused by the use of the mercury sealed valve are somewhat hard to estimate. It would probably fall between zero and one millimeter of mercury. Much larger errors are possible. The pressure error caused by deficient reference vacuum may be calculated from equation 6 as follows:

$$\Delta P = \Delta P_o \left[\frac{Z_1}{Z_1 + (760 - P)} \right] \quad (6)$$

where:

ΔP = the pressure error

ΔP_o = the error at 760 mm setting.

Z_1 = the height of the tube from the top of the mercury to the mercury sealed valve at 760 mm setting.

P = pressure being measured, mmHg.

Calculated altitude error using equation 6 as a function of altitude is shown in Table II. The results are based on a pressure error at 760 mm in the vacuum of 1 mmHg. If an error of only 0.1 mmHg occurs then the resulting ΔH is only 1/10th of the value indicated by Table II. Worthy of note is that the altitude error decreases with increasing altitude up to about 20,000 feet and then increases with increasing altitude to 100,000 feet. It should be noted that this error is systematic and that the pressure error is always positive.

TABLE II
CALCULATED NEGATIVE SYSTEMATIC ALTITUDE ERROR
DUE TO $\Delta P_o = 1$ mmHg. ABC.
(Equation 6)

ALTITUDE (Ft. $\times 10^{-3}$)	ALTITUDE ERROR (Ft.)
0	- 36
20	- 18
40	- 21
60	- 67
80	-170
100	-448

8. Air bubbles entrapped at mercury interfaces. This error will increase with decreasing pressure as given in equation 7 where Z_2 is height of mercury column above the bubble.

$$\Delta P = \Delta P_0 \left[\frac{760 + Z_2}{P + Z_2} \right] \quad (7)$$

Utilizing equation 7, the altitude error as a function of altitude has been calculated assuming $\Delta P_0 = 0.025$ mmHg. This is the error which would result from two hemispherical bubbles of 0.1 inch radius. Results are indicated in Table III. In the calculation of Table III, height Z_2 was assumed to be two inches. The results of Table III indicate that the altitude error due to air entrapment will increase rapidly with increasing altitude. In an attempt to verify this, experiments were conducted in the laboratory using an A-1 barometer. These were accomplished by pumping both on the reference tube and the cistern from atmospheric pressure to 80,000 foot pressure. Tests were performed at random after the mercury had been in extensive use and air bubbles were clearly visible at the mercury glass interface. The results of the tests repeated at least six random times, indicated the change in zero setting between atmospheric pressure and that conforming to 80,000 feet was within 0.05 mmHg. However, it was further noted that the air was continually escaping into the vacuum system as the tests were performed. As the pressure was reduced from atmospheric pressure, the air bubbles became increasingly larger as would be expected; however, they were unstable and many escaped into the vacuum system as the test proceeded. Hence, it must be concluded from these preliminary tests that the effect of air trapped in the mercury interfaces has small effect on shifting the zero when an active vacuum is maintained. Precision of the testing indicated that any such errors were five to ten times smaller than calculated for Table III.

TABLE III
CALCULATED POSITIVE SYSTEMATIC ALTITUDE ERROR
DUE TO $\Delta P_c = 0.025$ mmHg.
(Equation 7)

ALTITUDE (Ft. $\times 10^{-3}$)	ALTITUDE ERROR (Ft.)
0	0.9
20	3.4
40	15.5
60	74.5
80	287.0
100	932.5

9. Thermal lag. The thermal lag existing between the observed thermometer and the mercury column itself can result in an appreciable error. For example, in an area where the daily temperature may fluctuate 10°C , a lag of 3°C would probably be possible and this would correspond to an error of approximately 0.4 mmHg at a pressure of 760 mmHg.

3.2.1.4. Calculated Accuracies for A-1 Barometers as Presently Used for Air Force Altimeter Calibrations.

If the random errors only of section 3.2.1.3 are added, a maximum error of 0.50 mmHg results. However, if the random errors are combined by root-magnitude-square method, the RMS value is calculated at ± 0.27 mmHg. Combining this latter figure on an RMS basis with repeatability errors of 0.15 mmHg, the final computed error is ± 0.31 mmHg. This error is constant and independent of pressure level and when converted to altitude error the results are as shown in Table IV.

3.2.1.5. Calculated Barometer Error With Improved Operator Techniques.

The repeatability errors associated with the A-1 barometer are characteristic of this type instrument and, hence, cannot be improved without changing to a different design. From section 3.2.1.3, however, items 1, 2, 3 and 7 are the items of largest magnitude and, hence, in need of improvement as follows:

1. Item 1, if the scale correction chart is used to correct the reading, this error may be reduced to possibly 0.05 mmHg.

2. Item 2, use of the millimeter scale instead of the altitude scale will eliminate the stated error of ± 0.15 mmHg assigned to the altitude scale.

3. Item 3, with further emphasis to reduce mercury hysteresis in the capillary depression, the total error may be reduced from ± 0.2 mmHg to the figure of ± 0.1 mmHg which is included in the repeatability errors.

4. Item 7, the mercury sealed valve reference replaced by a continuous pumping vacuum system and monitoring of the vacuum level with a McLeod gage or equivalent vacuum gage will eliminate the systematic error assigned to the mercury sealed valve system and the figures given in Table II will be eliminated.

Making allowance for the changes indicated above, the resultant RMS value for all nonpressure dependent random errors is reduced from ± 0.31 mmHg to ± 0.16 mmHg. The altitude error as a function of altitude corresponding to the resultant RMS error of ± 0.16 mmHg is given as part of Table IV.

TABLE IV
ESTIMATED ALTIMETER ACCURACIES USING
MERCURIAL ALTITUDE TEST BAROMETER, TYPE A-1

Altitude (Ft. $\times 10^{-3}$)	ΔH Present Methods (Ft.)	ΔH Proposed Methods (Ft.)
0	± 11.3	± 5.8
20	± 21.2	± 10.9
40	± 45.0	± 23.7
60	± 119.9	± 61.9
80	± 341.9	± 161.8
100	± 873.5	± 432.3

3.3. DISCUSSION OF ALTIMETER CALIBRATION PROCEDURES.

The calibration of an instrument can rarely be performed under the exact conditions which will be encountered in normal service. The effects of a different environment such as temperature or vibration are often predominant changes although the time dependent and thermally induced inelastic errors are also generally significant for precision instruments.

The primary calibration of altimeters is conducted at approximately 25° C with secondary calibrations at higher and lower temperatures. It is believed, however, that in modern temperature controlled aircraft cabins that the altimeter normally operates at a temperature somewhat higher than 25° C because of the heat dissipated by other instruments in the immediate locale. In uncontrolled thermal environments, the operational temperature may vary widely. These factors require a calibration at more than one temperature. Such calibrations are generally considered to be quite repeatable since the thermally induced inelastic errors are usually small in comparison to the thermally induced dimensional changes; and in-service corrections conceivably could be made for thermal environmental changes in a normal service of an altimeter.

The inelastic errors are not so easily defined and the major portion of this section is given to a discussion of these errors.

3.3.1. General Consideration of Instrument Errors.

For this consideration the errors associated with an altimeter are divided into groups. The first group includes those errors normally referred to as scale error deviations and are herein defined as the discrepancy of instrument reading at a prescribed environment from a predefined relationship between pressure and altitude for a perfectly elastic mechanism, i. e., all inelastic effects such as hysteresis and drift are assumed to be zero. Conformance to a prescribed pressure-altitude relationship, then, is the major criterion for scale error figures. The second group of errors includes only those errors which appear as departures of a calibration curve from an ideal calibration curve due to inelastic effects at a given temperature. A third group might include only those errors due to temperature, however temperature errors may well contribute to either one or both of the above listed groups so that it is advantageous to consider effects of temperature changes on each of the groups separately.

Assuming that there are errors falling under the second classification which are of such a magnitude to warrant consideration, then some sort of average scale error calibration is desired about which the errors of this classification will be uniformly grouped. As an alternate, if scale errors are obtained in a manner such that the sign and magnitude of inelastic errors are known, then an average response may be predicted from the measured response. If the response of the instrument to a prescribed function is inherently linear and production techniques have been refined to the extent that no departures from uniformity are expected, then scale error calibration may consist of measurement at two points only, provided that the points are measured under known conditions of elasticity. However, if response is not linear and curve shaping is necessary within the instrument, the number of scale error calibration points required depends greatly on the complexity of the curve fitting mechanisms and the uniformity expected from a particular production facility. For example, if a cam is used for curve fitting, an irregularity on the cam could cause a large error to go undetected if calibration points straddled the irregularity. In general then, for maximum reliability of scale error calibration an infinite number of calibration points must be used. In practice of course, a reasonable compromise must be made. Regardless of the number of scale error calibration points, however, if inelastic errors are significant, the direction and magnitude of the inelastic errors should be known for each scale error calibration point. It is also necessary that environmental effects be known if they are of sufficient magnitude to warrant consideration. The complete problem then, is to select a schedule of testing such that the proper magnitude and sign of inelastic and environmental errors may be assigned to the measured scale error in order to determine the total error associated with any prescribed operational cycle.

Many attempts have been made in the past to describe in a general manner the relationship between force and deflection of a spring member but a review of this field of study is beyond the scope of this report. For precision force-deflection type instruments, however, it will be assumed that the force-deflection characteristics may be described by an envelope as shown in Figure 2.

The intersection of the abscissa and the ordinate represents a zero point which is a point at one extreme of the normal operational cycle and at which the spring member, i. e., altimeter, has been held for a long period of time. Curve A then represents the first cycle of operation after rest at the zero point. The curve A represents the worst possible combination as the portion from 0 to 1 is rapidly traversed and then held at point 1 until essentially all drifting is accomplished. This brings the measurement to point 2, where again it is rapidly traversed back to zero stress, point 3, and if held at zero stress for a long period of time the point will finally return back to zero. Curve B represents the condition under a sustained rapid cycling type of testing where a closed, symmetrical hysteresis loop is obtained. Curve C is shown to demonstrate what may happen under very slow cycling where the frequency of cycle traversing is low enough so that essentially all drifting is taken care of while the cycle is being made. Assuming that this representation is correct, it is clear that the maximum error zone that may occur is simply the drift error plus the hysteresis at the point of measurement. It should be recognized that the graph of Figure 2 is shown in greatly enlarged scale for illustrative purposes only and that the relative width of the drift and hysteresis curve, as shown in Figure 2, is not necessarily representative. It is assumed for this discussion that the center of the envelope (point 4) is fixed. This assumption requires that dimensional instability of instrument materials has been stabilized to a point where further shifts are minor compared to the inelastic errors considered herein.

The same envelope is shown in Figure 3, and here it is assumed that after reaching point 3 the cycle is immediately continued up-scale in a rapid manner back to point 2. The crosshatched area then represents the zone of possible readings for upscale traversing. This zone width is defined by the total drift at the ends and the curvature is defined by the hysteresis. A similar graph would hold for the zone of possible readings for downscale traversing.

If it can be shown that experimental data correlates with this representation, relatively simple tests corresponding to curves A and B (or other prescribed curves) could define the error envelope associated with a scale error calibration obtained under known conditions. The possibility exists that a fixed relationship exists between the hysteresis as defined by Curve A, and the drift curve which if known, could further simplify calibration procedures.

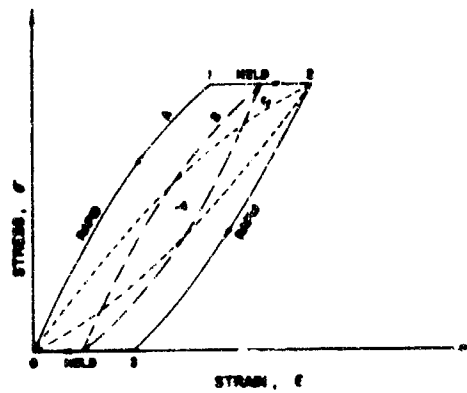


FIGURE 2
GRAPHICAL REPRESENTATION OF INELASTIC
ERRORS OBTAINED UNDER CYCLIC CONDITIONS.
— FIRST CYCLE AFTER REST
AT ARBITRARY ZERO POINT
- - - SUSTAINED RAPID CYCLING
- · - · - VERY SLOW CYCLING

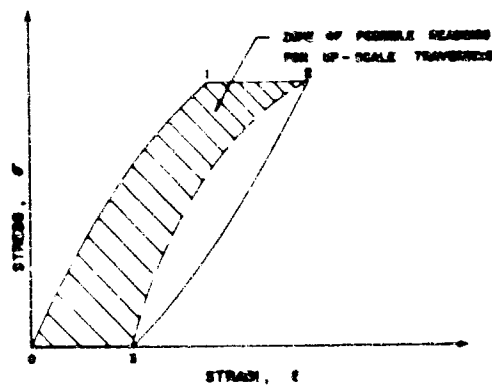


FIGURE 3
GRAPHICAL REPRESENTATION SHOWING INELASTIC
ERROR ZONE FOR UP-SCALE TRAVERSING

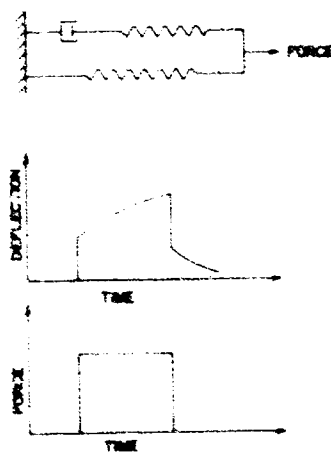


FIGURE 4
MECHANICAL MODEL AND DYNAMIC
BEHAVIOR OF STANDARD LINEAR SOLID.

Possibly the closest mechanical model of such a curve is that discussed by Zener (Ref. 13) and termed the "Standard Linear Solid." This model is shown in Figure 4 and has the analytical form:

$$\epsilon + a \dot{\epsilon} = b \sigma + c \dot{\sigma} \quad (8)$$

where:

ϵ = strain (displacement)

σ = stress (force)

$\dot{\epsilon}$ = time rate of strain

$\dot{\sigma}$ = time rate of stress

a, b, c = proportionality constants

The response to a unit step of stress may be readily obtained from expression (8) and is

$$\epsilon(t) = \left(\frac{c}{a} - b \right) e^{-t/a} + b \quad (9)$$

This model may be utilized in attempts to characterize drift patterns; however, it does not allow for the hysteresis obtained under conditions such that drift effects are negligible.

As a first approximation however, it may be assumed that the hysteresis curve is parabolic (Ref. 14, 15) which assumption gives the following expression for the shape of a closed loop hysteresis curve.

$$\delta/\delta_m = 4 \left(1 - \frac{\sigma}{\sigma_m} \right) \frac{\sigma}{\sigma_m} \quad (10)$$

where:

σ_m = stress range

δ = hysteresis

δ_m = maximum hysteresis for a given stress cycle

Although expressions (8) and (10) might be combined it seems advantageous to consider them separately until correlation could be shown for a particular instrument design.

As previously implied one might also expect to find fixed relationships between δ_m of expression (10) and the constants of the drift curve, expression (9).

It should be noted that expressions (9) and (10) are in terms of stress and strain and may be directly applied to a specific case of force and output only if the inter-relationships are known. Assuming that an altimeter employs a linear pressure capsule and curve shaping linkages, the respective altitude errors due to nominal values for hysteresis and drift are shown in Table V for an operational range of 0 - 70,000 ft. The midpoint of the stress range is approximately 17,000 ft. for this altitude range. The envelope of inelastic errors (described in Figure 2) would take the form of the last column of Table V for the hypothetical "linear" altimeter of Table V. No information is at hand to indicate a precise relationship of drift to stress range; however, it would be expected to be proportional to a power of stress greater than unity and possibly proportional to the hysteresis.

TABLE V
HYSTERESIS AND DRIFT FIGURES FOR NOMINAL VALUE OF
20 FT. AT 17,000 FT.

<u>H (Ft.)</u>	<u>δ/δ_m</u>	<u>Hysteresis δ (Ft.)</u>	<u>Drift (Ft.)</u>	<u>Hysteresis Plus Drift (Ft.)</u>
70,000	0.	0.	214	214
60,000	.113	14.5	128	142
50,000	.273	21.2	78	99
40,000	.502	24.6	49	74
30,000	.779	25.2	32	57
17,000	1.00	20.0	20	40
10,000	.87	13.9	16	30
0	0.	0	12	12

The effects of moderate temperature changes for precision instruments can be fully as significant as the pressure induced inelastic errors discussed above. This arises partially through use of materials having different thermal expansion characteristics or even the same material having different expansion characteristics in different

directions and would be quite prevalent, for example, if soft solders are used for joining active members. An additional source of stress, temperature induced, could arise through mechanically operated temperature compensating means. If the temperature induced stresses are moderate, however, the inelastic error envelope due to temperature changes will be similar to the envelope of Figure 2 and temperature effects may be analyzed in the same manner as loading effects. The only distinction being that the stress is now brought about by a temperature change rather than a direct loading.

3.3.2. Experimental Investigation of Altimeter Inelastic Errors.

A limited amount of testing of altimeters for inelastic errors was accomplished for comparison with the concepts outlined above. Data was obtained for two precision (MA-1 or AAU-8/A) altimeters on loan from ASD and two sensitive altimeters (Type C-12) which were purchased from a FAA authorized overhaul base. Hysteresis and drift data were obtained for two pressure ranges.

3.3.2.1. Testing Procedure.

The four altimeters and a vibrator were mounted on a table under a bell jar. Pressure was controlled manually using a C.E.C. type 6-201 piston gage for reference. The low pressure side of the piston gage was maintained below 20 microns as indicated on a McLeod gage which was connected via a separate pressure line into the low pressure chamber at a position across the chamber from the exhaust connection. A small bore mercury U-tube manometer was also tied into the system for a rough indication of absolute pressure. Appropriate valving was included for large pressure adjustments and an adjustable bellows was used for fine adjustment. Valving was also used to "disconnect" the piston gage from the remainder of the system during the large pressure cycles associated with the hysteresis testing.

The hysteresis data was obtained by running five continuous cycles over a pressure range and readings were made at the midpoint of the pressure range for both upscale and downscale traversing. (The pressure range midpoint was used in order to measure the maximum hysteresis in accord with the theory discussed herein.) The duration of each cycle was approximately 10 minutes, and fine adjustment and reading of the altimeters required approximately one minute.

Drift data was obtained by holding the altimeters at one pressure for at least 24 hours and then progressing rapidly to a pressure established with reference to the piston gage. The first readings (represented as zero on the time scale) were taken three minutes after starting the pressure change and efforts were made to accomplish the pressure change in two minutes at a constant rate.

3.3.2.2. Testing Results.

Results of hysteresis testing are shown graphically on Figure 5 and 6 and are summarized in Table VI. The data of Figure 5 give upscale and downscale readings at 20.4 inches Hg (essentially, the midpoint) for cycling between 28.9 inches Hg (1000 ft. altitude) and 12.3 inches Hg (22,700 ft. altitude.) The data of Figure 6 give upscale and downscale readings at 16.82 inches Hg for cycling between 28.9" Hg and 3.42" Hg (50,000 ft.). Average values of hysteresis measured at mid-pressure range are given in Table VI in feet of altitude, inches mercury and as a fraction of the pressure range. Although the altimeters employ "nonlinear" elements in order to read out directly in feet of altitude rather than pressure, it would seem fairly safe to assume that the integrated value of stress for all elements is directly proportional to the applied pressure. Accordingly, the maximum hysteresis, in terms of pressure, would occur at the midpoint of the pressure cycle. The fractional hysteresis increased with increased stress range for the two precision altimeters (1 and 2). The sensitive altimeters (4 and 5) do not show any well defined trend. The higher hysteresis values exhibited by the sensitive altimeters (approximately equal to ten times that for the precision altimeters) indicates a more highly stressed mechanism.

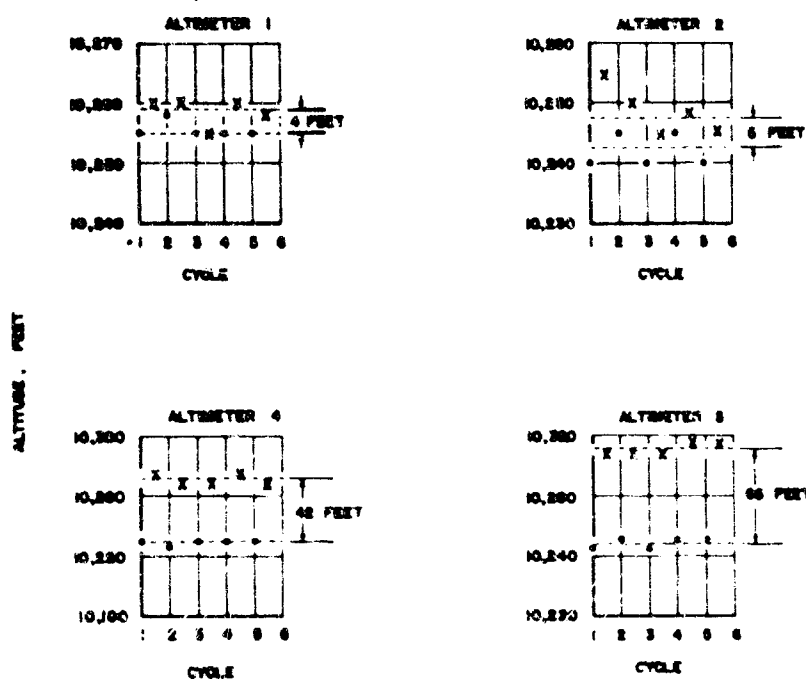


FIGURE 5
HYSTERESIS FOR 1,000 - 22,700 FT. RANGE
FOR FOUR TEST ALTIMETERS.

• DECREASING PRESSURE
X INCREASING PRESSURE

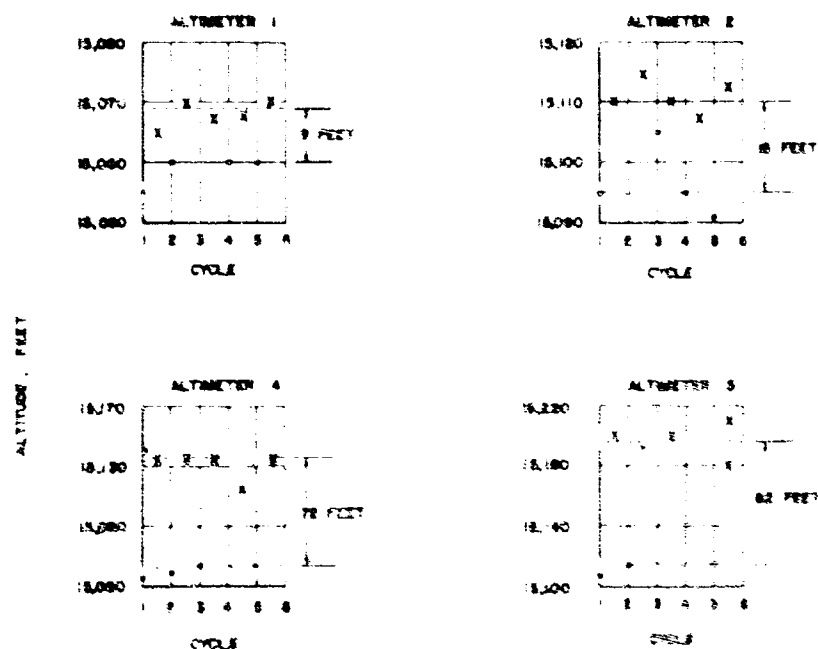


FIGURE 6
HYSTERESIS FOR 1,000 - 50,000 FT. RANGE
FOR FOUR TEST ALTIMETERS.

• DECREASING PRESSURE
X INCREASING PRESSURE

TABLE VI
HYSTERESIS RESULTS

Readings at Approx. 10,300 Ft.;
1000 Ft. to 22,700 Ft. Cycles (16.59 Hg)

Altimeter	Hysteresis (Ft.)	Hysteresis (In. Hg)	Fraction of Pressure Range
1	4	.0032	.019 percent
2	5	.004	.024 percent
4	42	.034	.20 percent
5	65	.052	.31 percent

Readings at Approx. 15,000 Ft.;
1000 Ft. to 50,000 Ft. Cycles (25.44 In. Hg)

Altimeter	Hysteresis (Ft.)	Hysteresis (In. Hg)	Fraction of Pressure Range
1	9	.0062	.024 percent
2	15	.010	.039 percent
4	70	.049	.19 percent
5	82	.056	.22 percent

Results of drift testing are shown on Figures 7, 8, and 9. Results of the first test, after approximately one hundred hours of "rest" at ambient pressure, is shown on Figure 7. As previously described the first data point recorded at zero time was taken three minutes after start of the pressure change and approximately one minute after the pressure was stabilized at test value. Readings were taken frequently for 20 to 30 minutes and then every hour or two until the end of the day. Ambient temperature variations were only about 2° F maximum during these tests. The altimeters were maintained "at pressure" overnight and several readings taken the following day, which readings are indicated as a dashed line after the time scale break on Figures 7, 8, and 9. Drift data shown on Figure 8 was obtained at approximately 1350 ft. altitude after "resting" at 22,700 ft. and similarly, the data of Figure 9 was obtained

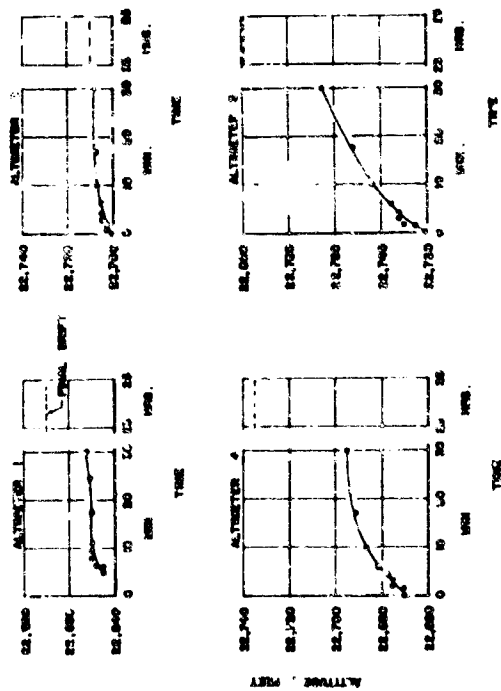


FIGURE 7
DRIFT AFTER 60 HOURS AT 800 FEET.

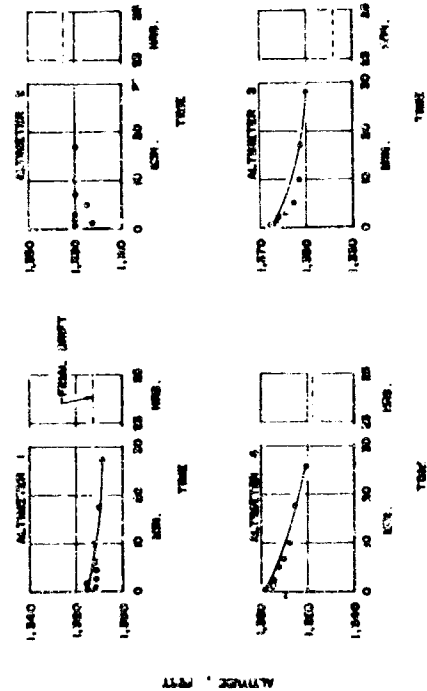


FIGURE 8
DRIFT AFTER 24 HOURS AT 22,700 FEET

EXPERIMENTAL DETERMINATION OF DRIFT FOR FOUR REPRESENTATIVE TEST ALTIMETERS.

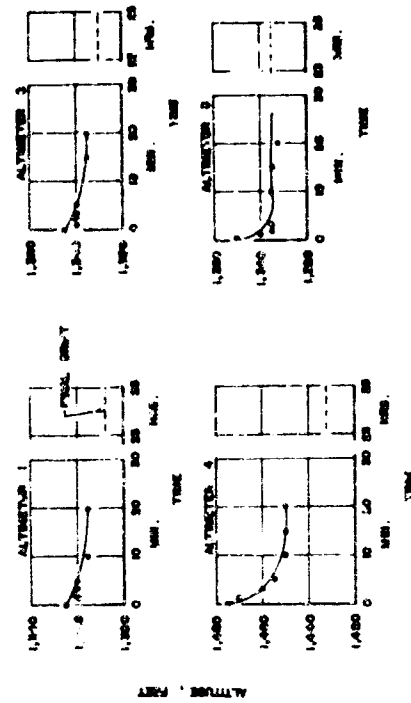


FIGURE 9
DRIFT AFTER 42 HOURS AT 30,000 FEET

after a 22 hour "rest" at 50,000 ft. altitude. The drift results associated with the precision altimeters show considerable scatter but in general, the drift after 24 hours for the sensitive altimeters is also of the same order of magnitude as the hysteresis. Analysis of the "Standard Linear Solid" model, Section 3.3.1, dictates a linear relationship between $\dot{\epsilon}_2 - \dot{\epsilon}_1$ and $\epsilon_2 - \epsilon_1$ where ϵ_1, ϵ_2 are indicated output values and $\dot{\epsilon}_1, \dot{\epsilon}_2$ are their first time derivatives respectively. The data for altimeter number 5 shown on Figure 5 was compared in this manner and no correlation was indicated. No attempts were made to compare the drift data for the precision altimeters to the Standard Linear Solid model because of the paucity of data. It is observed that the drift (as a fraction of the pressure range) is greater at 22,700 ft. than at 1350 ft. This result would be expected from the Standard Linear Solid model and would have the form shown in Figure 10 for a stress-time cycle of small magnitude after holding at one extremity of the normal stress range of the instrument for an extended period. This type of response has also been demonstrated in Reference 16 where it was found that drift and after-effect developed during a number of simulated short duration successive flights tended to accumulate. Drift is defined in Reference 16 as the change in altimeter reading with time when the instrument is subjected to a constant pressure and after-effect is defined as the hysteresis, at sea level pressure, at the completion of a pressure cycle.

3.3.3. General Discussion.

Test results indicate that hysteresis for the precision altimeter is an order of magnitude lower than for the sensitive altimeters. Drift accumulated over 24 hours was of the same order of magnitude as the hysteresis for the sensitive altimeters. Drift, over a 24 hour period, of the sensitive altimeters was two to five times the drift values exhibited by the precision altimeters. All comparisons were made on a pressure basis rather than altitude basis, since the integrated stress value for an altimeter is believed to be more closely proportional to pressure than to altitude.

Curvature of the drift response for the sensitive altimeter was found to be different than that predicted by the "Standard Linear Solid" model; however, phenomenological correlation was shown between this model and the accumulation of drift and after-effect under successive cycling at a low frequency as shown in Reference 16.

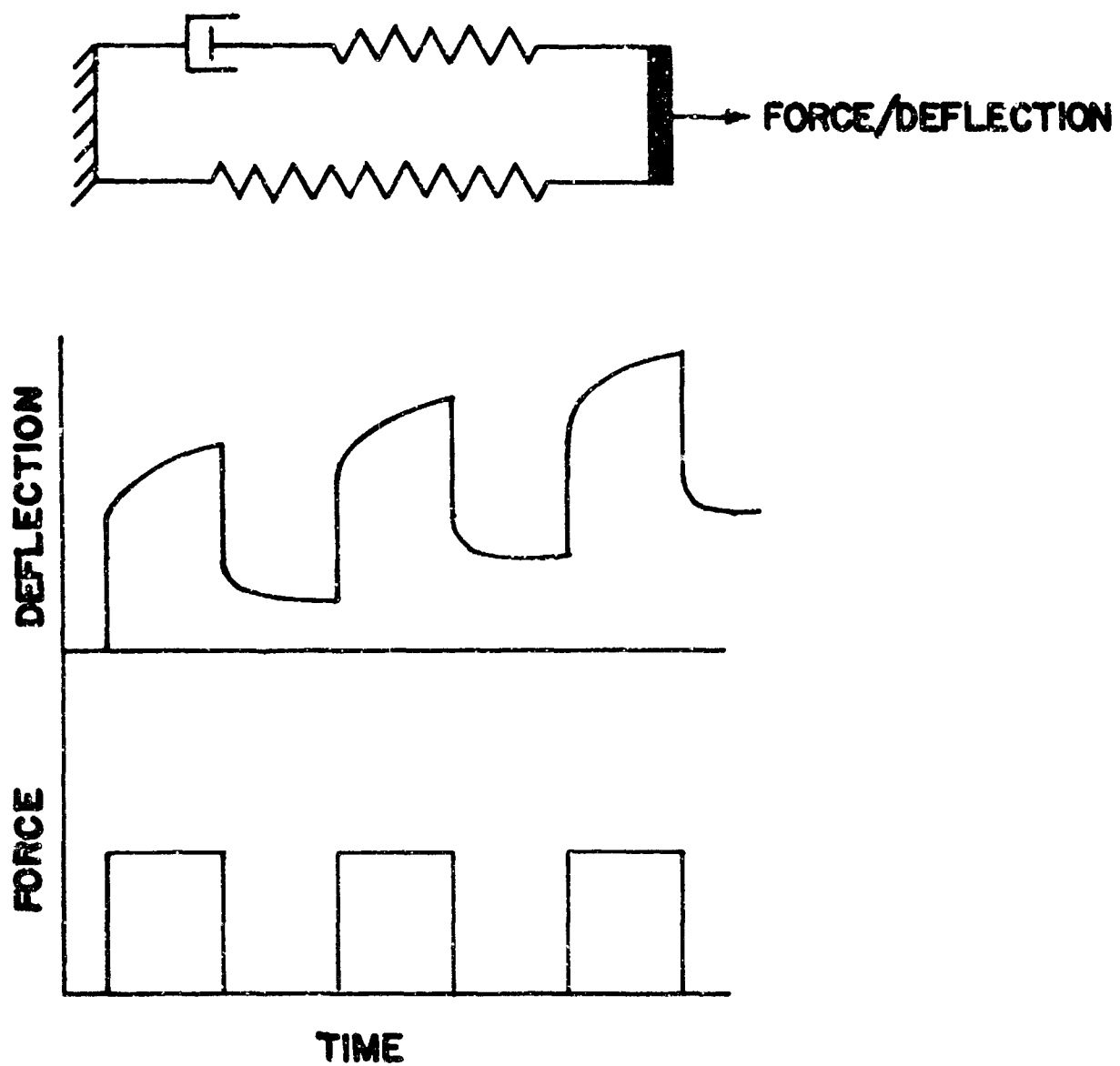


FIGURE 10

RESPONSE OF STANDARD LINEAR

SOLID MODEL TO SUCCESSIVE

FORCE CYCLING.

Fractional hysteresis values were roughly proportional to pressure range for the precision altimeters and roughly constant for the sensitive altimeters.

Existence of measurable frequency dependent inelastic effects requires that some attention be given to the calibration sequence. The calibration procedure adhered to by Air Force calibration facilities appears to be adequate in this respect for the precision altimeters since such calibrations tend toward the mean calibration of an inelastic error envelope (calibration is performed "slowly" so that a major portion of the drift takes place as the calibration cycle is performed) which is small relative to present values of overall scale error tolerances.

SECTION 4

FUTURE ALTIMETER CALIBRATION STANDARDS, TECHNIQUES, AND PROCEDURES

An objective of this contract was to survey the field for calibration equipment and techniques which might be utilized in achieving more satisfactory calibrations. Advertising literature on appropriate products was available from many manufacturers. Further information was obtained through a survey letter mailed to twelve organizations which have indicated capability in the pressure calibration equipment field.

4.1. ALTIMETER CALIBRATION STANDARDS PRESENTLY AVAILABLE.

The instruments which may be utilized in calibration of an altimeter are classified into two groups; Reference Standards and Working Standards.

4.1.1. Reference Standards for Altimeter Calibration.

The Reference Standards are characterized as pressure instruments which permit direct reference of the indicated reading to the fundamentals of mass, length, and time. A further restriction on this classification is that the instruments be constructed in such a manner that the accuracy values practically achieved are at least twice as good as the more versatile instruments of the second classification. The instruments surveyed which fall into this classification are listed in Table VII.

4.1.2. Working Standards for Altimeter Calibration.

The working standards are generally characterized as instruments having somewhat less accuracy than the reference standard but having greater flexibility and ease of operation. The instruments surveyed which fall within this classification are listed in Table VIII.

Items 1 through 6 are mercurial manometers and are generally considered capable of operation as a reference standard if careful attention is given to the measurement; however, the designs are such that ease of operation are favored over absolute accuracy. Item 5 requires special mention because of the exceptionally high accuracy reported. This instrument utilizes one fixed cistern and one movable cistern interconnected by flexible tubing. Mercury level within the cisterns is sensed through capacitive means

TABLE VII
Classification 1 (Reference Standards)

ITEM	INSTRUMENT TYPE	MANUFACTURER	IDENTIFICATION	APPLICABLE RANGES	ACCURACY	REFERENCE
1	Modified U-Tube	Hass	Type M8-2 Micrometer Standard Barometer	0-31" Hg 0-62" Hg 0-100" Hg	$\pm .001''$ Hg for each 30" section with occasional random deviation to .002" Hg	Manufacturers Literature
2	Pneumatic Piston-Cylinder	Dynometrics	Model PPS-500	0.2-15 psi (0.1 psi increments) 0.5-50 psi (0.5 psi increments) 1-150 psi (1 psi increments)	$\pm .015$ percent of range	Manufacturers Literature
3	Pneumatic Piston-Cylinder	Consolidated Electrodynamics Corporation	Model 8-201	0.3-1.5 psi 0.3-5 psi 1.5-15 psi (1 percent f.s. increments for all ranges)	$\pm .015$ percent of reading	Manufacturers Literature
4	Pneumatic Piston-Cylinder (Digital Readout)	Wallace O. Leonard, Inc.	Leonard Primary Pressure Standard	.4 to 250 psi	.01 percent f.s. to .02 percent of reading for each of three ranges	Manufacturers Literature
5	Tilting Pneumatic Piston-Cylinder	Ruska	---	.3-15 psig 2-600 psig 0-.3 psig 0-2 psig	Vertical* .01 percent f.s. .01 percent reading Inclined* .01 percent f.s. .01 percent reading	Manufacturers Letter

* Tentative Repeatability Figures, units expected to be marketed in 1962.

TABLE VIII
Classification 2 (Working Standards)

ITEM	INSTRUMENT TYPE	MANUFACTURER	IDENTIFICATION	APPLICABLE RANGES	ACCURACY	REFERENCE
1	Mercurial Manometer	Hass	A-1 Barometer	0-31" Hg	.026 percent f.s.	T.O. No. 33A7-4-2-1
2	Mercurial Manometer	Hass	0-31" Range Mercurial Barometer MIL Spec B-4308B	0-31" Hg	.004" Hg with use of calibration chart	Manufacturers Literature
3	Mercurial Manometer	Ideal-Aerosmith	OFF-SET Cistern	0-30" Hg	.005" Hg	Manufacturers Literature
4	Mercurial Manometer	Ideal-Aerosmith	U-Tube	0-30" Hg	.003" Hg	Manufacturers Literature
5	Mercurial Manometer	Ideal-Aerosmith	Double Cistern Nulling Manometer	0-33" Hg	.0003" Hg	Manufacturers Literature
6	Mercurial Manometer	Exactel	Series 500 Servomanometer	0-32" Hg	.004" Hg	Manufacturers Literature
7	Force Balanced Bellows	Consolidated Electrodynamics Corporation	Electromanometer System	± 1.5 psi ± 5.0 psi ± 15 psi	Less than .05 percent f.s. drift in 8 hours	Manufacturers Literature
8		Wiancko	Type Q3403	0-15 psi	.04 percent f.s.	Manufacturers Bulletin 106A
9	Quartz Pressure Gage	Buck	Fused Quartz Transfer Standard	0-1" Hg 0-40" Hg	.0033 percent f.s. repeatability	Manufacturers Literature
10	Diaphragm Gas Reference	Rosemount	Reference Pressure Cell Model 802A	0-200" Hg	$\pm (.001''$ Hg (.003 percent) per year stability (tentative)	Manufacturers Bulletin 46027
11		U.S. Science Corp.	Universal Barodyne	.8-120" Hg	$\pm .07$ percent of pressure or .002" Hg	Manufacturers Letter
12	Pressure Capsule	Fischer and Porter	Press-1-Cell	0-80,000 ft.	19 ft. at 10,000 58 ft. at 40,000 358 ft. at 80,000	Manufacturers Catalog 11-102 Spec. 11-1221-1
13	Servo-force balanced Piston Cylinder	Dynometrics	Model PB-500 Piston Beam	0-15 PSI	.025 percent f.s. .001 psi resolution	Manufacturers Letter

and rebalanced to a given position by vertical motion of the movable cistern. Column height is indicated through a lead screw.

Items 7 through 10 and 12 and possibly Item 11 (no descriptive literature is available on the sensing mechanism for Item 11) use high precision spring elements either directly or indirectly through a force balance system to give an analog signal of applied pressure. An evacuated chamber on one side of a precision spring seal serves as a pressure reference for these devices. Item 10 is unique in that the pressure reference chamber is not evacuated but is filled with gas to give one discrete pressure setting for the minimum energy position of the precision spring seal.

Item 13 is an adaptation of the conventional piston gage and is designed to give analog readings through force balancing of the piston rather than through direct use of dead weights.

With regard to the reference standards tabulated in Table VII, it is of interest to note the relative accuracy curves in terms of feet of altitude rather than units of pressure. Figure 11 shows the comparison between an accuracy specification given as .001 inch Hg and an accuracy specification defined as .015 percent of pressure. These figures correspond to the best accuracy figures quoted by the reference standard manufacturers. It should be noted that, in terms of feet of altitude, the .015 percent of pressure curve is almost flat compared to a rapidly increasing error at high altitude for a fixed pressure error of .001 inch Hg.

4.2. ADDITIONAL ALTIMETER CALIBRATION STANDARDS AND TECHNIQUES UNDER DEVELOPMENT.

In addition to the items documented in Tables VII and VIII, information has been received on several items recently developed or presently in a developmental state.

4.2.1. Manometry Development.

There have been many developments in the past ten years which have increased the ease of operation of the off-set system style barometers while preserving high accuracy. These developments include better cistern and cistern-tube passageways to minimize leaks and bubble entrapment, use of temperature controlled cabinets housing and manometer, electrical meniscus sighting devices with remote indication,

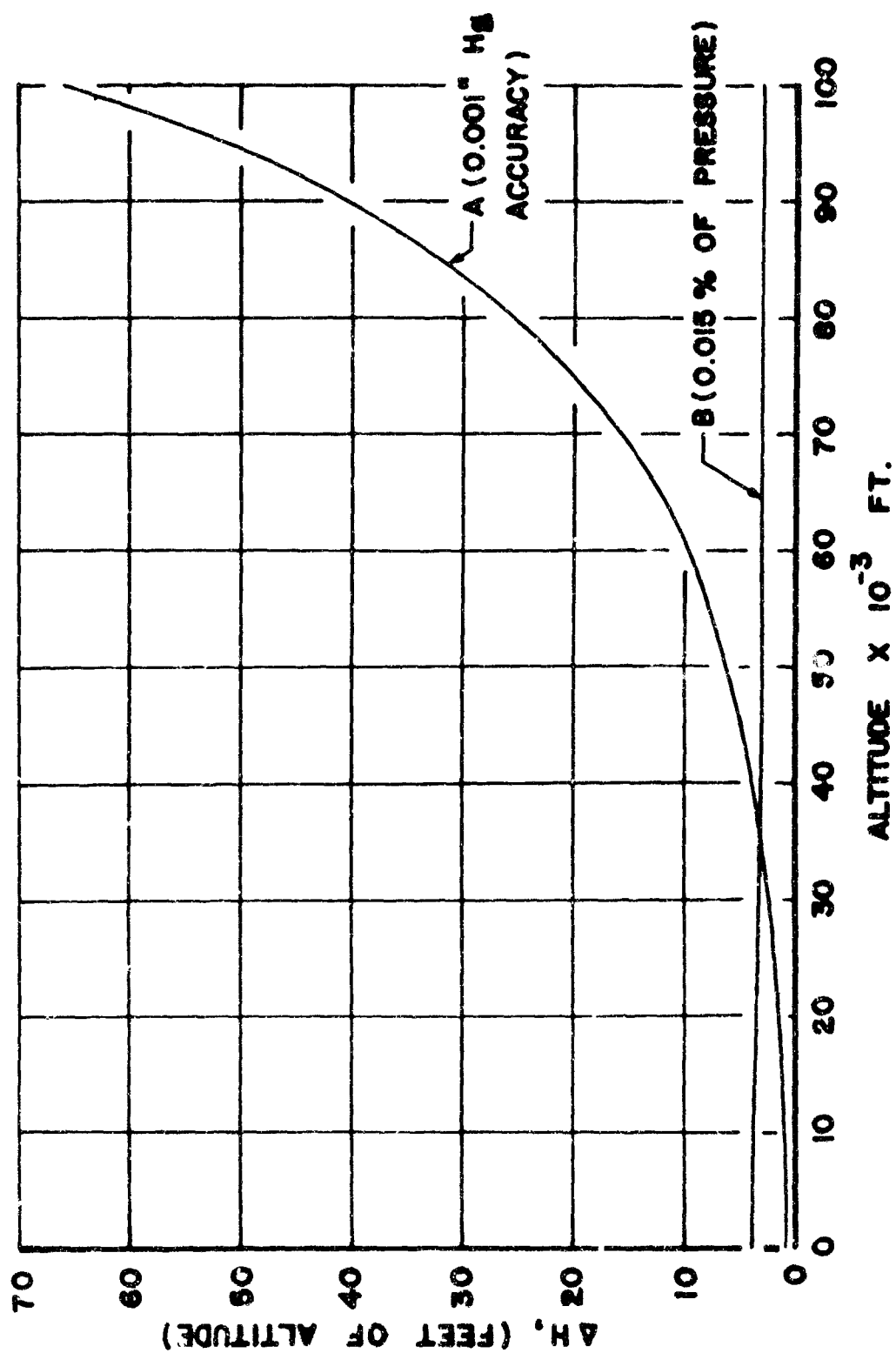


FIGURE 11
EQUIVALENT ALTITUDE DEVIATION FOR FIXED ERROR
AND FOR ERROR PROPORTIONAL TO PRESSURE .

pressure connections on the reference side so that the reference vacuum may be monitored continuously at the top of the reference tube, remote positioning mechanisms for positioning of the meniscus indicating apparatus, and precise pressure controllers which automatically hold a pressure setting on command of the electrical meniscus indicating apparatus. The development trend for the off-set cistern barometer systems is definitely toward remote console control and indication of a pressure setting.

The Hass Instrument Corporation expects to market a pushbutton control console for the offset cistern barometer before 1963. The pushbuttons will automatically establish a predetermined discrete pressure or altitude setting. Further development by this manufacturer calls for automatic stepping through a pre-set sequence of altitude points or photographic recording of altimeter indications.

The other off-set cistern barometer manufacturers also have remote indication and control features, along with their own precision servo actuated pressure controllers.

Exactel Instrument Company is developing a U-tube servo manometer incorporating two-inch bore tubes. This instrument will have facilities for verifying length calibration through use of gage blocks.

4.2.2. Non-Mercurial Calibration Standards Development.

The Buck Instrument Company is adding a servo valve to their fused quartz transfer standard which will be supplied as an accessory to allow presetting and maintaining of a given check point.

The Rosemount Engineering Company has modified a design of their Reference Pressure Cell in order to give an optional electrical adjustment of the setting of an individual RFC cell. This feature allows adjustment over an approximate range of 0.1 inches of mercury. This company is also developing accessory equipment which will permit semi-automatic and automatic altimeter calibration.

The TriDyne Corporation is developing a force balanced piston cylinder type instrument and the lowest standard range is 20 psia. Accuracy is reported as $\pm .025$ percent f.s. The force is supplied through a servo driven poise weight on a ball lead screw and an evacuated reference bellows serves as a pressure reference.

4.3. PROCEDURAL DEVELOPMENTS.

The developments that are presently taking place in the procedures of Air Force altimeter calibrations and that might be considered for further development have been divided into those pertaining directly to the calibration equipment and those pertaining to the calibration of the altimeter.

4.3.1. Altimeter Calibration Equipment.

The Air Force is presently in the process of renovating the procedure for maintaining accuracy on the altimeter calibration instruments. This is being accomplished through use of piston cylinder type reference standards, as listed in Table VII. These reference standards will be established at approximately 100 bases throughout the world and will be referenced periodically to similar standards maintained at the Heath facilities. The units at the Heath facility will be calibrated on a rotational basis at the Bureau of Standards. These reference standards then are utilized to maintain the accuracies of the A-1 type barometers. This procedural development, if coupled with the recommendations for improved operator techniques of the A-1 barometer given in Section 3.2, should result in an accuracy of the order of magnitude calculated in Section 3.2.1.5. If further improvement is required, the items listed in Table VIII and the items discussed in Section 4 must be considered to be used in lieu of the A-1 type barometer, or in some cases, in conjunction with the A-1 barometer. The improvements in manometry techniques given in Section 4.2 definitely tend toward greater ease of operation, but at the same time tend toward less portability. At the periodical calibration checks against a reference standard, the reference standard and the working standard must be brought together, which requires that one or the other be quite mobile or portable. An alternate solution is the use of a highly accurate and portable transfer standard. Items 7 through 12 and possibly item 13 have the advantage of being highly portable and some of these can also classify in the same accuracy range as the mercurial working standards. The nonmercurial working standards do not have the mercury contamination problems and periodic cleaning procedures that are associated with the mercurial standards. They also do not have the inertia of a column of mercury to contend with, so that their response time is generally much faster and in most cases they do not require a vacuum reference of an active nature.

4.3.2. Altimeter Calibration Procedures.

The small, but nevertheless significant magnitude of the inelastic errors of the precision altimeters, as discussed in Section 3.3, indicates that a better procedure for determining scale error envelope may be determined. For further improvement in this area, it is recommended that a large group of altimeters be subjected to testing along the pattern established in Section 3.3.2 and at temperatures corresponding to the extremes that can be expected under service conditions. This data would give envelopes analogous to the envelope shown on Figure 2, and under certain service conditions the calibration of the altimeter could be expected to fail anywhere within this envelope. A study of envelopes encountered by altimeters in service condition then could be utilized to give the best statistical calibration for scale error of any one altimeter, and expected deviations from this calibration for a different flight envelope could be estimated. With the advent of semi-automatic and automatic calibration facilities it appears that a superior procedure for determining the best statistical scale error calibration and deviations from this scale error calibration could be devised.

SECTION 5
INFLUENCE OF PRESSURE SYSTEM LEAKAGE AND PRESSURE LAG
ON AIRCRAFT STATIC PRESSURE MEASUREMENTS

A leak in the static pressure system of an aircraft will cause a flow of air through the connecting tubing of the system and therefore a breathing of air in and out of the pressure sensing orifices. The situation is identical to an aircraft in a dive or climb. In fact, leakage rates are usually specified in terms of rate of descent or feet/min. The rate of allowable static system leakage specified in Section 4.4.3.2 of MIL-P-26292 is 1000 ft./min at an initial condition of 50,000 ft. (test performed near sea level conditions). The specifications for altimeters are much tighter. Military Specification MIL-A-27229A (USAF) for the AAU-8/A Altimeter specifies 100 ft./min at an initial condition of 18,000 feet (test performed near sea level conditions).

Flow through the connecting tubing will subject the system instruments to a pressure different from the pressure sensed at the orifices. This is the well known pressure-lag error (see References 17 and 18) and is dependent on the static system instrument volumes as well as the length and internal diameter of the connecting tubings. A flow in or out of the static orifices will produce another error which is caused by a pressure drop across the orifices and disturbance of the external flow past the orifices. Both of these types of errors will be discussed in the following paragraphs.

5.1. PRESSURE LAG.

The maximum allowable lag for an aircraft's static pressure system is shown on Figure 4 of MIL-P-26292. The pressure lag at the major transducer and at the instrument panel is specified in terms of maximum rate of climb of a vehicle for an altitude of 50,000 feet. Altitude error equivalence for the allowable pressure lag can be obtained from:

$$\Delta H = \lambda \frac{dH}{dt} \quad (11)$$

where:

ΔH = Pressure-altitude error, ft.

λ = Pressure lag constant, sec.

$\frac{dH}{dt}$ = Rate of climb, ft./sec.

Under the conditions for determining system lag stated in paragraph 4.4.5.2 of MIL-P-26292, the lag constant will consist entirely of viscous and acoustic lag terms. The lag due to aerodynamic interference of the external flow caused by air breathing in or out of the static orifices, reported in Section 5.2, can be determined only under actual flight conditions or by wind tunnel testing. Assuming that acoustic lag is small compared to viscous lag, as explained later in Section 5.1.2, and that the temperature of the static pressure system is near sea level standard conditions, i. e., $T_0 = 518.69^\circ \text{R}$, the allowable system lag for any altitude can be approximated by using the viscous lag relationship

$$\lambda = \lambda_0 \left(\frac{P_0}{P} \right) \quad (12)$$

where P is the static pressure and subscript "0" refers to standard-atmosphere sea level conditions.

The allowable static lag at the major transducer and at the instrument panel as a function of altitude and maximum rate of climb of a vehicle is shown in terms of altitude error on Figures 12 and 13 respectively. The allowable error is considerably larger for the instrument panel than for the major transducer. It also increases with the maximum rate of climb capabilities of the aircraft, although for rates of climb beyond 60,000 ft/min there is a definite leveling off of the curve. Figures 12 and 13, therefore, indicate that supersonic, high performance aircraft can have a larger allowable pressure-altitude lag error than slower aircraft if they climb at rates near their maximum capabilities even though their allowable lag constant, λ , must be held to a lower value. However, it should be noted that the altitude errors shown correspond to maximum rates of climb and will be less, by direct proportion, for slower rates of climb.

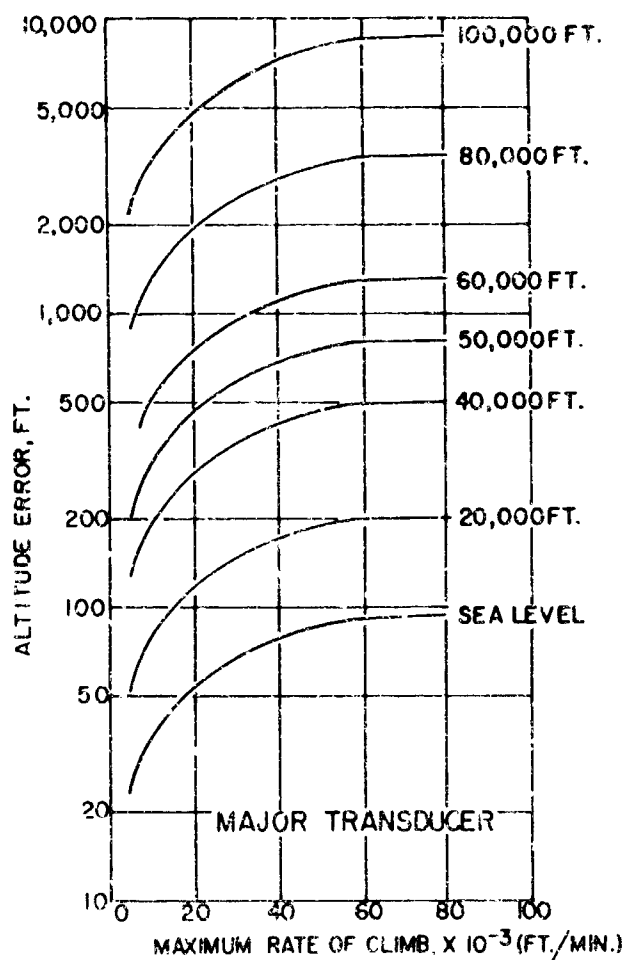


FIGURE 12

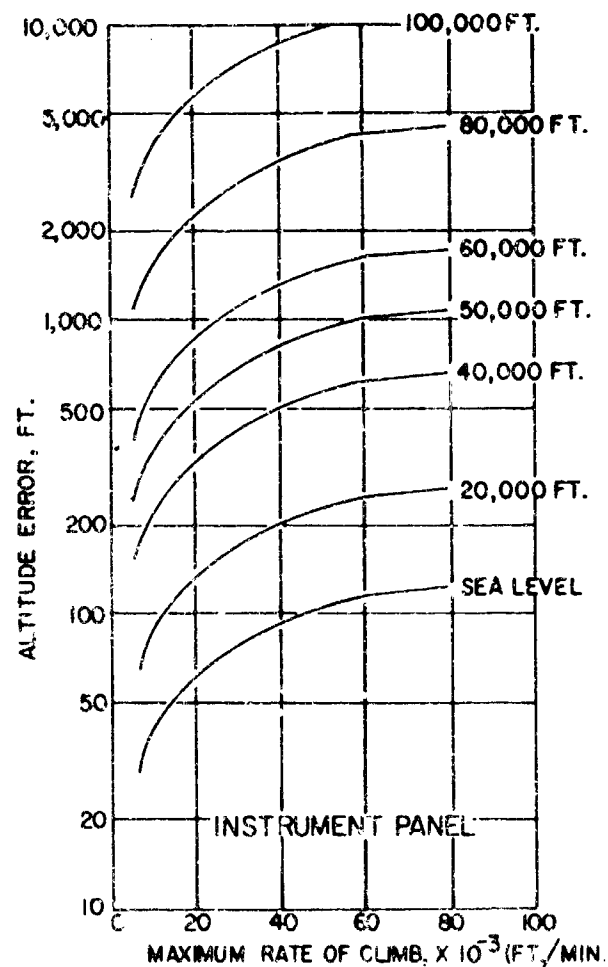


FIGURE 13

EQUIVALENT ALTITUDE ERROR FOR MAXIMUM ALLOWABLE STATIC PRESSURE SYSTEM LAG AS SHOWN ON FIGURE 4 OF MIL-P-26292 FOR AN ALTITUDE OF 50,000 FEET. ERRORS AT OTHER ALTITUDES COMPUTED USING STANDARD ATMOSPHERE PRESSURE VARIATIONS.

5.1.1. Viscous Lag.

Air flowing through the connecting tubing of an aircraft's static pressure system when there is a leak in the system, or when the vehicle is in a dive or climb, causes a pressure drop between the pressure ports and the receiving instruments. This is the viscous lag of the system and can be expressed for moderate flow rates as:

$$\lambda = \frac{128\mu L}{\pi D^4 P} \left[V_d + \frac{V_t}{2} \right] \quad (13)$$

where:

μ = coefficient of viscosity

L = length of tubing

D = internal diameter of tubing

P = static pressure

V_d = volume downstream of tubing

V_t = volume of tubing

In an actual aircraft installation, Equation (13) must be evaluated for each length of tubing between the static port and the instrument for which the lag is to be determined. All the individual lag constants are then added to obtain the total lag.

For this report we assumed a realistic total instrument system volume of 100 in.³ to determine what altitude error would exist for a leak in a pressure line 10 feet from the static orifices. The results are shown on Figure 15 as a function of internal diameter of the tubing. The leakage rate used was 1000 ft/min which is the allowable rate stated in Section 4.4.3.2 of MIL-P-26292 for an entire static system. The coefficient of viscosity, μ , was evaluated at sea level standard temperature. During flight the average temperature of the air in the static system could vary considerably from this value but, as shown on Figure 14, μ is not greatly dependent on temperature, i. e., a 100° R temperature change from sea level conditions, $T_o = 518.69^\circ \text{R}$, will cause only about a 15 percent change in the coefficient of viscosity.

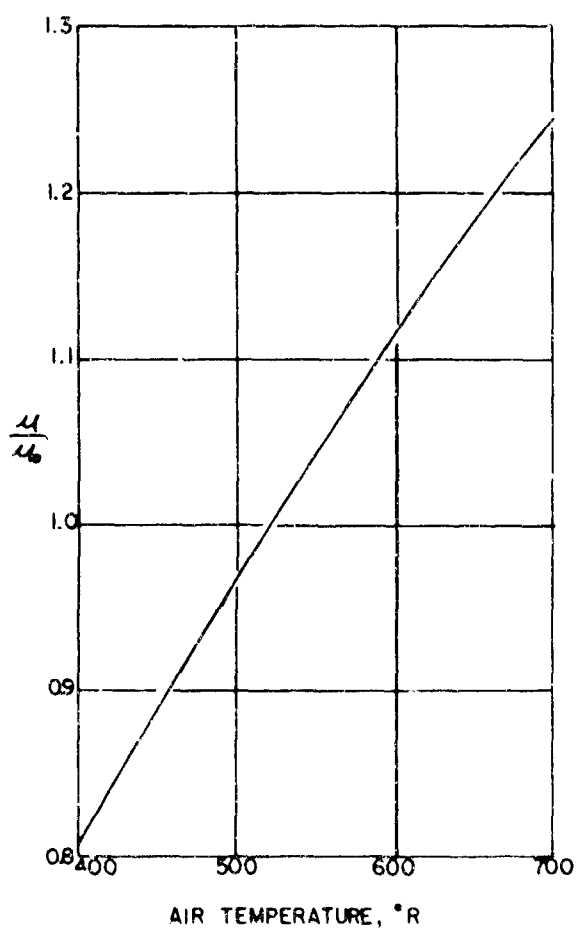


FIGURE 14

VISCOSITY RATIO FOR AIR AS A
FUNCTION OF TEMPERATURE

$$\mu_0 = 3.7373 \times 10^{-7} \text{ SLUGS / FT. SEC.}$$

= COEFFICIENT OF VISCOSITY AT
SEA LEVEL STANDARD TEMPERATURE
 $T_0 = 518.69^\circ \text{R}$

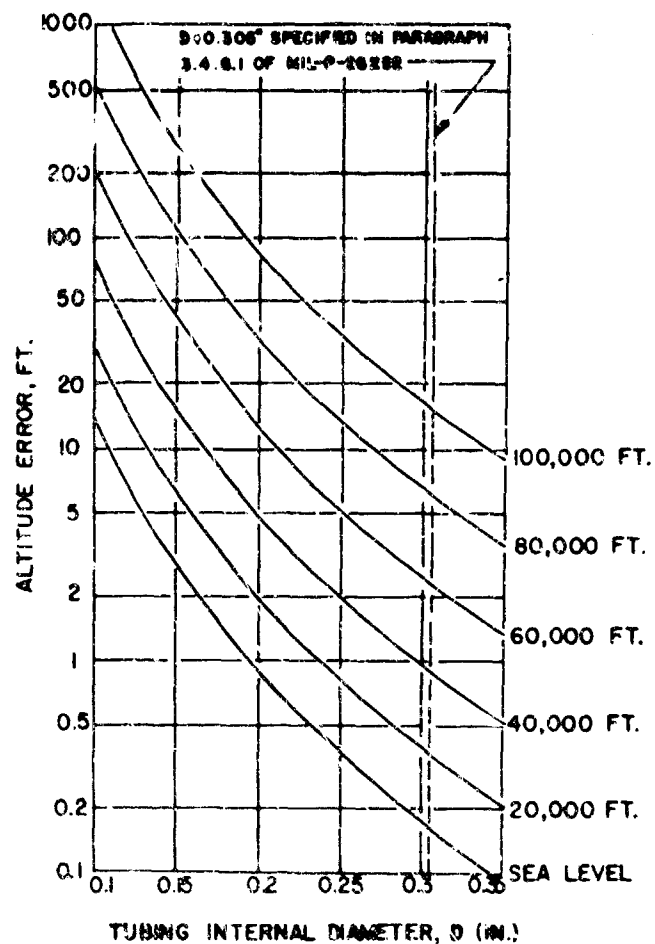


FIGURE 15

ALTITUDE ERROR EQUIVALENCE OF
VISCIOUS LAG ERROR.

$$\Delta H = \frac{128 \mu L}{\pi D^4 \rho} \left[V_0 + \frac{V_1}{2} \right] \frac{dH}{dt}$$

ASSUMING: $L = 10$ FEET

$$\mu = 3.7373 \times 10^{-7} \text{ SLUGS / FT. SEC.}$$

$$\frac{dH}{dt} = 1000 \text{ FT. / MIN.}$$

$$\left[V_0 + \frac{V_1}{2} \right] = 100 \text{ IN.}^2$$

The viscous lag error varies as the fourth power of the tubing diameter. For the example at 40,000 feet shown on Figure 15, the altitude error equivalence of viscous lag can be decreased from 15.3 ft. to 0.51 ft. by increasing the inside diameter of the tubing from 0.15 inch to 0.305 inch, the diameter specified in Paragraph 3.4.6.1 of MIL-P-26292. The altitude errors shown on Figure 15 for the recommended diameter of 0.305 inch and the allowable leakage rate of 1000 ft./min is small, reaching a value of only 15.5 feet for an altitude of 100,000 feet. However the errors shown are for a specific example and the magnitude of altitude error will be dependent on the location of a pressure leak in the system and will be largest if the leak is close to the instruments because L from leak to ports is maximum.

5.1.2. Acoustic Lag.

The acoustic lag is the time for pressure propagation through the static system tubing and is defined as follows:

$$\lambda_a = \frac{L}{a} \quad (14)$$

where: "a" is the local speed of sound inside the tubing.

From Eq. (11) we can obtain the equivalent altitude error:

$$\Delta H_a = \frac{L}{a} \frac{dH}{dt} \quad (15)$$

Using the above example for a pressure leak 10 feet from the static orifices, a leakage rate of $dH/dt = 1000$ ft./min, and assuming "a" = $a_0 = 1116.4$ ft./sec, the altitude error due to acoustic lag will be 0.15 ft. This value is small compared to the viscous lag errors shown on Figure 15.

The conclusions that may be reached regarding viscous and acoustic lag are that the resulting pressure-altitude errors will be small if the connecting tubing has an internal diameter of 0.305 inch or greater, if the leakage values are moderate (1000 ft of altitude per minute) and if the static system volumes are moderate (about 100 in.³). For higher values of leakage or climbing rate or larger system volumes, errors increase in direct proportion (see Equation 15 used to calculate Figure 15 results).

5.2. PRESSURE ERRORS CAUSED BY FLOW THROUGH STATIC PRESSURE ORIFICES.

A leak in an aircraft's static pressure system will produce a breathing of air in or out of the pressure sensing orifices. Flow through the static orifices will introduce two types of pressure errors; one is the pressure drop across the orifices and the other is caused by disturbance of the external flow field past the orifice.

The influence of external interference effects of flow through pitot-static tube static pressure orifices at supersonic Mach numbers and angles of attack has been investigated by the NASA, Reference 19. Results and parameters from Reference 19 have been incorporated in the present analysis, together with additional subsonic wind tunnel data obtained at REC, to predict typical leakage effects.

Wind tunnel tests were run at REC to determine the magnitude of the orifice errors for subsonic flow using the USAF Type MA-1 pitot-static tube. The test set-up for measuring the subsonic orifice pressure error as a function of mass flow through the orifices of an MA-1 is shown as Figure 16. Manometers, with 1.04 specific gravity oil, were used to obtain accurate differential pressure measurements. A static tap on the tunnel wall was used as a reference for measurements of the static pressure (P_s) variations. Mass flow through the static orifices was controlled by a mass flow measuring capillary temperature controlled in an ice bath. A pre-cooler coil, placed in LN_2 , was used to remove water vapor from the air before it passed through the control capillary. The tests were run in the REC Transonic Wind Tunnel, rectangular 3.6 inch x 17 inch test section, at $M = 0.5$ and 0.7 for 0 and 10° angles of attack. Atmospheric total pressure and total temperature conditions were used. Mass flow passing out through the orifices was varied from 0 to approximately 3.5×10^{-7} slugs/sec for each Mach number, angle of attack condition. Results of the experiment are shown on Figure 17; pressure error, $\epsilon_1 = (P_s - P_{ref})/P_{ref}$, is shown as a function of mass flow parameter $C_w = \dot{m}/(\rho_\infty V_\infty A_s)$.

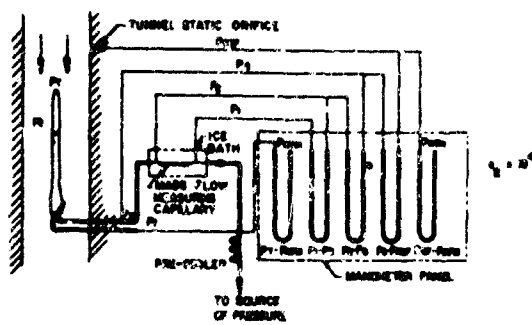


FIGURE 18
SKETCH SHOWING MASS-FLOW AND PRESSURE-MEASURING
SETUP FOR TESTING MA-1 PITOT STATIC TUBE.

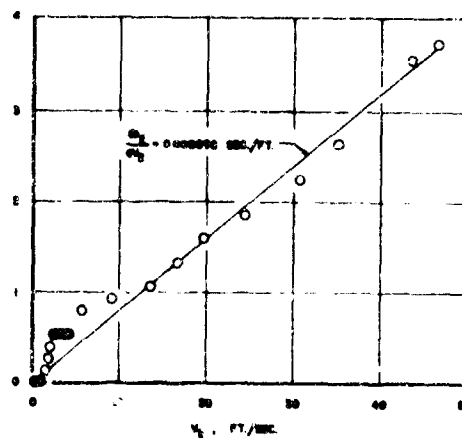


FIGURE 10
PRESSURE DROP ACROSS STATIC ORIFICES OF MA-1 PITOT-
STATIC TUBE AS A FUNCTION OF VELOCITY OF AIR THROUGH
THE ORIFICES.

$$v_2 = \frac{A_2 v_1}{A_1}$$

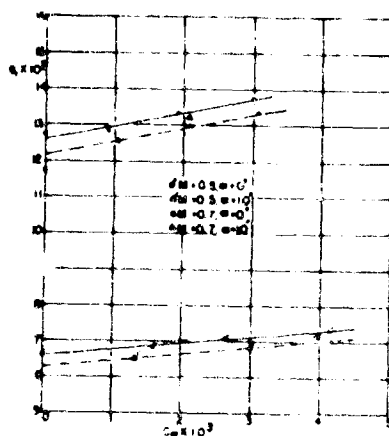


FIGURE 17
VARIATIONS OF STATIC PRESSURE ERROR OF MA-1 PITO
STATIC TUBE WITH MASS FLOW PARAMETER

• 1945

Trial	Control (C)	Washout (W)	Acute (A)
1	85	85	85
2	80	80	80
3	75	75	75
4	70	65	65
5	65	60	60

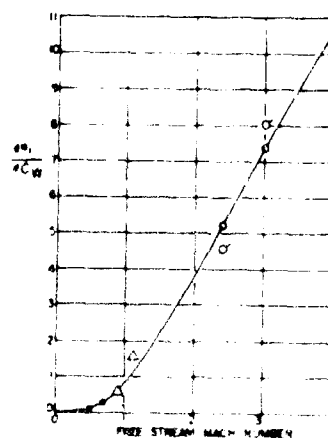


FIGURE 19
VARIATION OF CHANGE OF STATIC PRESSURE ERROR CAUSED
BY DISTURBANCE OF THE EXTERNAL FLOW WITH RATE OF
CHANGE OF MASS-FLOW COEFFICIENT

4. PRESENT REC RESULTS USING MA-1 PITCH STATIC TUBE
 5. FORWARD CRUISES OF RACA AIR-SPED HEAD REFERENCE (H)
 6. REAR CRUISES OF RACA AIR-SPED HEAD REFERENCE (H)
 7. ABORTION MARK 9A PITCH STATIC HEAD REFERENCE (H)

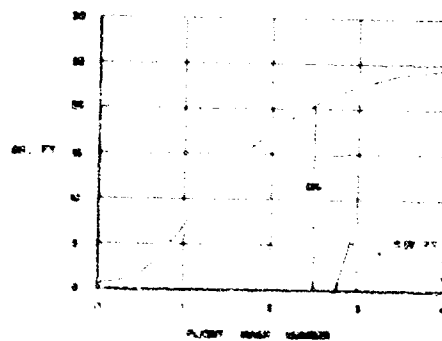


FIGURE 20
INFLUENCE OF LEAKAGE FROM A TYPICAL SUBURBAN RESIDENTIAL
SEWAGE TREATMENT PLANT

$$\Delta x, \Delta y, \Delta z$$

1948

where:

- P_s = static pressure at sensing orifices.
- P_{ref} = static pressure reference from tap located on wall of wind-tunnel test section.
- \dot{m} = mass flow, slugs/sec, determined from pressure drop across mass flow measuring capillary.
- ρ_∞ = wind-tunnel or free stream static density determined from P_{ref} and static temperature in the tunnel test section.
- V_∞ = wind-tunnel or free stream velocity
- A_s = total cross-sectional area of static orifices.

As shown on Figure 17, the pressure error did not go to zero for zero mass flow. This is due to an inherent pressure difference between the wall static reference used to set the tunnel Mach number and the static pressure as measured by the MA-1. The difference does not effect the reliability of the results since the change in pitot-static tube pressure reading with orifice flow rate (e_1 with C_w) is the measurement of concern.

Data plotted on Figure 17 includes the effect of pressure loss across the static orifices as well as the pressure error caused by disturbing the external flow past the orifices. Pressure drop across the static orifices of the MA-1 as a function of small air velocities through the orifices was determined separately and is shown as Figure 18. This data was obtained with no external flow over the tube. The dimensionless pressure error (e_2) in this low mass flow range is, within experimental accuracy, a linear function of velocity through the orifices. From the slope $de_2/dV_2 = 8 \times 10^{-6}$ sec/ft, the magnitude of the error due to pressure drop across the orifices with respect to the over-all pressure error with external flow, Figure 17, can be obtained from the relationship:

$$\frac{de_2}{dC_w} = \left(\frac{de_2}{dV_2} \right) \frac{V_2}{\frac{\dot{m}}{\rho_\infty V_\infty A_s}} = \left(\frac{de_2}{dV_2} \right) \cdot V_\infty \quad (16)$$

Using an average value of V_∞ from the experimental values for $M = 0.5$ and 0.7 , the pressure error due to pressure drop across the orifices, de_2/dc_2 was subtracted from the total error, de/dc_2 , to obtain the pressure error (de_1/dc_w) due to disturbance of external flow past the orifices.

Figure 19 shows the rate of change of static pressure error caused by disturbance of external flow past the orifice with rate of change of mass-flow coefficient, de_1/dc_w , as a function of Mach number. Also shown on Figure 19 are transonic and supersonic values of de_1/dc_w obtained from References 19 and 20. In Reference 19 the orifice errors were obtained to simulate an aircraft in steep angles of climb or dive and therefore the data was obtained over a greater range of mass flow than our present data, i. e., from 0 to about 2.2×10^{-6} , 2.9×10^{-6} and 3.7×10^{-6} slugs/sec. for the Mach numbers of 2.4, 3.0 and 4.0, respectively. The extensive data obtained in Reference 19 showed a linear variation of e_1 with C_w and therefore should be applicable to small leakage rates on the order of 5,000 ft/min in the tropopause, which was about the maximum mass flow rate used in the present investigation. Results from Reference 19 also indicate that de_1/dc_w is essentially independent of angle of attack up to $+15^\circ$. The data shown on Figure 17, for an angle of attack of 10° , appears to verify this postulation, although there was a fair amount of scatter in the $\alpha = 10^\circ$ data. The transonic data from Reference 20, shown on Figure 19, was obtained using a British Mark 9A Pitot-Static Head. This data was also for large mass flow leakage rates up to 2×10^{-5} slugs/sec., and for zero angle of attack.

A semi-empirical analysis for determining static pressure system leakage error is given in the following analysis. If a fixed volume system is considered as well as the perfect gas law,

$$p v = m R T \quad (17)$$

and

$$\frac{dp}{dt} = \frac{dm}{dt} \cdot \frac{R T}{v} + \frac{m R}{v} \cdot \frac{dT}{dt} \quad (17')$$

and if the system is at constant temperature or isothermal, which is the case for an aircraft system under moderate leakage or climb rates, then

$$\frac{dp}{dt} = \frac{dp}{dH} \cdot \frac{dH}{dt} = \dot{m} \frac{R T}{v} \quad (18)$$

or

$$\dot{m} = \frac{dp}{dH} \cdot \frac{dH}{dt} \cdot \frac{v}{R T} \quad (18')$$

$$\dot{m} = -\rho \frac{dH}{dt} \cdot \frac{v}{R T} \quad (18'')$$

where

$$-\frac{dp}{dH} = \rho = \text{density}$$

H = pressure altitude

The mass flow parameter was defined earlier as:

$$C_w = \dot{m} / (\rho_\infty V_\infty A_s) \quad (19)$$

where

\dot{m} = mass flow rate

ρ_∞ = free stream density

V_∞ = free stream velocity

A_s = area of static orifices

or from (18'')

$$C_w = \frac{-\rho_\infty \cdot \frac{dH}{dt} \cdot \frac{v}{R T}}{\rho_\infty V_\infty A_s} = \frac{-\frac{dH}{dt} \cdot \frac{v}{R T}}{V_\infty A_s} \quad (20)$$

The pressure ratio parameter is:

$$e_1 = \frac{\Delta P_1}{P_\infty} = \frac{P_1 - P_\infty}{P_\infty} \quad (21)$$

P_1 = indicated pressure with air flow through the static orifices

P_∞ = true static pressure

The results, for constant Mach number, have been shown to be nearly linear with gas flow rate and not largely dependent on angle of attack. Thus,

$$\frac{\Delta P_1}{P_\infty} = \frac{de_1}{dC_w} \cdot C_w \quad (22)$$

and

$$\Delta H = - \frac{\Delta P_1}{P_\infty} RT_\infty = - \frac{de_1}{dC_w} \cdot C_w \cdot RT_\infty \quad (23)$$

where

ΔH = altitude sensing error, ft.

T_∞ = atmospheric temperature, °R

then

$$\Delta H = \frac{de_1}{dC_w} \cdot \frac{dH}{dt} \cdot \frac{v_1}{RT_1} \cdot \frac{1}{v_\infty A_s} \cdot RT_\infty \quad (24)$$

where subscript "1" refers to instrument system

let $v_\infty = M_\infty a_\infty = M_\infty 49.1 (T_\infty)^{1/2}$, then

$$\begin{aligned} \Delta H_1 &= K_1 \left[(T_\infty)^{1/2} \right] \left[\frac{de_1}{dC_w} \cdot \frac{1}{M_\infty} \right] \left[\frac{v_1}{T_1 A_s} \right] \left[\frac{dH}{dt} \right], \text{ ft.} \quad (25) \\ &= K_1 \begin{bmatrix} A \end{bmatrix} \begin{bmatrix} B \end{bmatrix} \begin{bmatrix} C \end{bmatrix} \begin{bmatrix} D \end{bmatrix} \end{aligned}$$

where $K_1 = \text{constant} = 2.83 \times 10^{-5}$

$\left[A \right] = \text{Altitude parameter which is relatively constant in the standard atmosphere varying from 22.8 at sea level to 19.7 in the tropopause, } T_\infty \text{ in } ^\circ\text{R.}$

$\left[B \right] = \text{Experimentally determined influence of orifice outflow from Figure 19.}$

$\left[C \right] = \text{Static system design parameter.}$

$v_1 = \text{Instrument system volume, in.}^3$

$T_1 = \text{Instrument system temperature, } ^\circ\text{R}$

$A_s = \text{area of static orifices, in.}^2$

$\left[D \right] = \text{Rate of climb or leakage parameter. The form of this parameter is convenient since leakage rates are usually expressed as altitude rates. Units are in ft./min.}$

The resulting equation (25) permits the calculation of the external interference static pressure error due to leakage as a function of altitude, Mach number, static system geometry, and leakage or rate of climb.

The parameter for pressure drop across the orifices, e_2 , is independent of external Mach number and, as shown on Figure 13, varies linearly with velocity through the orifices. The following expression can be used to determine mass flow as a function of leakage rate, static pressure system parameters and altitude.

$$m = -\dot{m}_\infty \frac{e_2}{R} \frac{v_1}{T_1} \quad (26)$$

where ρ_∞ is the static density at altitude. Using the pressure-altitude error relationship;

$$\Delta H = - \frac{\Delta P}{P_\infty} R T_\infty \quad (27)$$

and

$$\frac{\Delta P_2}{P_\infty} = e_2 = \frac{d e_2}{d V_2} (V_2) \quad (28)$$

where $V_2 = \frac{\dot{m}}{\rho_\infty A_s}$ = velocity through the orifices, the following expression can be

obtained for altitude-position error due to pressure drop across the static orifices:

$$\Delta H_2 = K_2 \left[T_\infty \right] \left[\frac{de_2}{dV_2} \right] \left[\frac{V_1}{T_1 A_s} \right] \left[\frac{dH}{dt} \right], \text{ ft.} \quad (29)$$

The constant $K_2 = 1.39 \times 10^{-3}$

when

$$T_\infty = ^\circ R$$

$$de_2/dV_2 = 8 \times 10^{-6} \text{ sec/ft.}$$

$$V_1 = \text{in.}^3$$

$$T_1 = ^\circ R$$

$$A_s = \text{in.}^2$$

$$\frac{dH}{dt} = \text{ft./min.}$$

Equations (25) and (29) were used in an example as follows:

$$T_\infty = 390^\circ F$$

$$V_1 = 100 \text{ in.}^3$$

$$T_1 = 500^\circ R$$

$$A_s = \frac{\pi}{256} \text{ in.}^2 \text{ (defined by the geometry of the MA-1 pitot-static tube with four .0625 inch diameter static orifices).}$$

$$\frac{dH}{dt} = 1000 \text{ ft./min. (this number is defined by MIL-P-26292 and is assumed to exist in the example).}$$

The results of the calculation are indicated by Figure 20. At subsonic Mach numbers, the predicted leakage effect increased to 7.0 ft. at $M = 1.0$, and increased with increasing supersonic Mach numbers to 24.3 ft. at $M = 4.0$. The error due to the pressure drop across the static orifices, $\Delta H_2 = 0.07 \text{ ft.}$, is independent of flight Mach number in the above example and small when compared to the aerodynamic interference error, ΔH_1 .

The conclusions that may be reached regarding the aerodynamic interference effects of leakage are that they will be small (see example) but not negligible providing static system volumes are not excessive (200 in.³ or less) and leakage values are moderate (2,000 ft. of altitude per minute). It should be noted that the requirement of Section 4.4.2 of MIL-P-26292 allowable leakage rate of 1000 ft./min. at an initial condition of 50,000 feet, (test performed near sea level conditions) is severe since it requires the leakage test be performed with about 13 psid across the static system. However, in pressured aircraft, the differential may approach this value for components of the static system in the pressurized area.

The Air Force flush static port installation shown on Figure 1 of MIL-P-26292 has the same total static port area ($A_g = 0.012 \text{ in.}^2$) as the MA-1 Pitot-Static Tube. The flush fuselage installation requires seven 0.047" diameter orifices while the MA-1 requires four 0.0625" diameter orifices. Although not verified experimentally, it is expected that the orifice pressure drop through flush fuselage installations will be similar to the Figure 18 data. In the fuselage static port installation, the aerodynamic interference may be considerably less since the orifice flow exhausts into a relatively thick boundary layer as compared to the conditions at the MA-1 pitot-static tube orifice location.

EXAMPLE: Figures 15 and 20 may be used to solve any leakage or rate of climb altitude error problem. If we consider $V_i = 200 \text{ in.}^3$

$$\frac{dH}{dt} = 2000 \text{ ft./sec.}$$

$$H = 40,000 \text{ ft.}$$

$$D = 0.305" \text{ (dia. of static line)}$$

$$M = 1.0 \text{ (Mach No.)}$$

From Figure 15, viscous lag = 0.9 ft. for 100 in.³ volume and 1000 ft./sec.

$$\text{so total viscous lag (ft. of altitude)} = 0.9 \times 4 = 3.6 \text{ ft.}$$

From Figure 20, combined interference and orifice pressure drop = 7.0 ft (for 100 in.³ and 1000 ft./sec.)

$$\text{so total interference and orifice effect} = 7.0 \times 4 = 28.0 \text{ ft}$$

and

$$\text{all effects combined} = 3.6 + 28.0 = 31.6 \text{ ft.}$$

SECTION 6

PRESSURE ERRORS CAUSED BY DIMENSIONAL VARIATIONS AND IRREGULARITIES OF STATIC PRESSURE PORTS ON PITOT-STATIC TUBES

Wind tunnel tests were performed at REC on seven Model 852A Pitot-Static tubes that had variations in the angular displacement of their static ports. The REC Model 852A is an Air Force Type MA-1 deiced P-S tube and operates on 115 volts, AC or DC. It is manufactured in accordance with MIL-P-25632B. External dimensions of the MA-1 are identical to those of the USAF TRU-1/A (REC Model 850) which has a 28 volt AC or DC heating unit and is manufactured in accordance with MIL-P-25757B. Dimensional tolerances of these P-S tubes must be held to an accuracy that will permit interchangeability on aircraft without introducing unknown aerodynamic pressure errors. The external tolerances for the Type MA-1 are shown on Figure 1 of MIL-P-25632B. There are four 0.0625 inch diameter static holes which have tolerances of $\begin{matrix} +.005 \\ -.000 \end{matrix}$ inches. Angular displacement for each hole is $37.5^\circ \pm 0^\circ 15'$. Pressure errors introduced by angular displacements outside this $\pm 0^\circ 15'$ tolerance, which corresponds to only $\pm .0014$ inches on the circumference of the tube if the 0.620 inch nominal tube diameter is used, is discussed in the following paragraphs.

The seven P-S tubes tested at REC had the following angular displacements for the forward static holes:

TABLE IX

<u>Tube</u>	<u>Angular Displacement of Forward Static Ports</u>		<u>Included Angle Between Static Ports</u>
1	38° 16';	37° 30'	75° 46'
2	43° 15';	32° 15'	75° 30'
3	34° 50';	40° 10'	75° 0'
4	41° 18';	34° 48'	75° 7'
5	36° 0';	38° 27'	74° 33'
6	37° 30';	35° 36'	73° 6'
7	37° 11';	35° 44'	72° 55'

These P-S tubes were selected for testing because they represented a wide variation of static hole locations from the nominal 37.5° angular displacement from the vertical centerline of the tube. The $\pm 0^\circ 15'$ angular tolerance on the holes is exceeded for each tube. Although the port angles are given only for the forward ports, the inline rear ports exhibited approximately the same angular displacements. Two of the P-S tubes tested, No. 2 and No. 3, had external burrs in the immediate vicinity of the static ports. Tests were made with these burrs on and after the burrs were removed.

6.1. TESTING PROCEDURE.

Tests were performed in the REC 3.6 inch x 17 inch subsonic wind tunnel. The wind tunnel facility is described in Reference 21. Data was obtained using the accurate "pressure differential" method where a flush static pressure wall tap on the 3.6 inch side of the rectangular test section was used as a reference and pressure differential between the reference tap and the static ports on the P-S tubes was measured on a water manometer. One tube, No. 1, was selected as a reference. Measured pressure differential, $(P_s - P_r)$, for this tube was used as a reference, or zero value, and was subtracted from the $(P_s - P_r)$ values for the other six tubes to obtain $\Delta(P_s - P_r)$, the pressure difference due to variation in the angular displacement of the static holes. This method gives a very accurate determination of the minute pressure differences caused by small dimensional variations of the static ports and does not introduce the large measuring errors that would result if absolute values of static pressure were measured. Each P-S tube was tested at an angle of attack of $+10^\circ$ and Mach numbers of 0.3, 0.5, and 0.7. Two tubes, No. 1 and No. 3, were also tested at 0° and $+4^\circ$ angles of attack.

6.2. PRESENTATION OF DATA.

The pressure-altitude errors caused by angular displacement variations of static pressure ports on the seven Model 852A P-S tubes are shown on Figures 21 and 22. Also included on these graphs are the errors introduced when external burrs are present on the static ports of tubes No. 2 and No. 3. Sea level conditions and an angle of attack of $+10^\circ$ were used to illustrate the extreme altitude errors that could

occur. The pressure errors, $\Delta(P_s - P_r)$, were converted to altitude errors using the relationship

$$\Delta H_{SL} = \frac{-\Delta(P_s - P_r)}{P_r} RT_{SL} \quad (30)$$

Where R is the gas constant for air.

Altitude error will decrease in direct proportion with the absolute static temperature as illustrated in the following table for standard atmosphere temperature values.

TABLE X

<u>Altitude</u>	<u>Static Temperature</u>	<u>Static Temp. Ratio</u>	<u>ΔH</u>
Sea Level	518.69° R	1,000	100 ft.
10,000 ft.	483.04° R	0.9313	93 ft.
20,000 ft.	447.43° R	0.8626	86 ft.
30,000 ft.	411.86° R	0.7940	79 ft.
36,000 ft.	389.99° R	0.7519	75 ft.
to 80,000 ft.			

The + 10° angle of attack is severe with respect to normal flight conditions of an aircraft and can be realized usually only under low speed landing conditions. A typical flight envelope for an aircraft flying in a "clean" configuration, taken from Figure 6 of Reference 22, is shown as Figure 23. For a q_{cmin} of 187.2 lb/ft², the maximum angle of attack would range between 6° and 7° for flights from sea level to 50,000 ft. An indication of altitude errors present at angles of attack less than + 10° would be to use a linear variation with angle of attack for the errors shown in Figure 21; i.e., for $\alpha = + 5^\circ$, the errors would be 1/2 the values shown on Figure 21.

The tubes tested had a wide variation in the angular displacement of the static ports. Considering only the data on Figure 21 that was taken for tubes with no burrs present on the static holes, we see that very small errors are introduced at $M = 0.3$.

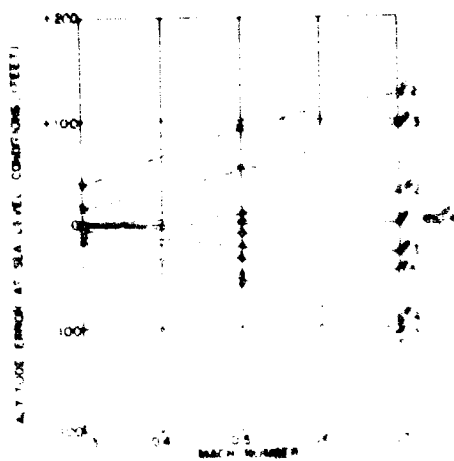


FIGURE 21
PRESSURE-ALTITUDE ERRORS CAUSED BY ANGULAR
DISPLACEMENT VARIATION OF STATIC PRESSURE PORTS
ON REC. MODEL BS2A PITOT-STATIC TUBE, #3

ANGLE OF ATTACK: 10°
NO NOTICEABLE BURRS ON STATIC PORTS
BURRS WERE PRESENT ON STATIC PORTS

ANGULAR DISPLACEMENT LINE OF VIEWING STATIC PORTS BETWEEN STATIC PORTS	MEASURED ANGLES	REMARKS
1. $30^\circ 15'$ AND $37^\circ 30'$	$75^\circ 45'$	USED AS A REFERENCE EXTERNAL BURRS ON STATIC PORTS WERE REMOVED
2. $45^\circ 15'$ AND $52^\circ 15'$	$73^\circ 30'$	EXTERNAL BURRS ON STATIC PORTS WERE REMOVED
3. $34^\circ 30'$ AND $40^\circ 10'$	$70^\circ 0'$	EXTERNAL BURRS ON STATIC PORTS WERE REMOVED
4. $41^\circ 19'$ AND $34^\circ 48'$	$73^\circ 7'$	
5. $46^\circ 0'$ AND $39^\circ 27'$	$72^\circ 27'$	
6. $47^\circ 30'$ AND $38^\circ 30'$	$73^\circ 6'$	
7. $47^\circ 11'$ AND $39^\circ 44'$	$72^\circ 55'$	

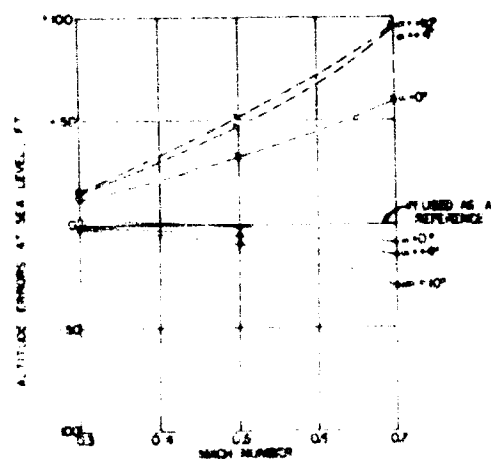


FIGURE 22
PRESSURE-ALTITUDE ERRORS CAUSED BY ANGULAR
DISPLACEMENT VARIATION OF STATIC PRESSURE PORTS
ON REC. MODEL BS2A PITOT-STATIC TUBE, #3

ANGLE OF ATTACK
NOTE

DATA TAKEN WITH EXTERNAL BURRS ON STATIC
PORTS (FIG 25)
DATA TAKEN AFTER THE BURRS WERE REMOVED

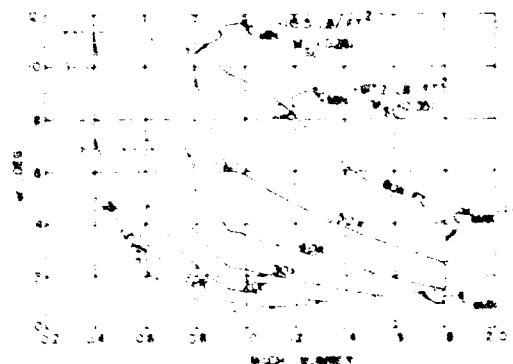


FIGURE 23
TOTAL ALTITUDE ERROR

At this Mach number, which is in the vicinity of an aircraft's landing speed, the total deviation of the data from all seven tubes is just 18.0 feet. At $M = 0.5$ and $M = 0.7$ the total deviations of the data is 68.0 feet and 143.1 feet, respectively. It should be noted that at these higher Mach numbers, the aircraft's angle of attack is usually considerably less than 10° and the aircraft would normally be at altitude. The above errors, reduced to correspond with the $q_{c\min.} = 187.2 \text{ lb/ft}^2$ line on Figure 23, are shown as column 5 on Table XI. It should be noted that following along this $q_{c\min.}$ line is also an extreme condition for operation of most aircraft. An indication of the accuracy of the data taken can be obtained from the two sets of data points for tube No. 7. This tube was run twice in the wind tunnel to verify the magnitude of its displacement errors and the data agreed within $\Delta H_{sl} = 10$ feet for all three Mach numbers.

To obtain a relative order of magnitude of the altitude errors shown on Figure 21, we will compare them with the errors permitted for altimeters and air data computers. The Air Force precision pressure altimeter, Type AAU-8/A, has its permissible scale errors specified in MIL-A-27229A (USAF). The Air Force Central Air Data Computer, Type MG-1A, has its scale error specified in MIL-C-25653B (USAF) as ± 40 feet or 0.2 percent of the indicated altitude whichever is greater. A readout indicator must accompany the air data computer. One of these indicators is the A/A24G-7 Amplifier - Indicator Group, Altitude - Vertical Speed, which has its scale error called out in MIL-A-27328 (USAF) as ± 25 feet. This error must be combined with the air data computer error to obtain the overall error of the system. An abbreviated tabulation of the above scale errors is shown in Table XI.

The total deviation of the data shown on Figure 21 can be used as an indication of repeatability of pitot-static tubes with the range of hole locations per Table IX. From the data there appears to be a definite error dependance on the included angle between the static ports. Two tubes tested, No. 6 and No. 7, had included angles for their ports considerably below the specified 75° . The errors for these tubes were larger than those for the remaining five tubes, all of which had included angles near 75° . Included angles of less than 75° gave a negative altitude error which

TABLE XI
COMPARISON OF ALTIMETER SCALE ERROR TOLERANCES
WITH THE ERRORS INTRODUCED BY
STATIC PRESSURE PORT ANGULARITY VARIATIONS

Standard Altitude (Feet)	Altitude Errors (Feet)					
	1	2	3	4	5	6
0	± 30	± 40	± 25	± 47	20	± 4.8
1,000	± 35	± 40	± 25	± 47	21	± 5.1
2,000	± 40	± 40	± 25	± 47	22	± 5.3
4,000	± 50	± 40	± 25	± 47	23	± 5.4
6,000	± 60	± 40	± 25	± 47	24	± 5.8
8,000	± 70	± 40	± 25	± 47	27	± 6.7
10,000	± 80	± 40	± 25	± 47	30	± 7.5
20,000	±130	± 40	± 25	± 47	42	±10.3
30,000	±180	± 60	± 25	± 65	62	±16.4
40,000	±230	± 80	± 25	± 84	91*	±25.1*
50,000	±280	±100	± 25	±103	149*	±42.4*
60,000	±800	±120	± 25	±123		

*Estimated Values

Column	Explanation
1.	Scale error tolerance of Air Force AAU-8/A Precision Altimeter, MIL-A-27229A (USAF).
2.	Scale error tolerance (including hysteresis) of Type MG-1A Central Air Data Computer, MIL-C-25653B (USAF).
3.	Scale error tolerance of Type A/A24G-7 Amplifier-Indicator Group, Altitude-Vertical Speed, MIL-A-27328 (USAF).
4.	Root-Magnitude-Squared, or random error addition, of Columns 2 and 3. This is the combined scale error of the Air Data Computer System.
5.	The total variation of the altitude errors of all seven tubes shown on Figure 21 reduced to correspond to the $q_{c\min} = 187.2 \text{ lb./ft}^2$ line on figure 23. This is <u>not</u> a randomized error.
6.	Maximum random altitude error deviations for the five tubes with included angles near 75° (Numbers 1, 2, 3, 4, and 5). The randomized errors correspond to the $q_{c\min} = 187.2 \text{ lb./ft}^2$ line on Figure 3. Effect of tube rotation relative to air stream are included. Maximum value tested was $5^\circ 45'$; Tube No. 2, Table IX.

corresponds to a positive pressure error, $\Delta(P_s - P_p)$. This trend is in the same direction that earlier experiments indicate, Reference 23.

A rotational displacement of the static ports, with a 75° included angle maintained, with respect to the rear mounting holes does not appear to produce a large pressure error. This rotation angle (for which the single port manufacturing tolerance of $37.5^\circ \pm 0^\circ 15'$ is specified in MIL-D-25632B) could also occur easily if the pitot boom on an aircraft is out of alignment. To obtain an idea of the random deviation of altitude error caused by rotation of the static ports, we took an average value of the errors that occurred for the five tubes with included angles near 75° , numbers 1, 2, 3, 4, and 5. The maximum deviation from this average will give a repeatability error for tubes with slightly rotated static ports. These maximum deviations which we shall assume as random deviations are $\Delta H_{sl} = \pm 4.0$ feet, ± 17.7 feet, and ± 38.6 feet for Mach numbers of 0.3, 0.5, and 0.7, respectively. Taking into account that these random values are for sea level conditions and an angle of attack of $\pm 10^\circ$, it can be concluded that they are indeed small when compared to randomized altimeter and air data computer errors. The errors, reduced to correspond to the $q_{cmin.} = 187.2 \text{ lb/ft}^2$ line on Figure 23, are tabulated in column 6 of Table XI. At zero degrees angle of attack, these errors will reduce to zero. It should also be noted that the ports on some of the tubes used in this analysis were rotated as much as $5^\circ 45'$.

6.3. EXTERNAL BURRS IN THE IMMEDIATE VICINITY OF THE STATIC PORTS.

As mentioned above, tests were also run on two tubes that had external burrs in the immediate vicinity of one or more of their static ports. These burrs could be formed when a hard instrument is used to clean out the holes or by inserting an indicating device into the holes. Photographs of the burrs are shown on Figures 24 and 25. On pitot-static tube, No. 2, Figure 24, the two forward ports on the tube had burrs. The largest burr had a height of only 0.006 inches. Number 3, Figure 25, also had two burrs with a height on the larger one of 0.004 inches. Earlier studies, Reference 24, indicated that external burrs or internal bevels on the static ports could cause sizeable pressure errors. Tests were run on both tubes, with the burrs on and after the burrs



FIGURE 24
PHOTOGRAPH OF BURRS ON STATIC PORTS
OF REC MODEL 852 A PITOT-STATIC TUBE NUMBER 2.



FIGURE 25
PHOTOGRAPH OF BURRS ON STATIC PORTS
OF REC MODEL 852 A PITOT-STATIC TUBE NUMBER 3.

had been removed. The results for a $+ 10^\circ$ angle of attack are shown on Figure 21. Although the burrs are small in height, they produce a noticeable pressure error. The equivalent sea level altitude errors for the burrs, taken from Figure 21, are as shown below in Table XII.

XII
 ΔH_{sl} FOR BURRS

M	Tube Number 2	Tube Number 3		
	$\alpha = 10^\circ$	$\alpha = 10^\circ$	$\alpha = 4^\circ$	$\alpha = 0^\circ$
0.3	+ 34.7 ft.	+ 17.1 ft.	+ 16.9 ft.	+ 9.0 ft.
0.5	+111.7 ft.	+ 61.0 ft.	+ 52.4 ft.	+33.9 ft.
0.7	+136.3 ft.	+125.9 ft.	+110.8 ft.	+68.7 ft.

The tube with the smaller burrs, No. 3, was also tested at 0° and 4° angles of attack before and after the burrs were removed. The results, listed on Table XII and shown on Figure 22, indicate that a pressure error due to the burrs exists for zero angle of attack, and that at $+ 4^\circ$ angle of attack the errors are nearly as large as for $\alpha = + 10^\circ$. Comparison between the tube used as a reference, No. 1, and No. 3 after the burrs had been removed show a very slight difference in the data taken at $\alpha = 0^\circ$. This difference is within the aforementioned accuracy of the wind tunnel data, but could also be due to other small variations between the two tubes.

6.4. CONCLUSIONS.

On the basis of the data presented above, the following conclusions can be reached.

1. From the data it can be concluded that the $\pm 0^\circ 30'$ manufacturing tolerance on the 75° included angle between the static ports is sufficient to provide excellent aerodynamic interchangeability, reference Column 6, Table XI.

2. The randomized altitude errors due to rotation of the static holes, maintaining the 75° included angle, are shown in column 6 on Table XI. Although angular variations as large as $5^\circ 45'$ are included in this average, the errors are small when compared to the stated accuracies of altimeters and air data computers. The $\pm 0^\circ 15'$ manufacturing tolerance on the 37.5° locations of the individual static ports from the ventral plane of the tube is conservative and could be relaxed to a tolerance of $\pm 1^\circ$ if the 75° included angle tolerance is specified as $\pm 0^\circ 30'$. The tolerance relaxation will cause no noticeable errors in the accuracy of the complete static pressure system, providing the pitot-static tube is installed on the aircraft with an accuracy of about $\pm 1^\circ$.

3. Burrs in the vicinity of the static ports, even if only a few thousandths of an inch in height, will cause noticeable pressure errors. As shown in Table XII, these errors do not decrease rapidly with decreasing angle of attack. They will cause a relatively large residual error at zero angle of attack, whereas pressure errors due to angular variations of the static ports will decay with decreasing angle of attack and will cause no pressure error at $\alpha = 0^\circ$.

Extreme care should be taken if measuring or cleaning instruments are inserted into the static ports as these instruments could cause burring or internal beveling of the ports.

4. The total variation of the altitude errors of all seven REC Model 852A Pitot-Static Tubes tested falls within the scale error tolerance of other components of an aircraft's static pressure system. Although the pitot-static tubes tested covered an extreme range of (1) singular angular variations of the static ports and (2) the included angle between sets of static ports, the total variation of all the errors, shown on Column 5 of Table XI are compatible with the stated accuracies of altimeters and air data computers shown as Columns 1 and 4 on Table XI. The total variation errors shown on Column 5 of Table XI are also extreme cases because they follow the $q_{c_{min}} = 187.2 \text{ lb/ft}^2$ line on Figure 23 and operation along this line will be at an angle of attack of over 6° . Lower angles of attack would give proportionately lower errors.

SECTION 7

FUSELAGE SKIN IRREGULARITIES IN THE VICINITY OF FUSELAGE STATIC PRESSURE PORTS AND FUSELAGE MOUNTED AERODYNAMICALLY COMPENSATED PITOT-STATIC TUBES

7.1. FUSELAGE STATIC PRESSURE PORTS.

This section presents a brief analysis of the pressure-altitude errors that would result if, in the vicinity of the static ports, an aircraft's fuselage skin is deformed from its specified manufacturing contour. Fuselage static ports on aircraft with high subsonic flight capabilities normally have a residual altitude-position error due to the local flow field of the aircraft. This error is primarily a function of Mach number but could also be dependent on angle of attack, angle of sideslip, and Reynold's number. The position error is usually different for each aircraft model produced and flight tests are performed on at least one aircraft of each model to determine its position correction. If the fuselage contours of subsequent aircraft of the same model deviates from the contour of the flight tested aircraft, the master calibration curve of position error for these aircraft will be in error. Both manufacturing tolerances during production and damage to the aircraft's skin in service could cause unknown residual position errors.

To arrive at a criterion for allowable skin deformation, corresponding to equivalent altitude errors and as a function of length and width of the deformation and distance of the deformation from the static ports, a smooth wave deflection was chosen as shown on Figure 26. The deflection has the shape of a 360° cosine wave with a deflection depth, D , equal to the double amplitude of the cosine wave. The wave is assumed to start a distance L_1 , from the port and extend for equal distance $\pm y$ on either side of the static port location. The pressure error felt at the port caused by specific skin deflections were computed on the REC LGP digital computer using numerical integration of three-dimensional wavy-wall, small-perturbation theory, Reference 25.

It should be noted that if the wave is a depression in the surface and the static ports are located upstream of the depression, as shown on Figure 26, the pressure error, $P - P_\infty$, felt at the port will be negative. The equivalent altitude error, ΔH , will therefore be positive which means that an altimeter will indicate too high an altitude. If the ports are located downstream of the depression, $(P - P_\infty)$ will also be

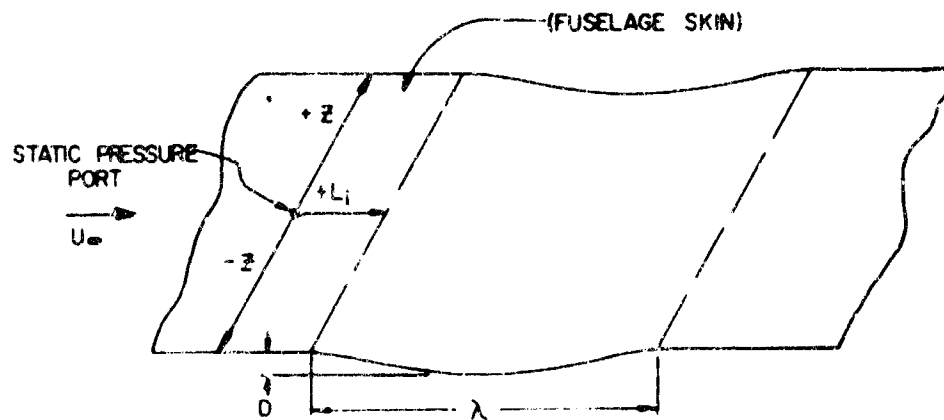


FIGURE 26
NOTATION USED FOR 360° COSINE WAVE FUSELAGE SKIN DEFORMATIONS.

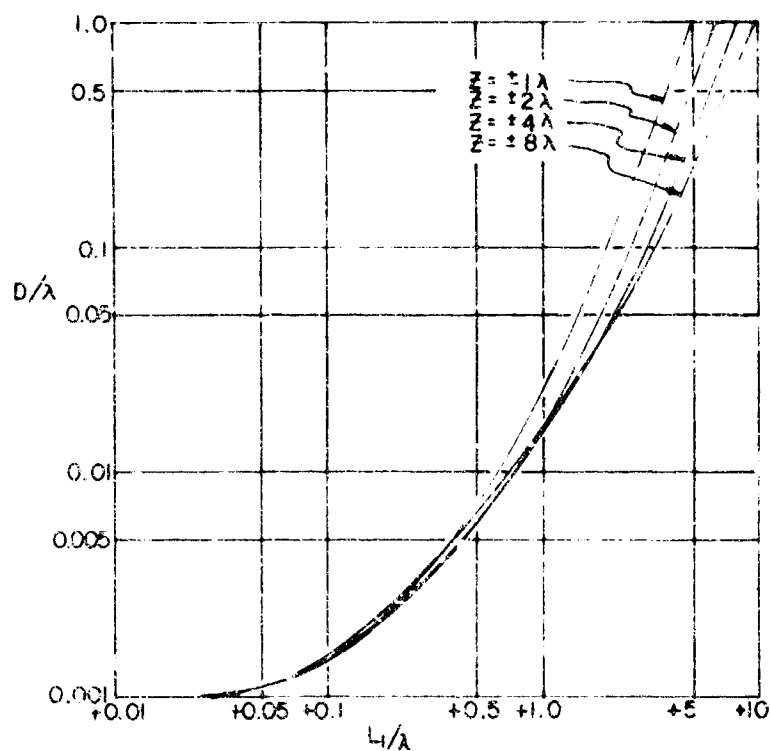


FIGURE 27
ALLOWABLE WAVE DEPTH FOR AN EQUIVALENT ALTITUDE ERROR AT
SEA LEVEL OF ± 50 FT. AS A FUNCTION OF z

$M_\infty = 0.8$
 λ = LENGTH OF WAVE DEFLECTION.
 L_1 = DISTANCE FROM THE STATIC PORTS TO THE START OF THE WAVE
 DEFLECTION.
 D = MAXIMUM WAVE DEPTH.
 z = LENGTH OF WAVE IN DIRECTION PERPENDICULAR TO THE FLOW
 DIRECTION.

negative and ΔH will be positive. If the wave protrudes from the nominal surface, the reverse will be true, i. e., if the ports are upstream or downstream of a protruding wave, $(P - P_\infty) > 0$, and $\Delta H < 0$.

For a free stream Mach number of 0.8, the allowable wave depth for an equivalent altitude error at sea level of ± 50 feet is as shown on Figure 27. The dimensions are all given as fractions of wave length, λ . The right extremity of the four curves shown on Figure 27 was used to determine the tightest tolerance needed to assure an error of $\Delta H_{SL} = 50$ feet. These tolerances are shown on Figure 30. The allowable wave depth shown on Figure 30 would be increased for free stream Mach number less than 0.8, but would be decreased for $M > 0.8$. The greatest deviation with Mach number will occur for waves in close proximity to the static ports i. e., for small values of L and short wave lengths. Also superimposed on Figure 30 are the dent limitations for structural repair specified by the Boeing Aircraft Company for the Boeing 720 Aircraft. This is shown as an example of desired tolerances of a manufacturer and should result in altitude errors of $\Delta H_{SL} < \pm 50$ feet for a single deformation if $L > 12$ inches but would allow altitude errors at sea level in excess of ± 50 feet for $L < 12$ inches. The approximate theory limit line shown on Figure 30 corresponds to a maximum angle of 15° on the slope of the cosine wave deflection.

It should be noted that the tolerances shown for sea-level conditions will give a slightly reduced altitude error as altitude increases. The error will decrease in direct proportion with the absolute static temperature and will reach a minimum of 0.75 times the sea-level value for altitudes from 36,000 feet to 82,000 feet in the standard atmosphere, i. e., $\Delta H_{SL} = \pm 50$ feet would correspond to $H_{36,000 - 82,000 \text{ ft.}} = \pm 37.5$ ft.

The allowable wave depths for altitude errors at sea-level of ± 10 ft. and ± 100 ft., obtained from graphs similar to the one shown on Figure 27 for ± 50 ft., are shown as Figures 28 and 29 respectively.

From Figures 28, 29, and 30, one can obtain an idea of the tolerances needed for smooth skin deformations outside a 3 inch radius from the static ports. If the skin deformation is located off to the side of the static ports, with respect to the flow direction, or if the length of the wave is less than would be indicated from the right-hand extremity of the curves shown on Figure 27, the pressure errors induced by

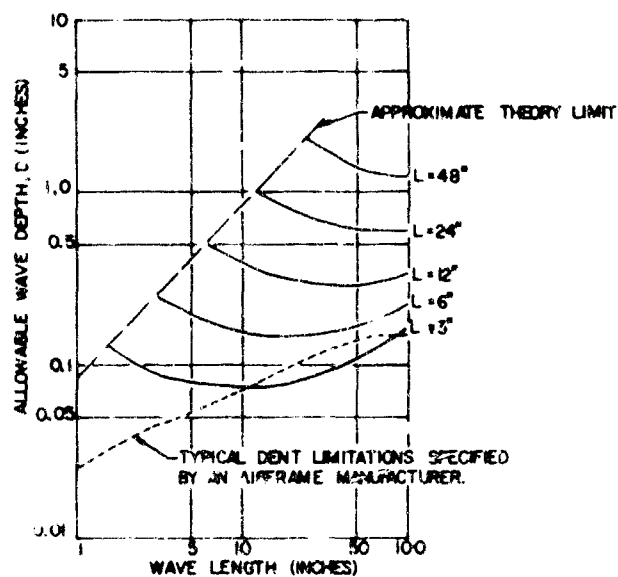


FIGURE 28
ALLOWABLE WAVE DEPTH FOR AN EQUIVALENT
ALTITUDE ERROR AT SEA LEVEL OF ± 100 FT.
 $M_\infty = 0.8$
"L" IS THE DISTANCE FROM THE STATIC PORTS TO
THE START OF A WAVE DEFLECTION.

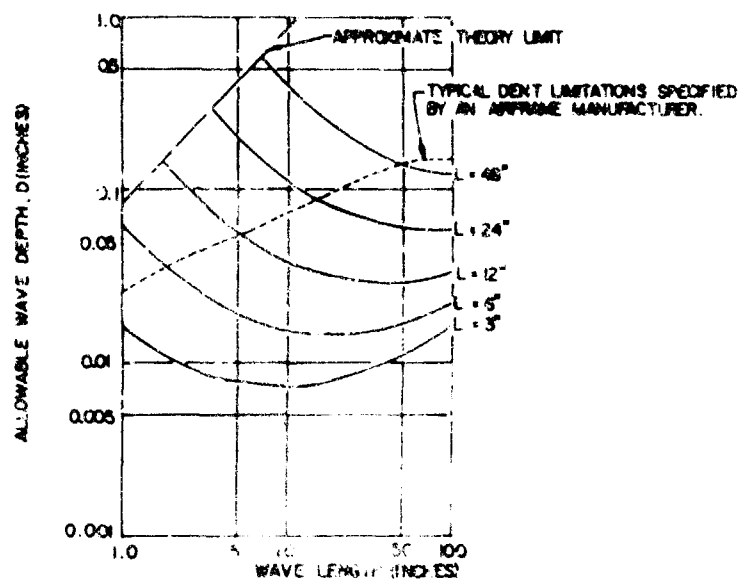


FIGURE 29
ALLOWABLE WAVE DEPTH FOR AN EQUIVALENT
ALTITUDE ERROR AT SEA LEVEL OF ± 10 FT.
 $M_\infty = 0.8$
"L" IS THE DISTANCE FROM THE STATIC PORTS TO
THE START OF A WAVE DEFLECTION.

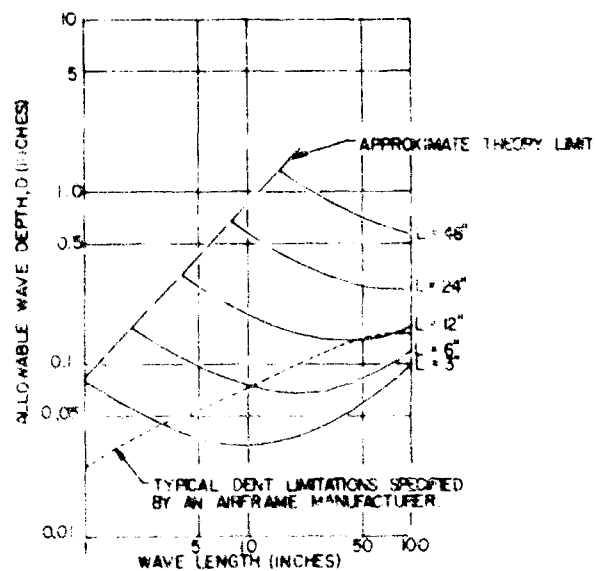


FIGURE 30
ALLOWABLE WAVE DEPTH FOR AN EQUIVALENT
ALTITUDE ERROR AT SEA LEVEL OF ± 50 FT.
 $M_\infty = 0.8$
"L" IS THE DISTANCE FROM THE STATIC PORTS TO
THE START OF A WAVE DEFLECTION.

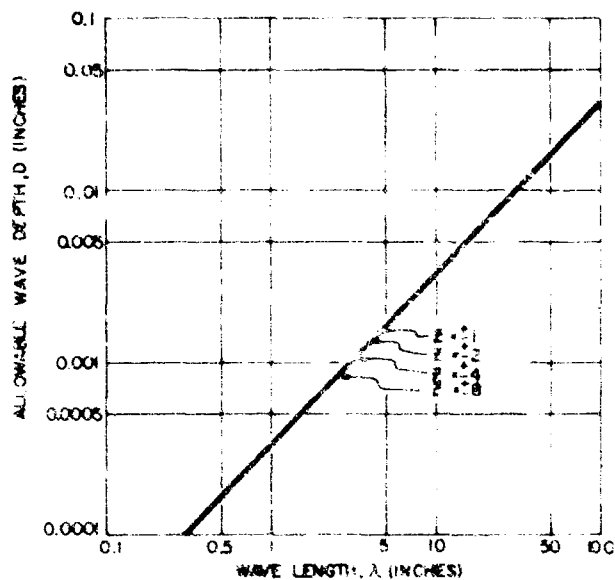


FIGURE 31
ALLOWABLE WAVE DEPTH FOR AN EQUIVALENT
ALTITUDE ERROR AT SEA LEVEL OF ± 50 FT.
 $M_\infty = 0.8$
STATIC PORTS ARE LOCATED AT BOTTOM OF
DEFLECTION AT $L_1 = -0.5\lambda$.

the waves would be less and the tolerances could consequently be increased from the values indicated. However, if more than one skin deformation occurs in the vicinity of the static ports, the allowable depth for each skin deformation would have to be decreased proportionally.

If the static ports are located in the center of a skin deflection, the allowable depth tolerances could become extremely tight. Figure 31 shows the allowable wave depth for $\Delta H_{SL} = \pm 50$ ft. at $M_{\infty} = 0.8$ for fuselage ports located in the center of a 360° cosine wave skin deflection. The allowable wave depth is practically independent on the length of the wave in the "x" direction and is directly proportional to altitude error. For an equivalent altitude error of $\Delta H_{SL} = \pm 500$ ft., the wave depth would be 10 times the value shown on Figure 31.

Location of the ports in the center of the wave represents the extreme case with respect to allowable wave depths. If the ports are displaced off the center of the wave, but still inside the wave, the allowable depth could be slightly larger. For ports located on the edge of the wave the allowable depth would be increased to approximately 2.4 times the value if located at the center of the wave.

7.2. FUSELAGE-MOUNTED AERODYNAMICALLY COMPENSATED PITOT-STATIC TUBES.

The same wave shape used in the preceding section was used as a criterion to determine how much the allowable fuselage skin deformation tolerance could be reduced if a fuselage mounted pitot-static tube were used instead of flush static ports. By moving the static port location away from the fuselage skin, the pressure influence at the ports due to small skin irregularities in the vicinity of the ports can be greatly reduced. The difference between the allowable wave depth for flush static ports located on the fuselage and static ports located 8 inches from the fuselage on a pitot-static tube is shown on Figures 32 through 35 for an equivalent altitude error at sea level of ± 50 ft. and a free stream Mach number of 0.8. The wave, in the x-direction perpendicular to the flow direction, is symmetrical about the static ports. Two values of x are given: $x = \pm 1\lambda$ and $x = \pm 4\lambda$, where λ is the length of the wave in the flow direction. The allowable depth values for ports located on the surface are

identical to those explained in Section 7.1 and shown on Figure 27.

Another way of presentation of the data would be to show the equivalent altitude error for each specific wave length and distance of the wave from the static ports measured in a direction on the surface and parallel to the flow direction. However, for sake of comparison, the fixed value of $\Delta H_{SL} = \pm 50$ feet will give a realistic indication of the advantage of using fuselage mounted pitot-static tubes.

The greatest increase in allowable wave depth will be, as shown on Figure 32, when the static ports are located in the center of the 360° cosine wave skin deformation.

For $\lambda = 3$ inches and $z = \pm 1\lambda$ or 6 inches, the allowable wave depth could increase from 0.001 inch to 0.072 inch for the same equivalent error of $\Delta H_{SL} = \pm 50$ ft. For $\lambda = 20$ inches and $y = \pm 1\lambda$ or 40 inches, the allowable wave depth could still be increased from 0.007 inch to 0.02 inch for the same equivalent error. Greater increases in allowable depth will exist if the wave length is longer, i.e., $z = \pm 4\lambda$. Other locations of the port within the wave deflection, from $L_1 = 0.5\lambda$ to $L_1 = 0$, will give varying degrees of allowable wave depth, but the location, $L_1 = -0.5\lambda$, is the extreme case.

A sizable increase in allowable wave depth also exists when the static ports are located at the edge of the deformation, at $L_1 = 0$, as shown on Figure 33. As the skin deflection moves away from the static ports, as shown on Figures 34 and 35, the increase in allowable wave depth diminishes, except for very small wave lengths, but in this region the allowable depth is already quite large and, therefore, not as critical as when the wave is in close proximity to the ports.

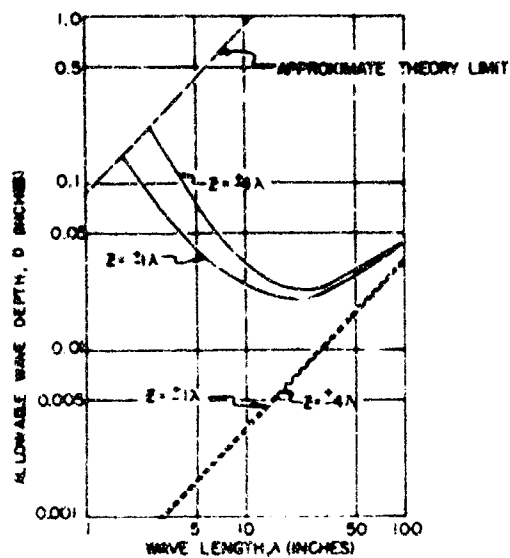


FIGURE 32
STATIC PORTS ARE LOCATED AT CENTER OF
360° COSINE WAVE SKIN DEFORMATION, AT
 $L_1 = 0.5\lambda$.

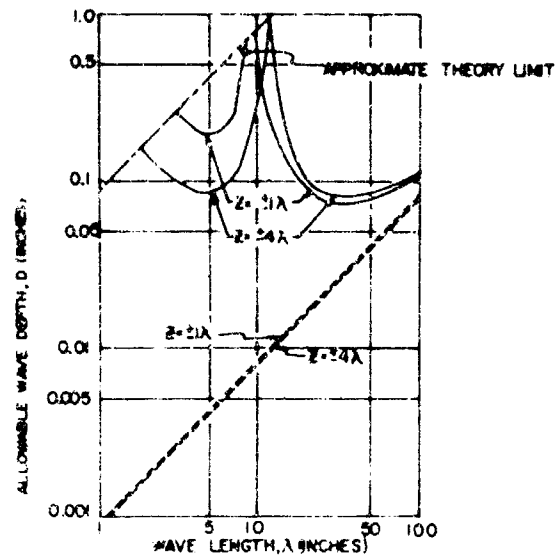


FIGURE 33
STATIC PORTS ARE LOCATED AT EDGE OF 360°
COSINE WAVE SKIN DEFORMATION, AT $L_1 = 0$.

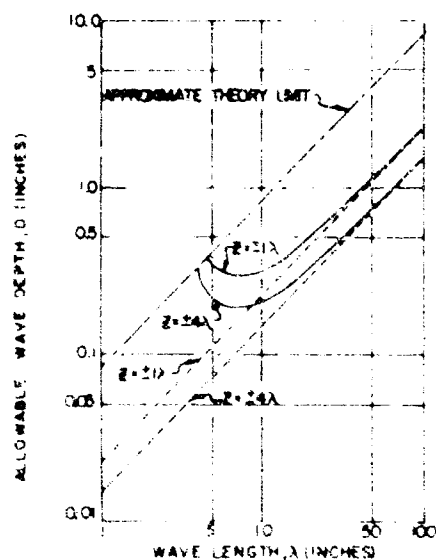


FIGURE 34
STATIC PORTS ARE LOCATED 1λ AWAY FROM
EDGE OF 360° COSINE WAVE SKIN DEFORMATION,
AT $L_1 = \lambda$.

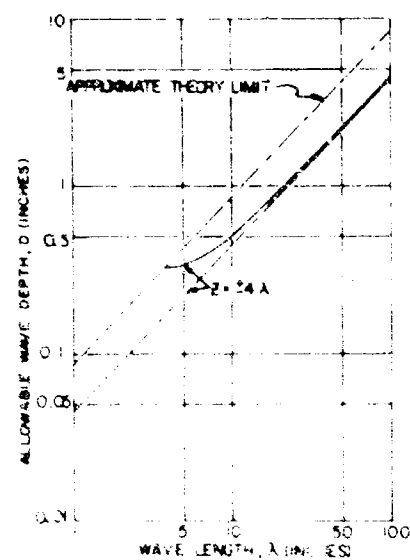


FIGURE 35
STATIC PORTS ARE LOCATED 2λ AWAY FROM
EDGE OF 360° COSINE WAVE SKIN DEFORMATION,
AT $L_1 = 2\lambda$.

ALLOWABLE WAVE DEPTH FOR AN EQUIVALENT ALTITUDE
ERROR AT SEA LEVEL OF $\pm 50\text{ FT}$ ($M_{\text{sea}} = 0.8$)
--- STATIC PORTS ARE LOCATED ON THE FUSELAGE.
--- STATIC PORTS ARE LOCATED 8" FROM THE FUSELAGE
ON A PITOT-STATIC TUBE

SECTION 8

AIRCRAFT SKIN CONTOUR MEASUREMENTS ADJACENT TO FLUSH STATIC PORTS ON MILITARY TRANSPORT TYPE AIRCRAFT

8.1. INTRODUCTION.

A survey of flush mounted static port assemblies and the surrounding aircraft skin area on three military type transports was conducted by Rosemount Engineering Company. The aircraft were stationed at McGuire Air Force Base during this survey which began on November 13, 1961, and ended on November 22, 1961. At about the same time, but extending for a longer period, flight tests were conducted by the Air Force and NASA to determine the static pressure error of the co-pilot's altimeter system. Results from the flight test phase are given in Reference 26. This section describes primarily the techniques used by Rosemount Engineering Company to measure surfaces near the static ports and the results of the survey. In addition, results of the measurements were used to predict the static pressure differences between the aircraft. Predicted position error differences are compared with the flight test data.

8.2. AIRCRAFT SKIN CONTOUR MEASUREMENTS ADJACENT TO FLUSH MOUNTED STATIC PORT ASSEMBLIES.

8.2.1. Aircraft Surveyed.

The skin contour in the area adjacent to the static port assembly was surveyed on the following aircraft:

Aircraft Type A (C-131)

<u>NASA and REC Aircraft No.</u>	<u>Aircraft S/N</u>	<u>Remarks</u>
1	25781	
2	25786	
3	25792	
4	25799	
5	53-7087	No skin measurements taken.

Aircraft Type B (C-118)

<u>NASA and REC Aircraft No.</u>	<u>Aircraft S/N</u>	<u>Remarks</u>
1	3821	
2	3270	
3	3825	
4	3834	
5	3266	
6	3823	
7	3290	This aircraft not flight tested.

Aircraft Type C (C-135)

<u>NASA and REC Aircraft No.</u>	<u>Aircraft S/N</u>	<u>Remarks</u>
1	00370	No skin measurements taken.
2	00371	
3	00374	No skin measurements taken.
4	00377	
5	00378	
6	10326	
7	00372	This aircraft not flight tested.
8	00373	This aircraft not flight tested.
9	00376	This aircraft not flight tested.

8.2.2. Survey, Apparatus and Techniques.

Devices to measure skin contours in the area of flush static ports were designed and constructed specifically for this measurement program. Two devices were fabricated and they are shown as Figures 36 and 37. Figure 37 shows the assembly that was used for measurements on Aircraft Type C. This assembly consists of an aluminum angle frame to which is mounted a longitudinal traverse assembly. The traverse assembly is made of two 33 inch steel rules with a strip reinforcing element

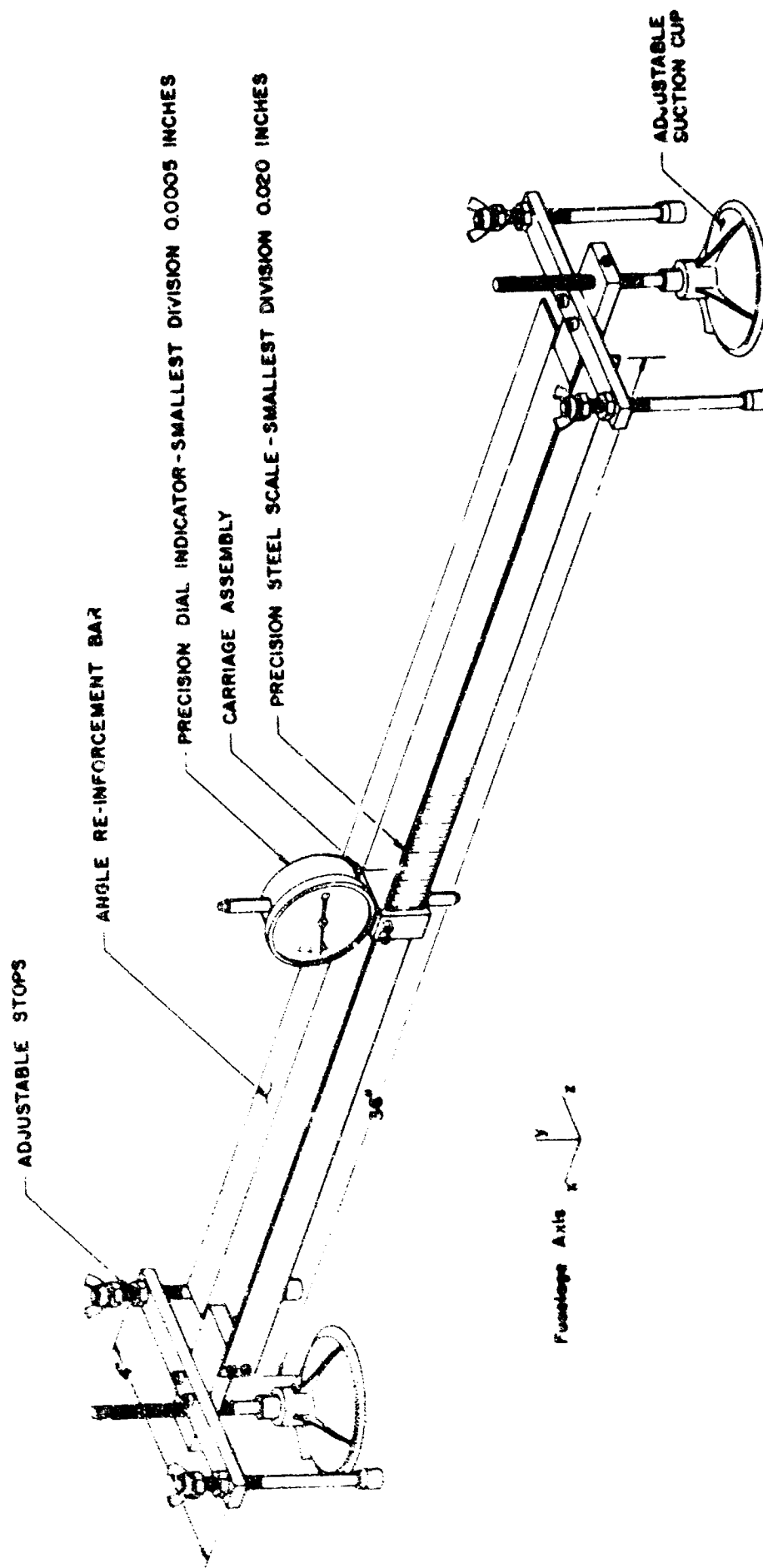


FIGURE 36. THE ASSEMBLY USED TO MEASURE SKIN DEFORMATIONS ON THE TYPE A AND B AIRCRAFT

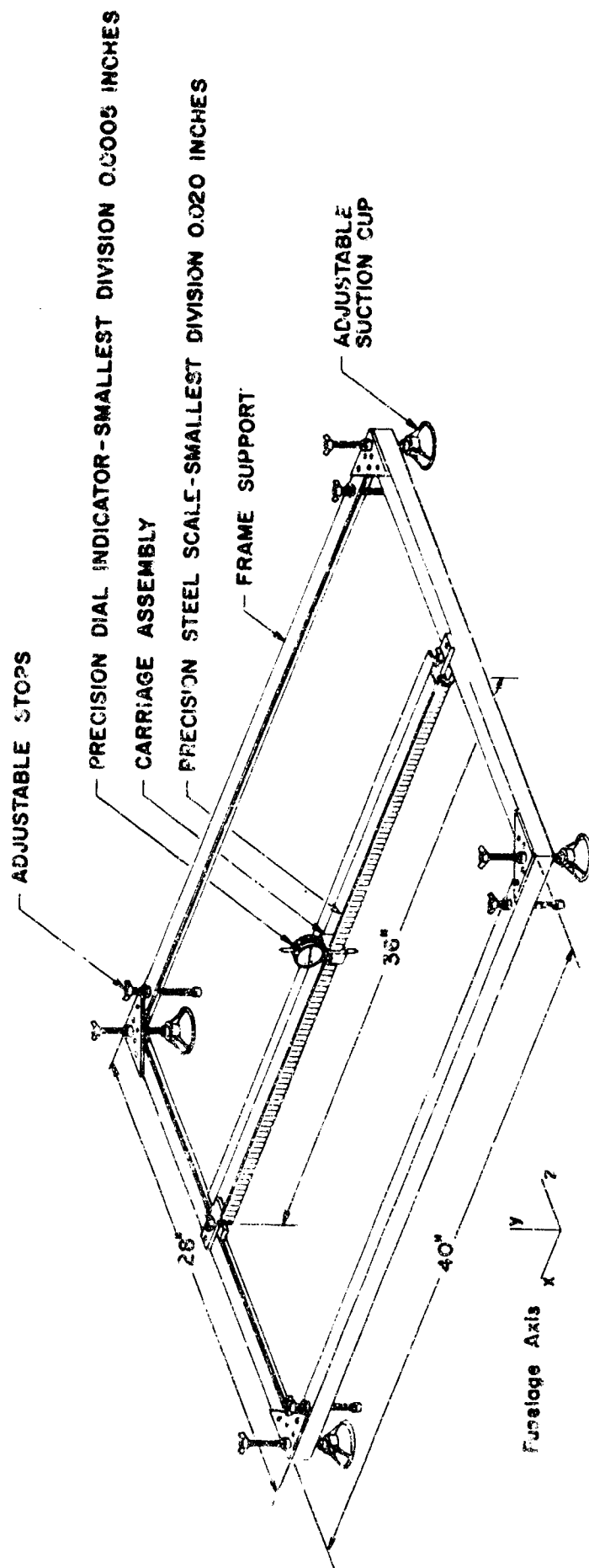


FIGURE 37. THE ASSEMBLY USED TO MEASURE SKIN DEFORMATIONS ON THE TYPE C AIRCRAFT

of aluminum angle to add rigidity. The rulers have no movement in or out, thus providing a reference plane from which all skin measurements were taken. The two steel rules were placed on edge approximately one inch apart providing a track for the carriage assembly to slide on. The carriage assembly holds the dial indicator and the foot of the indicator can move in and out as it is moved along the skin of the aircraft without any change in the reference plane fixed by the rulers. The position of the assembly on the steel rules and readings of the dial indicator give the x and y coordinates required to correlate this data. The coordinate z may be obtained by adjusting the transverse assembly with respect to the frame.

The assembly shown in Figure 37, used on Type C Aircraft, could not be used on Type A and B Aircraft because of high axial curvature of the skin and smaller radii of the fuselage. The assembly that was used is shown in Figure 36. This assembly utilizes the carriage assembly, and the precision scales of Figure 37, but the large 28 x 40 inch frame is replaced by 4 inch cross bars. In the case of Figure 37 configuration, the device was secured to the aircraft by use of four rubber suction cups. Figure 36 configuration utilized two rubber suction cups. Any movement of the assemblies due to the suction cups were eliminated by threaded feet which were snugged down to the aircraft surface. This configuration kept the distance between the aircraft and the steel scales constant during individual survey. A polaroid camera was used to record some observations.

Measurements were taken in a plane $z = 0$ through the co-pilot's static port centerline and at z positions above and below the ports. This data is presented as Figures 41 through 44. The center of the static port assembly was used to designate the center of coordinates system as far as the z and x coordinates are concerned as shown in Figure 38. This figure also indicates the sign convention used. Port assemblies were the same as used by NASA personnel for altitude position error measurements. Along the centerline through the static ports, dial readings were taken at the center of the static port, at each edge of the static port assembly to determine the flushness of the static port with respect to the surrounding skin, and

thereafter in one inch increments forward and aft of static ports for a total length of 34 inches. The area surveyed was a rectangular area 8 inches wide, 34 inches long with the static port assembly at the center. The accuracies of the measurements taken were within ± 0.05 inches for the lateral positions (x direction) and ± 0.001 inch for the vertical movement (y direction). The lateral movement was recorded from the steel scale reading and the vertical movement from the dial indicator.

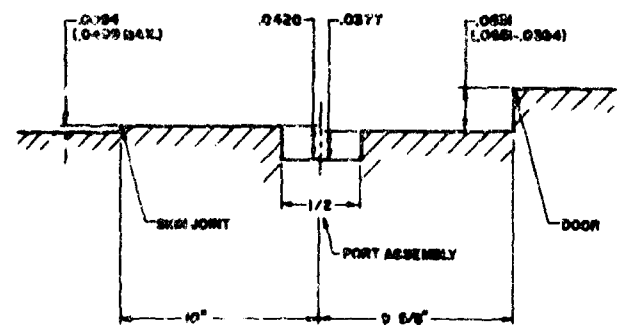
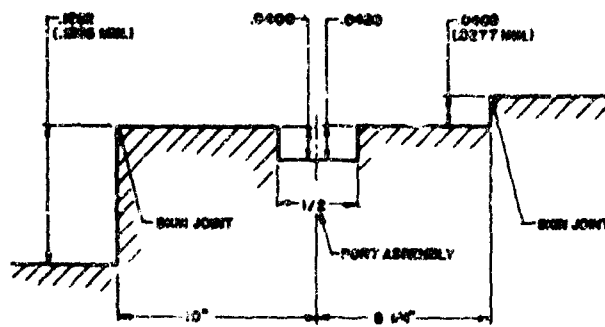
Use of the measuring device described gives only relative values of the airplane contour and these values will not be repeatable from aircraft to aircraft since the scales may be displaced at a different y distance on each aircraft. In addition to the y displacement being different, the scales can be skewed at a different angle with respect to the skin, thus forcing the y measurements to vary. The variables mentioned were corrected mathematically by forcing the reference plane to pass through the same two points on each aircraft, thus correcting for any variable in the vertical displacement and skewing angle. The two referenced or fixed points were at ± 6 inches from the center of the static port assembly. This method of data reduction was used on aircraft Types B and C. The average y measurements for the Type B and C aircraft is shown on Figure 40. Since only four aircraft of Type A were measured and major steps in the aircraft skin were present, the contour data has not been reduced and only the flushness of the static port assembly and the magnitude of the skin steps have been recorded in this report.

8.2.3. Experimental Results.

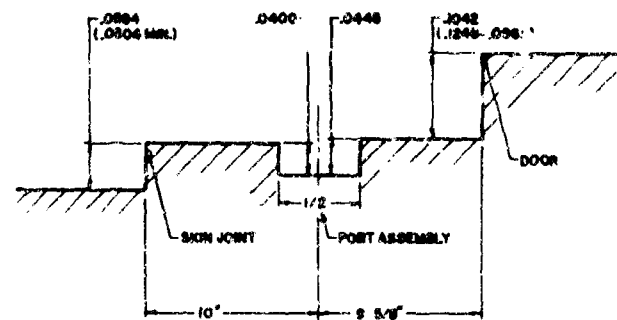
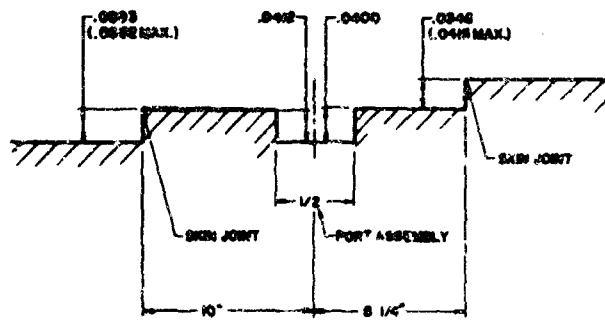
8.2.3.1. Aircraft A.

Limited presentation of data of Aircraft A is shown on Figure 39. The schematics indicate step variations. On the left side of the aircraft skin joints were located $8 \frac{1}{4}$ inches forward of the static port centerline and 10 inches aft of the port centerline. Height of the forward skin joint varied from 0.042 inches maximum to 0.009 inches minimum. The skin joints 10 inches aft of the port centerline on both the right and left hand side of the aircraft were even larger than this, varying between 0.009 inches and 0.168 inches. On the right side of the aircraft an access door to the airplane was

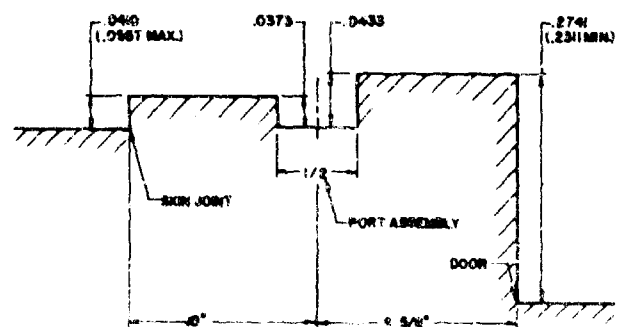
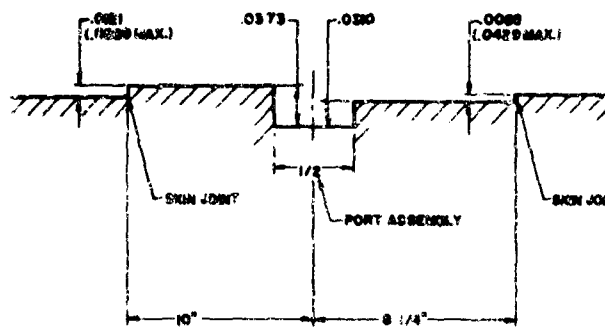
AIRCRAFT NUMBER 1



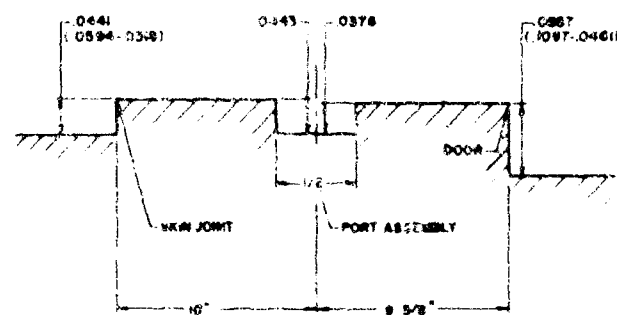
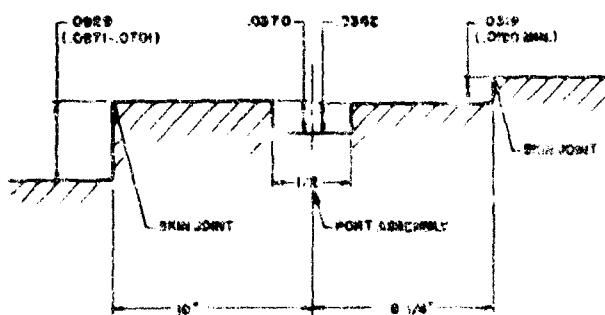
AIRCRAFT NUMBER 2



AIRCRAFT NUMBER 3



AIRCRAFT NUMBER 4



AFT ← FORWARD
LEFT SIDE

AFT ← FORWARD
RIGHT SIDE

FIGURE 39. VARIATIONS IN SKIN CONTOUR ON THE TYPE A AIRCRAFT

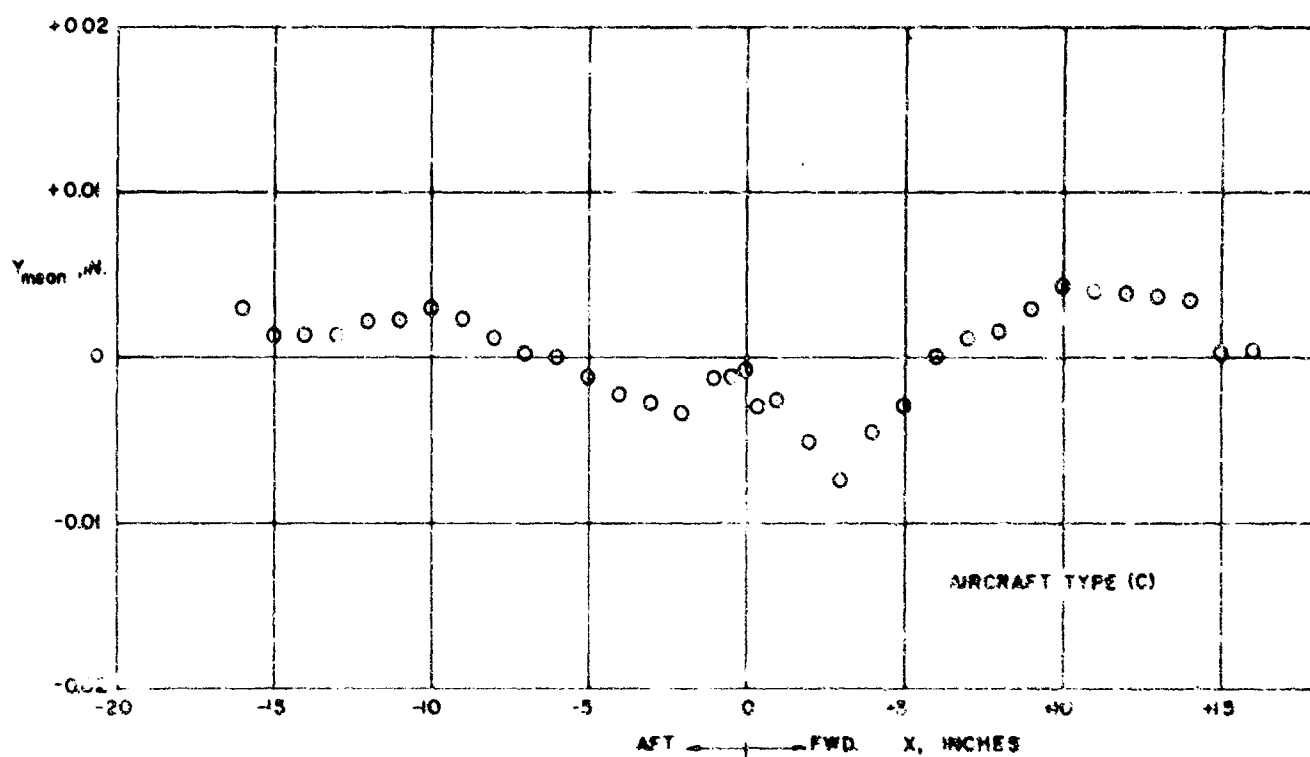
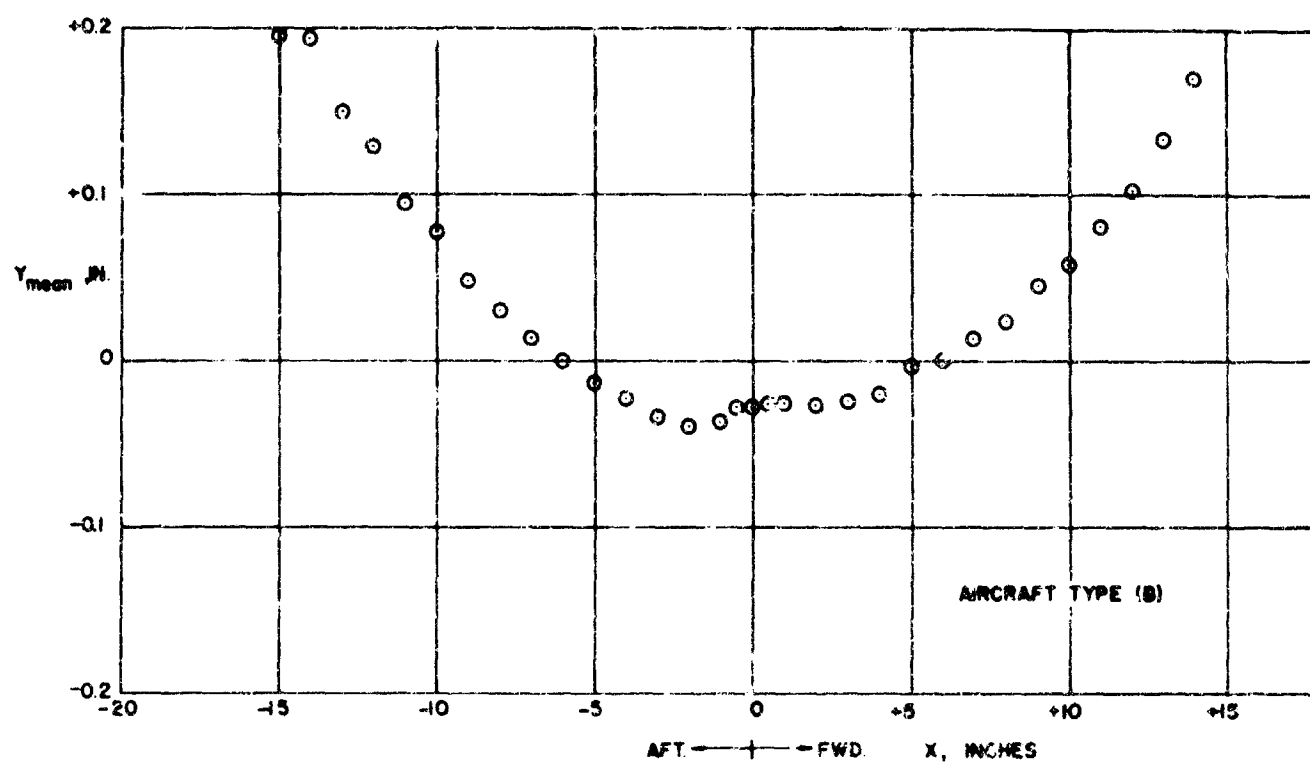


FIGURE 40
 Y_{MEAN} VALUES FOR AIRCRAFT TYPES (B) AND (C)

located 9 5/8 inches forward of the port centerline. Flushness of this door varied to a large extent between aircraft, varying from 0.274 inches in to 0.125 inches out. Static port assemblies were consistently mounted flush to the inside of the skin rather than to the outside skin as in other aircraft survey. Amount of the step was reasonably consistent, varying between 0.031 to 0.043.

8.2.3.2. Aircraft B.

Measured skin contours for Aircraft B, along the centerline through the static port assembly, is shown in Figure 41. Measurements are shown for the right and left hand side of the aircraft for x locations from - 16 inches to + 16 inches. Flushness of the static port assembly with respect to the surrounding skin is also indicated by the sketches in the center of the page. The data shows substantial profile irregularities. Aircraft 2, 6 and 3 have skin irregularities to 0.040 inches within ± 5 inches of the static port. Aircraft Number 5, has skin contour data closest to the mean skin contour. It should be noted on Figure 41 that all surface measurement data between stations ± 10 inches from the static ports fell within ± 0.060 inches. Measurements at transverse positions above and below the static port assembly is shown on Figure 42 for the Type B Aircraft. The contours at z of ± 4 inches although indicating definite presence of waves, shows less evidence to random data scatter when compared to the centerline distributions. Much of the random distribution scatter is caused by the deflection of the skin locally when the static port assembly is riveted to the aircraft skin.

The indication of flushness of the static port assembly with respect to the surrounding skin is shown on Figure 41. The maximum outward position of the static port assembly was 0.0564 inches for Aircraft Number 6. The maximum inward position step was 0.0270 inches for Aircraft Number 4.

8.2.3.3. Aircraft C.

Most of the skin surface measurements for Aircraft C are shown in Figures 43 and 44. Centerline measurement data is shown in Figure 43 which shows the same erratic tendency as in the area of the static port of Aircraft B. However the magnitude of the

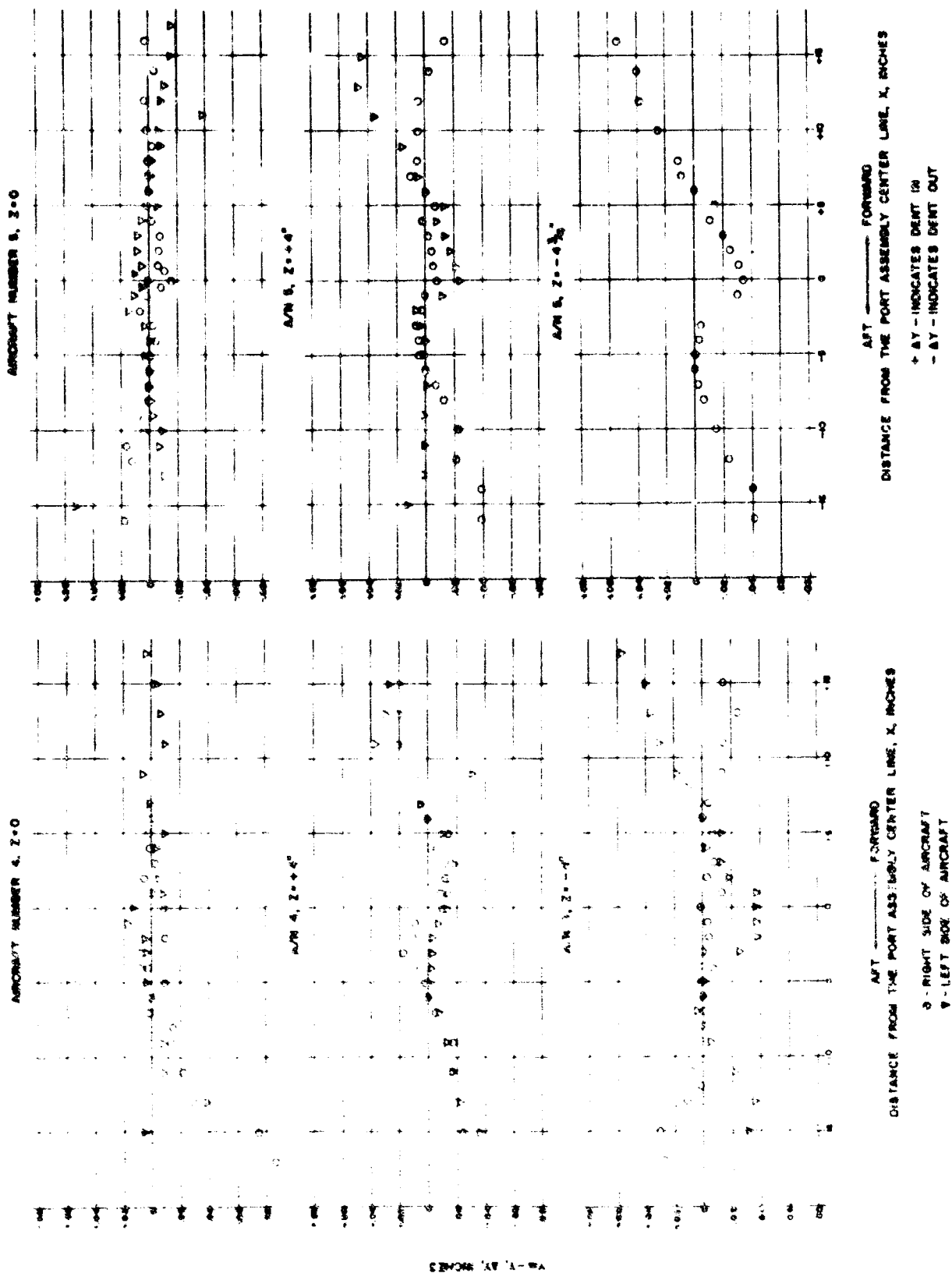


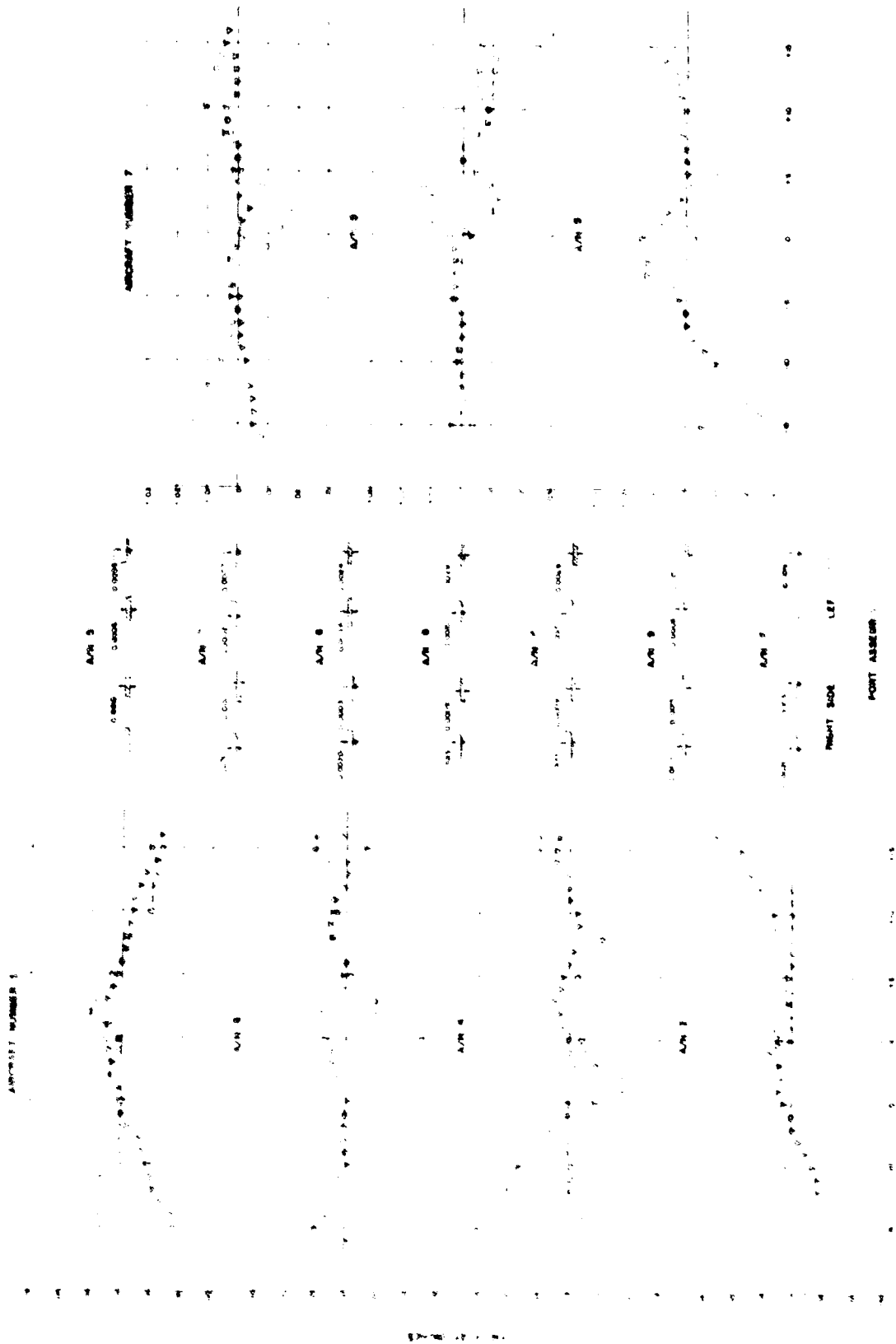
FIGURE 42 VARIATION FROM THE MEAN SKIN CONTOUR AT THE CENTER LINE AND ± 4 \" LOCATION FOR THE TYPE 8 AIRCRAFT

deviations are considerably less than for aircraft Type B. For Aircraft C all surface measurement data taken between ± 10 inches of the aircraft's port centerline fall within ± 0.025 inches. Aircraft Number 6 shows a large dent centered at the static port with a total of 0.025 inches deflection occurring within the length of ± 5 inches from the center of the port. Aircraft 7, 8 and 9 all have deviations within ± 5 inches of the aircraft's static port of 0.010 to 0.020 inches. The y deviation scale of Figures 43 and 44 have been increased by a factor of 2 as compared to Figures 41 and 42. It may be noted from Figure 43 that flushness of the static ports was extremely good with a maximum deviation out being 0.0045 inches and a maximum deviation in being 0.0034 inches. Measurements taken at ± 4 inches from the port centerline is shown in Figure 44; although definite skin waves are present, these data indicate elimination of any erratic skin deformations right in the area of the static port.

8.2.3.4. Data, Summary and Mean Skin Contours.

The mean skin contours for Aircraft Type B and C are shown in Figure 40. The mean skin contour for Aircraft B shows appreciable curvature as indicated by the upper curve of Figure 40. A skin bump just aft of the static port may be noted from the mean contour plot. The mean contour of Aircraft C is shown in the lower graph of Figure 40. It should be noted that the scale for this graph has been increased by a factor of 10 over the upper graph. The contour is essentially a straight line with all deviations falling between $+ 0.004$ inches and $- 0.007$ inches from a straight line. The consistent deformation right at the static ports is shown by the mean skin contour of Aircraft C. This is caused by warpage of the skin area when the static port assembly is riveted to the skin.

The root-mean-square of the individual deviations from the mean contour, shown in Figure 40 for Aircraft B (360 readings taken into account), is 0.012 inches. The root-mean-square deviation for Aircraft C based on 455 readings is 0.0070 inches. Numbers apply to the aircraft centerline surveys through the static ports only. They indicate that the Type C aircraft, which were relatively new (most of them had less than 100 hours of flight) were two to three times smoother than the older Type B aircraft.



AIRCRAFT NUMBER 1
AIRCRAFT NUMBER 2
AIRCRAFT NUMBER 3
AIRCRAFT NUMBER 4
AIRCRAFT NUMBER 5
AIRCRAFT NUMBER 6
AIRCRAFT NUMBER 7

AIRCRAFT NUMBER 1
AIRCRAFT NUMBER 2
AIRCRAFT NUMBER 3
AIRCRAFT NUMBER 4
AIRCRAFT NUMBER 5
AIRCRAFT NUMBER 6
AIRCRAFT NUMBER 7

FIGURE 43 VARIATION FROM THE MEAN SKIN CONTOUR AT THE CENTER LINE LOCATION FOR THE C TYPE AIRCRAFT

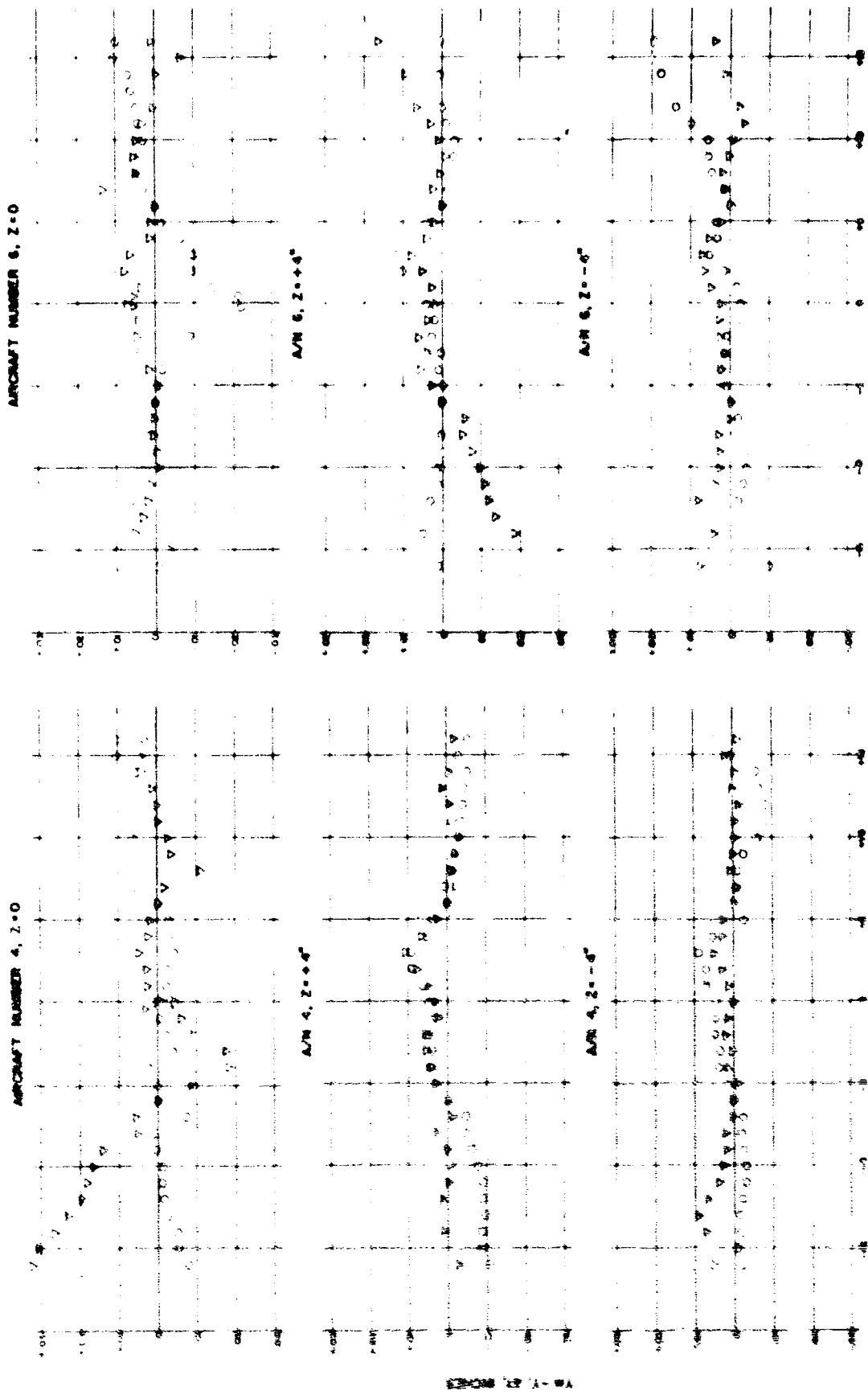


FIGURE 4-4 VIBRATION FROM THE MEAN SKIN CONTOUR AT THE CENTER LINE AND 20" LOCATION FOR THE TYPE C AIRCRAFT

In regard to port flushness, the root-mean-squared of 28 port deviations for Aircraft C were 0.0018 inches and for Aircraft B was 0.016 inches. Thus the flushness of the port installation on Aircraft C was observed to be ten times better than the flushness on Aircraft B. The maximum step observed at static port for Aircraft B was 0.0564 inches and for Aircraft C was 0.0045 inches.

8.2.3.5. Maintenance of Static Ports.

During the measurements performed on 18 aircraft, the condition of the static ports and surrounding area was noted. The presence of foreign material such as wax or dirt was found in only one port assembly out of 72 examined (18 aircraft - both sides - both pilot and co-pilot ports). In the one case a slight amount of wax was found in 2 of the 7 holes blocking about 1/3 of the area of the 2 holes. The cleanliness of the ports was, therefore, found to be very good.

No burrs at the edges of the static holes were larger than about 0.005 inches and in most cases no measurable burr existed. There was no evidence of burring from insertion of a cleaning rod into the ports.

The use of paint adjacent to the port assembly (Aircraft B) for lettering "U.S. AIR FORCE" is not considered the best practice from the static port maintenance standpoint. Paint was generally found to be in good condition. Some chipping near the ports was noted. The influence of the paint is concluded to be of minor significance compared to surface waves and port flushness.

8.3. ALTITUDE POSITION ERRORS DUE TO SKIN IRREGULARITIES IN THE VICINITY OF FUSELAGE STATIC PRESSURE PORTS.

An analytical study was conducted to estimate position errors caused by deviations of fuselage skin from the aircraft's mean surface curvature. The study was made for a number of aircraft that were both surveyed by REC and flight-tested by combined USAF and NASA personnel. The aircraft corresponding to those listed previously in Section 8.2.1 have been designated as follows:

Type B, Number 1	Type C, Number 1
Type B, Number 2	Type C, Number 3
Type B, Number 3	Type C, Number 5
Type B, Number 4	Type C, Number 6
Type B, Number 5	
Type B, Number 6	

Fuselage skin deviations from the mean contour in the vicinity of the co-pilot's static ports have been discussed in the previous sub-sections. The mean contour of the fuselage at the static ports, as estimated by REC, for both Type B and Type C aircraft is shown on Figure 40. A schematic showing the area over which fuselage skin measurements were taken is shown on Figure 38.

The "linearized small perturbation" theory used for the present analytical study has been well documented in Reference 25. The integral equation for pressure coefficient can be expressed as

$$C_P = \frac{\frac{P_1}{\gamma} - P}{\frac{\gamma}{2} P M^2} = \int_{z_1}^{z_2} \int_{x_1}^{x_2} \frac{x m dx dz}{\pi \left[x^2 + (1-M^2)z^2 \right]^{3/2}} \quad (31)$$

where x and z are the coordinates shown on Figures 38 with the center of the static port located at $x = 0$ and $z = 0$, M = local Mach number, and m is the slope of the fuselage, $\frac{\delta y}{\delta x}$, at a point x, z . The coordinate y is zero at the static port and a plus y deflection on the surface is a dent into the fuselage skin. For numerical integration purposes $m = (y_{n+1} - y_n) / \Delta x = \Delta y / \Delta x$. If we assume that surface deformations are actually uniform waves of constant Δy extending from z_1 to z_2 , Equation 31 becomes:

$$C_P = \sum_{x_1}^{x_n} \frac{\Delta y}{\pi x} \left[\frac{z_2}{x^2 + (1-M^2)z_2^2} \right]^{1/2} - \left[\frac{z_1}{x^2 + (1-M^2)z_1^2} \right]^{1/2} \quad (32)$$

Equation (32) was evaluated for both the right and left sides of the aircraft fuselage using the exact surface deformation measurements shown on Figures 41, 42, 43, and 44. $C_{P_{right}}$ and $C_{P_{left}}$ were then averaged to obtain an overall pressure error of the co-pilot's static pressure system. For purposes of comparison with flight test data, Mach number has been converted to indicated airspeed assuming standard sea level conditions and omitting any aircraft position error. The relationship is as follows:

<u>V_1 (Sea Level)</u>	<u>Mach Number</u>
100	0.151
200	0.303
300	0.454
400	0.605
500	0.756
600	0.908

The predicted position errors for four aircraft, Type B numbers 5 and 4 and Type C numbers 6 and 4, were computed using both centerline skin measurements and measurements taken at $z = \pm 4$ inches, as shown on Figure 38. Predicted position errors for the remaining aircraft were computed using only fuselage measurements along the centerline at $z = 0$. The area bands of effectiveness of the skin measurements in the z direction were varied to obtain an indication of sensitivity of predicted position error with the width of the band, over which the skin deformation (Δy) is assumed constant.

Variations in predicted position errors between aircraft are shown on Figure 45 for the Type B aircraft and on Figure 46 for the Type C aircraft. The errors are given for assumptions that the centerline data measurements of $\Delta y = y - y_m$ extend over bands from $z_1 = -2$ inches to $z_2 = +2$ inches and from $z_1 = -5$ inches and $z_2 = +3$ inches. For the aircraft on which surface measurements at $z = +4$ inches and -4 inches were available, i.e. Type B numbers 5 and 4 and Type C numbers 6 and 4, complete data was used. For example, if the centerline data for Δy was assumed effective for a band from $z = -2$ inches to $+2$ inches, the Δy data at $z = +4$ inches was assumed effective for an area band from $z = +2$ inches to $+6$ inches and the Δy data at $z = -4$ inches was assumed effective for a band from $z = -6$ inches to -2 inches. The pressure errors due to each of these three bands were then added to obtain a "complete data" pressure error. The theoretical prediction curves show only a minute dependence of position error on the width of the effective data bands in the $\pm z$ direction.

Superimposed on Figures 45 and 46 are variations in position errors between aircraft determined from flight tests conducted by NASA, Reference 26. The flight test data has been resown as Figures 47(A), 47(B), and 47(C) of this report. The flight test values indicated on Figures 45 and 46 are differences in the absolute ΔH errors of aircraft shown on Figures 47(B) and 47(C). There is reasonably good agreement between the theoretical prediction and flight test data. Agreement is better for Type C aircraft which is to be expected because of a generally smoother aircraft skin on these aircraft compared to the surface irregularities for the Type B aircraft. It should also be noted that the static port assemblies were not always flush with the fuselage skin. The resulting "steps" will cause pressure errors which can not be predicted from theory. The "step" errors, therefore, have not been incorporated in this report.

8.4. SUMMARY.

8.4.1. The correlation between predicted static pressure error (based on skin measurements) and flight test measurements was good for the Type C aircraft, Figure 46. Most of the important skin deviations occurred near the ports and were apparently caused by the riveting of the port assembly to the surrounding skin.

8.4.2. Comparison of predicted static pressure error and flight test results are not as good for the Type B aircraft, Figure 45. The differences are probably caused by the following.

1. The ports are located on a curved surface near the nose and shifts in fore and aft location of the ports will produce a shift in static pressure.

2. The port assemblies were in general not flush and since ports were located only six feet from the nose in relatively thin boundary layer, the effect of flushness may have been significant. The predictions take into account only surface waves and not port flushness. It may be noted from the report that port flushness was 10 times better for the Type C than the Type B.

3. Surface deformations on the Type B aircraft were 2.5 times larger than for the Type C aircraft. It is probable that some waves influencing the static pressure were not taken into account in the calculations. The Type B aircraft had been in service thousands of hours and therefore subject to random surface damage.

4. The Type C aircraft port location was on a cylindrical section of the aircraft and accessible from the ground. Measurements were made with the apparatus of Figure 37 and are probably more precise than those obtained on the Type B aircraft.

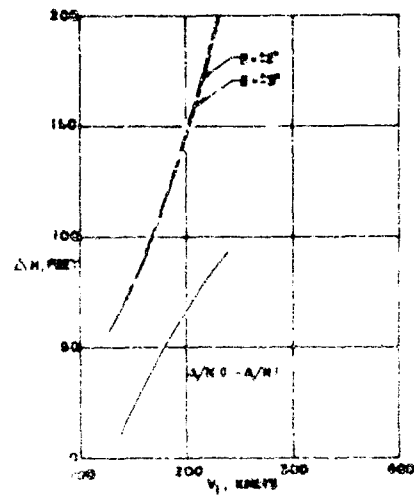
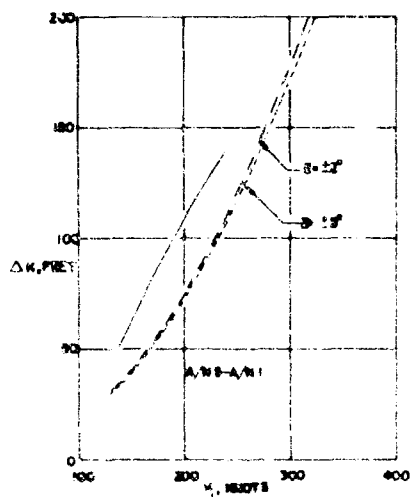
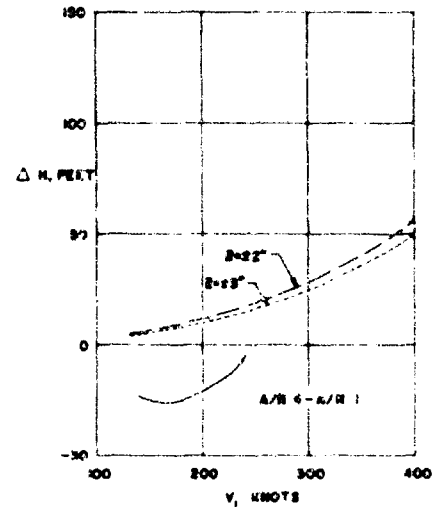
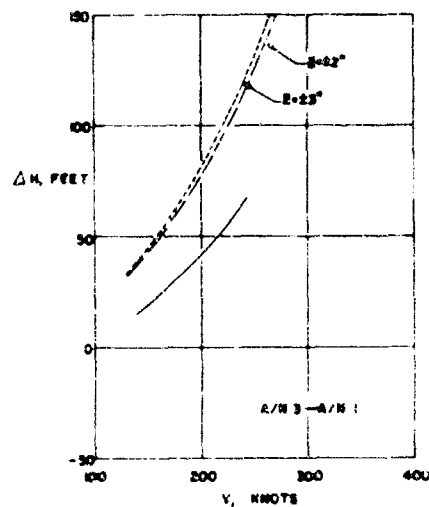
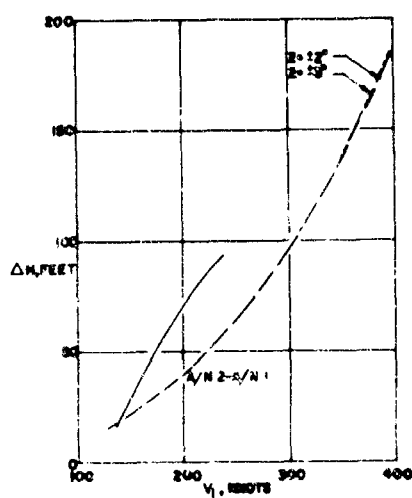


FIGURE 45
 VARIATIONS IN ALTITUDE POSITION ERRORS BETWEEN TYPE B AIRCRAFT
 AIRCRAFT NUMBER 1 USED AS A BASE
 — FLIGHT TEST DATA
 - - - THEORETICAL PREDICTIONS (STANDARD SEA LEVEL CONDITIONS)

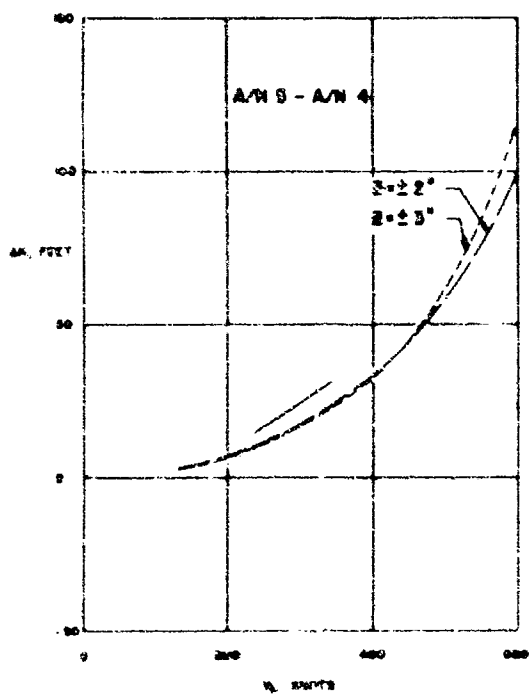
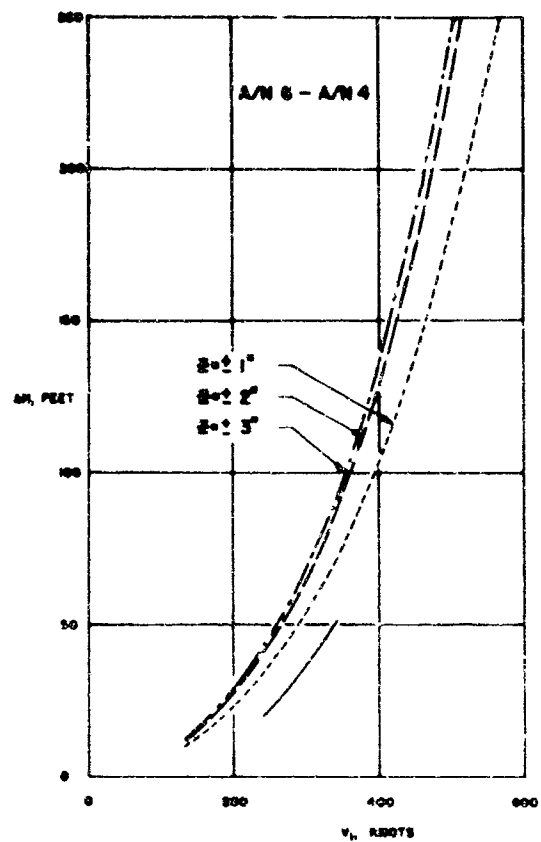
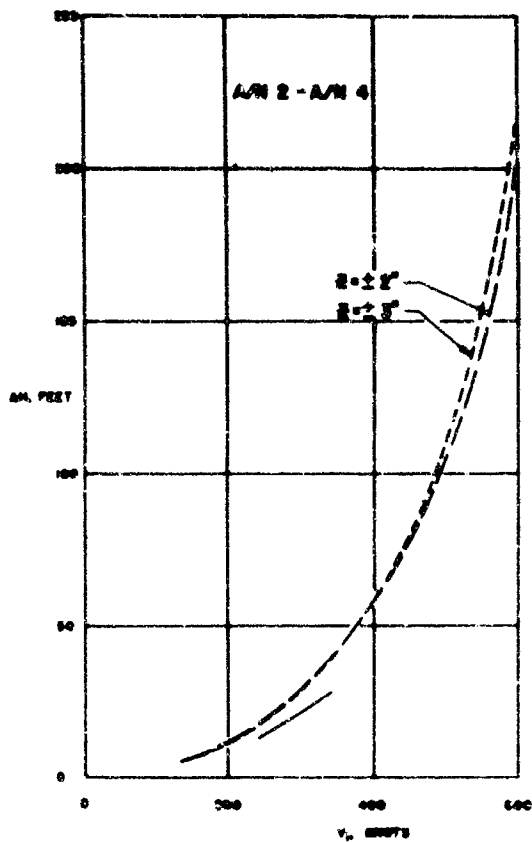


FIGURE 46
 VARIATIONS IN ALTITUDE POSITION ERRORS BETWEEN
 TYPE (C) AIRCRAFT.
 AIRCRAFT NUMBER 4 USED AS A BASE
 — FLIGHT TEST DATA
 ---- THEORETICAL PREDICTION (STANDARD SEA LEVEL CONDITIONS)

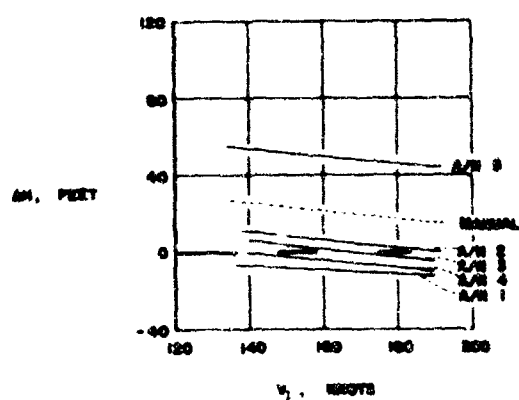


FIGURE 47(A)
TYPE A AIRCRAFT

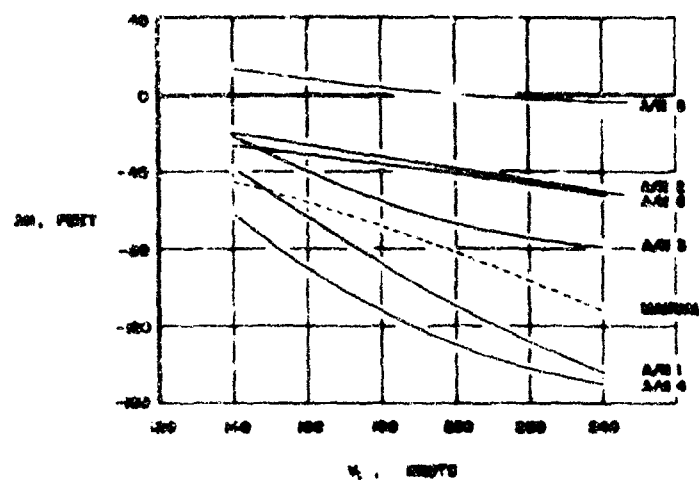


FIGURE 47(B)
TYPE B AIRCRAFT

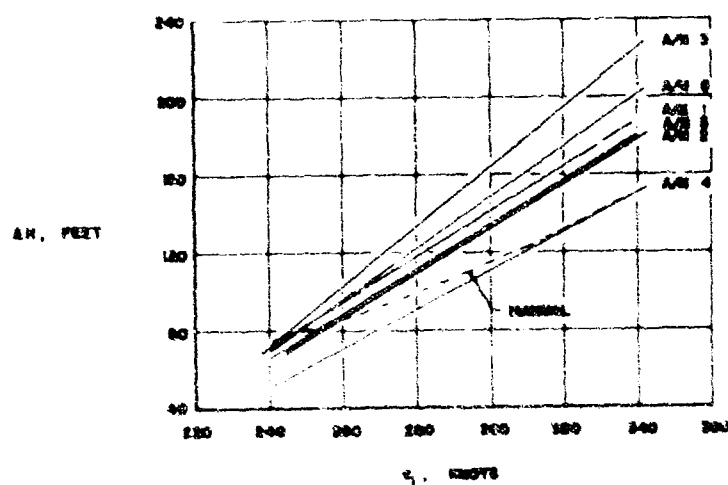


FIGURE 47(C)
TYPE C AIRCRAFT

FIGURE 47
COMPARISON OF THE COPILOT'S STATIC-PRESSURE-SYSTEM ERROR WITH THE MANUFACTURER'S CALIBRATION FOR THE THREE TYPES OF AIRCRAFT (NASA FLIGHT TEST DATA, REFERENCE 26)
AE = INDICATED ALTITUDE - TRUE PRESSURE ALTITUDE

SECTION 9

FLIGHT TEST METHODS FOR THE CALIBRATION OF AIRCRAFT STATIC PRESSURE SYSTEMS

9.1. INTRODUCTION.

Results of a previous study conducted under Air Force Contract AF33(600)37359, Reference 22, indicated through error analysis, the probable accuracies of several methods for in-flight calibration of aircraft static pressure systems. The current military specification, MIL-P-26292, for the design, installation, and inspection of pitot and static pressure systems requires experimental in-flight determination of installation error per paragraph 4.4.6. The flight test methods are optional but subject to approval of the procuring activity. The accuracies of flight test methods should be equal to or superior to results obtainable from the following:

a. The Tower Fly-By Method. - The aircraft is flown close to an aircraft control tower and the altitude of the aircraft is measured by photographing its position on a measured grid.

b. The Radar Phototheodolite Method. - The aircraft is tracked by radar using a boresight camera to correct the azimuth and elevation angles read from the radar scales.

c. The Pacer Technique. - The pacer aircraft and the aircraft being calibrated are flown together in close formation while the altitude and airspeed indications are compared.

d. The Fly-By Parallax Technique. - The pacer aircraft is flown at a constant speed and altitude while the aircraft to be calibrated, alternately decelerates and accelerates while keeping the pacer aircraft in line with the horizon.

It is the purpose of this section to review the Reference 22 work with a re-summary of probable accuracies of the above techniques and provide certain recommendations for standardization of calibration procedures.

9.2. THE TOWER FLY-BY METHOD.

9.2.1. Techniques and Accuracy.

This method is one of the oldest and most accurate calibration methods, if performed correctly. Fundamental to the accuracy is the fact that the pressure differential between low altitude fly-by and a reference point (runway or tower) may be predicted accurately. The accuracy of the absolute value of pressure is unimportant. For example, an absolute pressure error of 0.008 inch Hg. results in a pressure differential error of 0.1 ft. for an air column 200 ft. high. The air pressure should be continuously monitored at a reference point (tower or ground) probably using a Fortin type barometer. The atmospheric temperature should be continuously monitored, preferably at tower elevation. Additional details are discussed in Sections 2.1.1 and 2.1.2 of Reference 22.

The calibration accuracy of the tower fly-by method was arrived at through error analysis (Reference 22) for two different pressure gages on the test aircraft. Case I was for a full range altimeter with an assumed accuracy of $\pm (10 \text{ ft.} + 0.00125H)$ where H is altitude in feet. The predicted accuracy of fly-by calibration with full range altimeter was $\pm 17.3 \text{ ft.}$ and independent of flight speed. Case II utilized a differential pressure gage or limited range altimeter. Prior to take off, a temperature controlled reference tank vented to the atmosphere, could be sealed at constant pressure, and all subsequent flight pressure would be taken as a differential against the reference pressure. The accuracy of the temperature control system and pressure gage were assumed at $\pm 0.05 \text{ in. H}_2\text{O}$ or $\pm 3.4 \text{ ft.}$ of air at sea level. The overall predicted accuracy of the fly-by calibration was $\pm 5.4 \text{ ft.}$

9.2.2. Calibration of Low Speed Aircraft and Probable Accuracy At Altitude.

9.2.2.1. Aircraft With Flush Static Ports.

Fuselage mounted static ports are usually located carefully by the airframe manufacturer at a position on the fuselage such that the pressure over a given airspeed range will be relatively insensitive to angle of attack. Usually, however, up to a Mach number of 0.7 the variation is larger than the compressibility effects. Flight tests are

usually, therefore, performed at certain values of impact pressure, q_c , and the results presented as $\Delta P/q_c$, ΔP , or ΔH as a function of indicated airspeed. Unfortunately, although $\Delta P/q_c$ will remain constant at altitude, the altitude error (ΔH) will increase as indicated by the equation

$$\Delta H = \Delta H_{sl} (\rho_{sl}/\rho) \quad (33)$$

where ρ is the static density and subscript "sl" represents standard sea level conditions.

The variation of altitude error at various altitudes is indicated by Table XIII below.

TABLE XIII
Calibration Accuracy at Altitude for Low Speed Aircraft
($M \leq 0.7$) At Constant Angle of Attack

<u>Altitude, Feet</u>	<u>ρ_{sl}/ρ</u>	<u>ΔH_1, Feet</u>	<u>ΔH_2, Feet</u>
0	1.000	± 17.3	± 5.4
10,000	1.354	± 23.4	± 7.3
20,000	1.877	± 32.5	± 10.1
30,000	2.669	± 46.2	± 14.4
40,000	4.047	± 70.1	± 21.9
50,000	6.531	± 113.0	± 35.3

ΔH_1 = Altitude error using full range altimeter for tower fly-by calibration.

ΔH_2 = Altitude error using limited range altimeter for tower fly-by calibration.

In addition to the altitude effect which assumes constant $\Delta P/q_c$, compressibility effect will tend to increase $\Delta P/q_c$ with increasing Mach number. To estimate the magnitude of compressibility, the pressure variation on a body of revolution as a

function of Mach number has been considered between $M = 0$ and $M = 0.7$. If the local pressure results in $\Delta P/q_c = 0.02$, the maximum allowable from MIL-P-26292 at low speed, then the maximum compressibility effect from $M = 0$ to $M = 0.7$ will be $\Delta C_p = 0.004$. The maximum effect of compressibility has been calculated and shown in Table XIV.

TABLE XIV
Maximum Effect of Compressibility Between $M = 0$ and $M = 0.7$
For Fuselage Mounted Static Ports

<u>Altitude, Feet</u>	<u>ΔH_c, Feet</u>	<u>$\Delta H_1 + \Delta H_c$, Feet</u>	<u>$\Delta H_2 + \Delta H_c$, Feet</u>
0	0*	17.3	5.4
10,000	41.9	65.3	49.2
20,000	38.4	70.9	48.5
30,000	35.7	91.9	50.1
40,000	33.5	105.6	55.4
50,000	33.5	145.3	68.8

ΔH_c = Altitude error due to compressibility effects.

* = Error is zero since tower fly-by calibrations include compressibility effects.

ΔH_1 = From Table XIII.

ΔH_2 = From Table XIII.

The advantages of using the limited range altimeter for calibration is obvious from Tables XIII and XIV. The uncertainty of tower fly-by calibration with full range altimeter is magnified by the altitude effect. It should be noted that the compressibility effects listed above should be larger than normally expected. If the aircraft flight envelope extends beyond $M = 0.7$, it is recommended that flight calibrations be performed at altitude by an alternate method. The tower fly-by procedure is still a useful calibration check method, however, even for higher speed aircraft as discussed in Section 9.2.2.2.

9.2.2.2. Aircraft With Nose or Wing Tip Boom Installation.

If an aircraft with nose or wing boom is calibrated at tower fly-by as a function of indicated airspeed, $\Delta P/q_c$, the accuracies of the calibration at altitude will follow the predictions of Table XIII. Nose installations are less subject to compressibility effects, hence, the results may be used with good accuracy up to $M = 0.8$. However, if a pitot-static tube configuration (such as USAF Types MA-1 or TRU-1/A) is utilized, which is insensitive to positive angles of attack, the variation of pressure at the sensing ports is only caused by the variations in the fuselage flow field. Since the sensing ports are not located on the fuselage or wing, the variation of pressure with angle of attack could be expected to be small. The influence is discussed in detail in Reference 22, Section 2.1.3.3. Results are resummarized in Table XV for three lengths of nose booms and three Mach numbers. As indicated by Reference 22 (which includes both the effect of angle and compressibility) the angle of attack effects are conservative, since the Prandtl Glauert correction for compressibility for locations ahead of the body will over-correct. On the other hand, the results are based on a particular angle of attack-Mach number-altitude flight envelope which is probably typical of a high performance fighter type aircraft. Heavier wing loadings would result in increased angles of attack at altitudes.

9.2.3. Calibration of High Speed Aircraft and Probable Accuracy at Altitude.

It was recommended in a previous section, 9.2.2.1, aircraft with flush static ports capable of Mach numbers in excess of 0.7 should be calibrated at altitude to duplicate both angle of attack and compressible effects. Aircraft with wing tip or nose booms may be calibrated up to $M = 0.9$ (the usual limit for tower fly-by procedures) and the calibrations may be used at altitude (based on the predictions of Table XIV). If the aircraft is capable of flights above a Mach number of 0.9, then calibrations at altitude are recommended.

The most common flight calibration methods at altitude are as follows:

- a. Pacer Technique.
- b. Fly-by Parallax Technique.
- c. Ground Tracking Techniques.

TABLE XV

TOWER FLY-BY PREDICTIONS USED AT ALTITUDE-VARIATION OF ANGLE
OF ATTACK EFFECT FOR NOSE BOOM CONFIGURATIONS ONLY

ΔH_{α} for Full Range Altimeter, Feet

Altitude (Feet)	M = 0.7			M = 0.8			M = 0.9		
	$\frac{X}{D} = 1.5$	1.0	0.5	$\frac{X}{D} = 1.5$	1.0	0.5	$\frac{X}{D} = 1.5$	1.0	0.5
0	±17	±17	±17	±17	±17	±17	±17	±17	±17
10,000	16	19	20	17	20	22	20	23	27
20,000	15	21	24	17	24	28	22	30	37
30,000	14	25	31	19	30	38	28	42	56
40,000	14	33	43	22	42	56	38	62	87
50,000				28	64	89	53	92	131

ΔH_{α} for Limited Range Altimeter, Feet

Altitude (Feet)	M = 0.7			M = 0.8			M = 0.9		
	$\frac{X}{D} = 1.5$	1.0	0.5	$\frac{X}{D} = 1.5$	1.0	0.5	$\frac{X}{D} = 1.5$	1.0	0.5
0	± 5	± 5	± 5	± 5	± 5	± 5	± 5	± 5	± 5
10,000	5	7	8	6	9	11	9	12	16
20,000	5	11	14	7	13	17	12	19	26
30,000	5	15	21	9	21	29	18	32	36
40,000	5	24	34	13	33	47	29	53	78
50,000				19	54	79	43	82	121

9.2.3.1. Fly-by and Pacer Methods.

The use of the fly-by method usually involves calibrating a reference aircraft using the tower fly-by technique and subsequently utilizing the reference aircraft for an altitude fly-by. In the altitude fly-by, the reference aircraft takes the place of a tower reference at sea level. Usually the reference aircraft is equipped with a long nose boom to minimize disturbance of flow field by fuselage and reduce angle of attack and compressibility effects. The results of Table XV indicate that for a long nose boom, $X/D = 1.5$, an aircraft at $M = 0.7$, or below, will serve as a very accurate reference. The accuracy of the procedure has been analyzed in Reference 22 and the results are repeated in Table XVI for the columns labeled ΔH_2 . Two types of instrumentation are considered:

- a. Full range altimeter with accuracy corresponding to $\Delta H = \pm (10 \text{ feet} + 0.00125H)$ where H = altitude in feet.
- b. A limited range altimeter with 0.5 percent accuracy with two ranges:
0 - 10 in. H_2 full scale for use to 50,000 ft. and 0 - 5 in. H_2 full range for use from 50,000 ft. to 100,000 ft.

The advantages of the limited range altimeter method are readily apparent.

TABLE XVI
CALIBRATION ACCURACIES OF TWO METHODS OF CALIBRATION
AT ALTITUDE FOR FUSELAGE STATIC PORTS: $M \leq 0.7$

or

Nose Booms $M < 0.9$

Wing Booms $M < 0.9$

ΔH_1 = Total error in test aircraft including

- a. Calibration of a reference aircraft at sea level by tower fly-by method.
- b. Transfer of reference aircraft calibration to a pacer aircraft using a fly-by procedure at altitude.
- c. Calibration of test aircraft by pacer method at altitude.

ΔH_2 = Total error in the test aircraft including

- a. Calibration of a reference aircraft at sea level by tower fly-by method.
- b. Calibration of test aircraft by reference aircraft in a fly-by procedure at altitude.

Altitude (Feet)	Full Range Altimeter		Limited* Range Altimeter	
	ΔH_1 , Feet	ΔH_2 , Feet	ΔH_1 , Feet	ΔH_2 , Feet
10,000	54	42	27	23
20,000	76	57	28	24
30,000	100	73	31	25
40,000	124	89	37	29
50,000	148	106	36	27
60,000	173	123	44	34
70,000	197	141	64	47
80,000	222	158	99	71
90,000	247	175	157	112
100,000	272	193	250	178

*0 - 10 inches H_2O gage range used to 50,000 feet.

0 - 5 inches H_2O gage range used from 50,000 to 100,000 feet.

Since a pacer aircraft may only be tower calibrated to $M = 0.9$, calibrations above $M = 0.9$ must be obtained at altitude using fly-by with a reference aircraft. An alternate method is to recalibrate at higher Mach numbers at altitude using ground tracking techniques as will be discussed in the next section. The accuracy of the pacer calibration using the reference aircraft fly-by is given by the ΔH_2 column of Table XVI. After calibration, the pacer may be used to calibrate many aircraft. The estimated accuracy from Reference 22 is given in columns ΔH_1 of Table XVI. The main advantage of the limited range altimeter method is the elimination of repeated large altimeter errors. As an example, for a calibration by a pacer at 40,000 feet the following probable altimeter errors may occur:

Tower Fly-by altimeter error = ± 10 ft. (Reference 22)

Pacer calibration at 40,000 ft.

Reference aircraft altimeter error = ± 60 ft.

Pacer aircraft altimeter error = ± 60 ft.

Test aircraft calibration at 40,000 ft.

Pacer aircraft altimeter error = ± 60 ft.

Test aircraft altimeter error = ± 60 ft.

Root-magnitude-square of all altimeter errors =

$$\left[(10)^2 + 4(60)^2 \right]^{1/2} = \pm 120.4 \text{ ft.}$$

Root-magnitude-square of all errors (Table XVI) = ± 124 ft.

In the case of the limited range altimeter method, the ± 10 ft. error at sea level is replaced by a ± 5.4 ft. error (Reference 22) and the ± 60 ft. errors at 40,000 ft. replaced by a ± 13.8 ft. error.

9.2.3.2. Calibrations At Altitude Utilizing Ground Tracking Equipment.

This method appears ideal when a suitable ground tracking facility is available such as located at Edwards Air Force Base. The method eliminates the need for a pacer or reference aircraft at altitude. The method is described in detail in Section 2.4.4, Reference 22. The most practical method appears to calibrate the test aircraft in a tower fly-by procedure at one value of indicated airspeed and/or Mach

number. This calibration provides a reference or calibrated condition. The aircraft at altitude is flown at the reference condition and a survey of pressure vs altitude is made using the ground tracking equipment. An alternate method which saves flight time is to fly level in the reference condition, measure the total temperature, calculate the static temperature from the corrected Mach number, and compute the pressure variation assuming a standard temperature lapse rate at the altitude involved.

Following atmospheric calibration, the aircraft is flown over the tracking range in a series of variable speed conditions. For certain tracking ranges, e.g., Edwards Air Force Base, using multiple phototheodolites along an extended path, an accelerating and/or decelerating speed run is fast and accurate. At the end of the calibration runs, the atmospheric survey should be repeated.

An error analysis has been performed in Section 2.4.4 of Reference 22 for both the limited and full range altimeters. In the case of the limited range altimeter, the reference tank may be vented to the atmosphere with the aircraft flying in the reference condition. The tank is then sealed off and the subsequent calibration flights are performed with the pilot instructed to maintain zero pressure differential. As the position error changes with Mach number, the aircraft will increase or decrease altitude to maintain zero differential. The difference in altitude between the reference and test condition converted to pressure plus the position error at the reference condition then equals the pressure error at the test condition. The following equations describe the calibration.

For the aircraft flying in the reference condition at constant Mach number

$$p = p_{\text{ref}} = p_m - \left(\frac{p_m - p_{\text{ref}}}{p_m} \right) p_m \quad (34)$$

or at constant indicated airspeed

$$p = p_{\text{ref}} = p_m - \left(\frac{p_m - p_{\text{ref}}}{q_{\text{cm}}} \right) q_{\text{cm}} \quad (35)$$

For the aircraft flying in the test condition

$$p_{\text{test}} = p_{\text{ref}} \exp \left(- \frac{H_{\text{test}} - H_{\text{ref}}}{RT_{\text{ave}}} \right) \quad (36)$$

The pressures p_{test} and p_{ref} are true static pressures corresponding to pressure altitudes H_{test} and H_{ref} , respectively. The average static temperature at H_{test} and H_{ref} is T_{ave} . Because zero pressure differential is maintained on the limited range altimeter, the measured static pressure, p_m , is the same at both reference and test altitudes. Also, if pitot pressure error does not change from the reference to test condition, the measured impact pressure, q_{cm} , can be used as a correlation parameter. Position error for the aircraft at the test condition is then

$$\frac{p_m - p}{p_m} = \frac{p_m - p_{\text{test}}}{p_m} = 1 - \left(1 - \frac{p_m - p_{\text{ref}}}{p_m}\right) \exp\left(-\frac{H_{\text{test}} - H_{\text{ref}}}{RT_{\text{ave}}}\right), \quad (37)$$

or

$$\frac{p_m - p}{q_{\text{cm}}} = \frac{p_m - p_{\text{test}}}{q_{\text{cm}}} = \frac{p_m}{q_{\text{cm}}} - \left(\frac{p_m}{q_{\text{cm}}} - \frac{p_m - p_{\text{ref}}}{q_{\text{cm}}}\right) \exp\left(-\frac{H_{\text{test}} - H_{\text{ref}}}{RT_{\text{ave}}}\right) \quad (38)$$

The accuracies of the calibration using a full range or limited range altimeter from Reference 22 are summarized in the following table.

TABLE XVII
ATMOSPHERIC SURVEY FOLLOWING TOWER FLY-BY AND
SUBSEQUENT CALIBRATION AT ALTITUDE USING GROUND
TRACKING

	<u>Full Range</u> <u>Altimeter</u>	<u>Limited Range</u> <u>Altimeter*</u>
<u>Altitude</u> <u>(Feet)</u>	<u>ΔH, Feet</u>	<u>ΔH, Feet</u>
10,000	38	18
20,000	55	20
30,000	72	24
40,000	89	30
50,000	107	28
60,000	124	36
70,000	141	49
80,000	159	72
90,000	176	112
100,000	193	178

* 0 - 10" H_2O range used to 50,000 feet.

0 - 5" H_2O range used from 50,000 to 100,000 feet.

A comparison of the results of Table XVII with the fly-by at altitude and pacer at altitude results. Table XVI, indicate comparable accuracies with the fly-by calibrations, ΔH_2 . Comparisons hold for both the full range and limited range altimeter methods. The tracking method has the advantage of utilizing only one aircraft and one set of instrumentation.

9.2.3.3. Trailing Probe Method.

A standard method of determining the position error for low speed aircraft has been by use of trailing bomb or probe. The probe is stabilized by use of fins such as to maintain approximately at zero angle of attack. The probe is suspended from an aircraft by a cable. The maximum speeds for calibration by this method are usually limited to about 275 miles per hour.

Work on this method of calibration was continued by the British and instead of employing a tote bomb, a small airplane configuration was attached to the end of the cable. Additional work in this country was conducted by the Douglas Aircraft Company. Tests indicated the device could be flown stable, at least up to a Mach number of 0.9. The accuracy quoted by the British and Douglas was $\frac{\Delta P}{q_c} = \pm 0.005$. Recently the Douglas Aircraft Company Flight Test Department has continued with flight test on a light weight cone configuration. To date only verbal communications are available on the results. Experiments on a twin jet Navy aircraft over the range from 100 to 500 knots up to $M = 0.9$ have been rather successful. Results indicate the calibrations can be performed within $\frac{\Delta P}{q_c} = 0.005$. Preliminary data indicates that trailing the cone at a distance of one wing span and aft of the aircraft will be more than sufficient to provide the above accuracy. An aircraft with an 80 foot wing span indicated that the pressure was constant up to a point within 30 feet of the aircraft.

The advantages of utilizing the trailing probe configuration are immediately apparent in that the position correction may be determined as a direct measurement utilizing a differential pressure gage between the pressure port to be calibrated and the trailing probe. The device may be used on a test aircraft directly. Another possibility is to use the trailing probe on a reference aircraft during fly-by procedures

with a test aircraft. The trailing airplane previously used was a rather heavy device and offered considerable damage potential if the system became unstable. The use of a light weight trailing cone appears to overcome this serious deficiency. It will probably be desirable to utilize a reel in the carrying aircraft for extending and retracting the trailing cone although this feature may not be absolutely necessary. A disadvantage to this system is that considerable time lag is encountered due to the long leads from the trailing probe to the aircraft itself. Hence, this method had best be used only for steady flight conditions. If the general method can be developed to perfection, it offers substantial advantages over all the calibration methods in that the reference static pressure is carried with the aircraft to be tested.

9.2.4. Conclusions and Recommendations.

9.2.4.1. Tower Fly-By Calibrations.

A review of previous work, Reference 22, indicates that the tower fly by method of calibration is probably the most accurate known method. It may be utilized successfully up to a Mach number of 0.9. With a full range altimeter used for flight instrumentation, accuracies on the order of ± 17.3 feet may be obtained in the tower fly-by method. If a limited range altimeter is utilized, accuracies on the order of ± 5.4 feet of altitude may be obtained.

9.2.4.2. Calibration Accuracy of Altitude of Tower Calibrated Aircraft.

(1) For aircraft with flush static ports, whose Mach number at altitude does not exceed $M = 0.7$, it is recommended that the tower fly-by calibration be utilized at all altitudes providing the calibration is performed as a function of indicated airspeed.

(2) Aircraft with flush static ports with Mach numbers in excess of 0.7 should be calibrated at altitude utilizing an alternate method.

(3) For aircraft with nose or wing tip booms, whose Mach number at altitude does not exceed 0.9, it is recommended that the tower fly-by calibrations shall be utilized at all altitudes providing the calibration is performed as a function of Mach number.

(4) Aircraft with nose or wing tip booms, capable Mach number at altitude is in excess of 0.9, should use recalibration at altitude by an alternate method.

9.2.4.3. Calibration Methods at Altitude.

(1) Comparison of aircraft fly-by methods at altitude and single aircraft method utilizing ground tracking indicate the two methods are comparable in accuracy.

(2) If it is necessary to transfer the calibration from the reference aircraft to a pacer aircraft and hence to a test aircraft, then the single aircraft method utilizing ground tracking is more accurate.

(3) In the interest of standardization and insuring compatibility of instrumentation and for obtaining probably the best accuracy, it is recommended that the single aircraft method utilizing ground tracking be adapted by the USAF as a standard calibration at altitude procedure. In addition, it is recommended that the ground tracking equipment, radar-phototheodolite and phototheodolite range, at Edwards Air Force Base, California, be utilized for all calibrations of USAF aircraft.

(4) The use of the limited range altimeter method for flight test instrumentation has been analyzed and compared with conventional altimeter instrumentation offers a reduction in calibration errors of about 50 percent. It is recommended that the USAF conduct flight tests on equipment furnished for previous study, Reference 22, to prove the feasibility of this equipment under flight test conditions. If feasibility of limited altimeter instrumentation is proven, it is recommended that it be adapted as standard instrumentation for all Air Force Flight Test procedures.

SECTION 10
REFERENCES

1. Diehl, Walter J.; Standard Atmosphere -- Tables and Data, NACA Report No. 218, 1925. (Reprint 1940)
2. Brombacher, W. G.; Altitude-Pressure Tables Based on the United States Standard Atmosphere, NACA Report No. 538, 1935.
3. Aiken, Jr., William S.; Standard Nomenclature for Airspeeds with Tables and Charts for Use in Calculation of Airspeed, NACA Report No. 837, 1946.
4. Kollsman Instrument Corporation Listing of 20 April 1961, Various Standards of Pressure Versus Altitude Equivalent Pressure in In. Hg. at 0° C.
5. Williams, D. T.; Bell J. C.; of Battelle Memorial Institute and Nash, W. F. of Aircraft Laboratory; A New Standard Atmosphere: The WADC 1952 Model Atmosphere. WADC Tech Report 54-215, March 1954.
6. Standard Atmosphere -- Tables and Data for Altitudes to 65,800 Feet, NACA Report 1235, 1955.
7. Minzner, R. A.; and Ripley, W. S.; The ARDC Model Atmosphere, 1956. No. 86, 1956.
8. Minzner, R. A.; Champion, K.S.W.; and Pond, H. L.; The ARDC Model Atmosphere, 1959, AFRCR-TR-267, 1959.
9. Livingston, Sadie P.; and Gracey, William; Tables of Airspeed, Altitude, and Mach Number Based on Latest International Values for Atmospheric Properties and Physical Constants, NASA Technical Note D-822, 1961.
10. International Civil Aviation Organization, Montreal, Canada, and Langely Aeronautical Laboratory, Langely Field, Va., Manual of the ICAO Standard Atmosphere - Calculations by the NACA, NACA Technical Note 3182, May 1954.
11. International Civil Aviation Organization, Montreal, Canada, Manual of the ICAO Standard Atmosphere, ICAO Document 7488, May 1954.
12. International Civil Aviation Organization, Montreal, Canada, and Langely Aeronautical Laboratory, Langely Field, Va., Standard Atmosphere - Tables and Data for Altitudes to 65,800 Ft., NACA Report 1235, 1955.
13. Zener, Clarence; Elasticity and Anelasticity of Metals, University of Chicago Press 1948.
14. Bulletin 6626 Rosemount Engineering Company, Appendix 9.6.
15. Keulegan, G. H.; Static Hysteresis in the Flexure of Bars, Technologic Papers of the Bureau of Standards, Vol. 21, 1926.

16. Gracey, William, and Stell, Richard E.; Repeatability, Drift, and After-effect of Three Types of Aircraft Altimeters, NASA TN D-922, July 1961.
17. Lamb, J. P., Jr.; The Influence of Geometry Parameter Upon Lag Error in Airborne Pressure Measuring Systems, WADC TR 57-351, July 1957.
18. Huston, Wilbur B.; Accuracy of Airspeed Measurements and Flight Calibration Procedure, NACA Report 919, 1949.
19. Silsby, Norman S.; External Interference Effects of Flow Through Static Pressure Orifices of an Airspeed Head at Several Supersonic Mach Numbers and Angles of Attack, NASA Memo 2-13-59L, March 1959.
20. Mabey, D. G.; The Calibration at Transonic Speeds of a Mark 9A Pitot Static Head with and Without Flow Through the Static Slots, C.P. No. 384, British A.R.C., 1958.
21. REC Bulletin 106021, REC Transonic Wind Tunnel Facility.
22. DeLeo, Richard V.; Cannon, Peter J.; and Hagen, Floyd W.; Evaluation of New Methods for Flight Calibration of Aircraft Instrument Systems, Part I: Analysis of Altimeter, Airspeed, and Free-Air-Temperature Systems, WADC TR59-295, Part I, June 1959.
23. Ritchie, Virgil S.; Several Methods for Aerodynamic Reduction of Static-Pressure Sensing Errors for Aircraft at Subsonic, Near-Sonic, and Low Supersonic Speeds, NASA Report 18, 1959.
24. Gracey, William; Measurement of Static Pressure on Aircraft, NACA Report 1364, 1958.
25. Werner, Frank D. and Teigen, Mary J., An Investigation of the Effect of Random Fuselage Wall Irregularities on Flush Static Pressure Port Calibrations, WADC Technical Report 57-365, April 1957.
26. Silsby, Norman S., and Stickle, Joseph W., Flight Calibrations of Fuselage Static-Pressure-Vent Installations for Three Types of Transports, NASA TN D-1356, May 1962.
27. DeLeo, Richard V., and Hagen, Floyd W.; Evaluation of New Methods for Flight Calibration of Aircraft Instrument Systems, Part III Development of Altimeter, Airspeed, and Free-Air-Temperature Calibration Systems, WADC TR 59-295, Part III, February 1961.
28. Recommended Test Procedures for Altimeters, Air Transport Association of America, June 1961, Revised December 1961.

APPENDIX A

Suggested Changes to MIL-P-26292 (USAF)

Pitot and Static Pressure Systems, Installation and Inspection of

SUMMARY.

Subject specification has been reviewed as part of the work under Contract AF33(600)-42754. In order to update the specifications to meet present Air Force requirements a number of specification changes and additions are suggested in the following paragraphs. The numbering system pertains to the numbering system used in the Military Specifications. If no changes are recommended to this specification, then those numbers are omitted from the following listing:

1. SCOPE: 1.1

In the third line change the word "total" to "pitot".

Pitot pressure is defined as the absolute pressure at the impact source. Total pressure equals pitot pressure subsonically, but is not equal to the pitot pressure supersonically because of the normal shock loss.

2. APPLICABLE DOCUMENTS.

2.1. SPECIFICATIONS.

Military.

Add MIL-P-27478, Pitot Tube TRU-42/A, electrically heated, 8-inch mast.

Delete MIL-T-5420 tubes, pitot-static, electrically heated aircraft.

The latter specification is deemed incompatible with Air Force deicing requirements. For example, deicing requirements are specified at 100 knots tunnel speed at $-15^{\circ} \pm 5^{\circ} \text{C}$. High performance requirements require testing at 350 knots indicated tunnel speed at $-30^{\circ} \text{C} \pm 5^{\circ} \text{C}$.

3. REQUIREMENTS.

3.4.1.2. Pitot-Static Tubes.

Delete AN5814, AN5816, MIL-T-5420. Considering present Air Force requirements, these specifications are considered obsolete.

3.4.1.3. Pitot Tubes.

Add MIL-P-27478.

3.4.2.1. Pitot-Static Tubes.

Nose boom mounted supersonic pitot-static tubes shall be utilized where ever possible on high performance aircraft. Wing booms are acceptable for aircraft operating up to a Mach number of 1.0. The approximate recommended length for nose booms shall be within 0.5 to 1.0 maximum equivalent fuselage diameter. (Equivalent fuselage diameter is defined as the diameter of a circle having an area equivalent to the maximum cross sectional area of the aircraft.) If an aerodynamically compensated pitot-static tube is utilized, the shortest nose boom length compatible with the aerodynamic compensation available with the tube shall be selected. If other forms of pressure compensation are available in the aircraft, nose boom length shall be selected as short as practicable, however, uncorrected pressure must fall within the requirements of section 4.4.6.4. Boom shall be equipped with aligning device with markings to insure that the boom is always installed with the pitot-static tube mounting holes in the same position. The boom should also be provided with a removable sleeve to aid in maintenance of the pitot-static tube and couplings.

The above specification change incorporates elimination of the wing tip boom of above Mach number 1.0. Primary reason for this change is the very erratic behavior of static pressure vs Mach number in the range 0.8 to approximately 1.4 Mach number. Illustrations of this phenomena are contained in Reference 24, Figures 29 and 33 for both a swept and unswept wing configuration. Additional difficulties with the wing pitot-static tube installation are that the pneumatic lines are excessively long when the tube is mounted at the wing tip, hence, pneumatic time constant is larger. In addition, the local angle of attack range forward of the wing is considerably larger than the airplane angle of attack due to the induced up-wash effects of the wing itself. For an aircraft pitching through the range from 0 to 15°, the local flow angle at the pitot-static tube as mounted on the wing tip could easily vary between 0 and 30°. It appears that the above combination of deficiencies are enough to eliminate the wing tip nose boom from consideration for Mach numbers above 1.0. Additional deviations of the specification are included to permit use of an

aerodynamically compensated pitot-static tube. This unit would allow the nose boom length to be considerably shortened, possibly to about 0.25 as maximum fuselage diameter. In addition, if other means of compensation are provided, such as an air data computer, the shorter nose boom length can be utilized.

3.4.3. System Anti-Icing Capability.

- a. Altitude - 10,000 feet
- b. Mach Number - 0.60

The altitude and Mach number specifications have been changed from 40,000 feet and 0.75, respectively. Demonstrating deicing capability at 40,000 feet is not as severe as demonstrating deicing capability at 10,000 feet, because the density at 40,000 feet is approximately 1/4 of the density near sea level. Hence, the convection heat transfer at 40,000 feet between the tube and the air passing over the tube is approximately one-half the magnitude at sea level. The Mach number has been changed from 0.75 to 0.6 since there will be appreciable aerodynamic heating due to this relatively high Mach number, which will tend to minimize deicing heater requirements. The combination of 10,000 feet altitude at Mach number 0.6 tends to represent the most severe deicing requirements when coupled with an outside air temperature of -35° C per the original specification.

3.4.5. Flush Static Port.

When a multiple flush static port configuration is utilized, all static ports shall be located on the square plate with the primary static system centered within the area of the square plate.

FIGURE 3 PITOT TUBE AND FLUSH STATIC PORT SYSTEM.

Per Page 8, MIL-P-26292 has been modified and is included as part of this appendix. Changes provide a completely separate static system for pilot's and co-pilot's instruments. Manifolding per Figure 3 of the original specification has been eliminated.

4.4.6. Installation Error.

Present specification requires that contractor shall submit plans to the procuring activity for approval regarding details of Flight Test Programs to determine pitot-static pressure installation errors. Four in-flight calibration methods are listed. No change in the present specification is recommended at this time. However, the Air Force has supported studies under contract AF33(600)-37359, Reference 22 and 27. Calibration methods were analyzed by error analysis. In general, the analysis showed that each of the four methods listed in the present specification have near comparable accuracy for calibrations at altitude. Accuracy of the calibration can be considerably increased in each case if a full range altimeter or 15 pound absolute pressure gage is replaced with a limited range differential gage. Limited range differential gage has been called a limited range altimeter or sometimes referred to as a statoscope. Fabrication of two limited range altimeters was completed under reference contract, Reference 27. These have been furnished to the Air Force for flight test evaluation. Up to this time only a very limited amount of flight test data is available on the calibrators. Information available shows excellent sensitivity of the units but to date only quantitative data has been obtained. If this program or others are more successful in obtaining improved accuracy over present calibration methods, it appears that the specification should be rewritten specifying exactly the flight test configuration and instrumentation utilized. This will insure comparable accuracies for all flight test data obtained by various manufacturers. In addition, within the Air Force at least, consideration should be given for performing the flight test at one standard location using one standard set of ground instrumentation. The capabilities of the Edwards Air Force Base, with the availability of considerable tracking equipment, satisfy the necessary facility requirements. Disagreement has often occurred between the flight test results obtained from contractors and the subsequent Air Force calibrations. Standardizing the instrumentation and method for calibration, as well as the location where the experiments are performed, will tend to eliminate these discrepancies. It appears that systematic errors existing between different calibration methods, instrumentation and locations now exist which contribute to the non-agreement between contractor furnished and

subsequent Air Force calibrations. The reader is referred to Section 9 of this report which reviews in-flight calibration methods. This section compares the expected experimental accuracies utilizing fully each altimeter and limited range altimeters. The use of the limited range altimeter appears very beneficial. If the flight tests on this device prove satisfactory, the Air Force should give consideration to standardizing of this type of installation. Recommendations on the use of various calibration methods are summarized in Section 9.

4.4.6.2.

Eliminate the words 'or wing tip boom installations'.

Figure 5 position error tolerance, page 16, MIL-P-26292, change the definition of q_c from "true dynamic pressure" to "impact pressure".

4.4.6.3.

The measured pitot pressure shall not differ from the true pitot pressure by more than 0.4 percent throughout the entire Mach number range of the aircraft.

In the above paragraph the word 'total' is replaced by the word 'pitot' and the word 'exceed' is replaced by the word 'differ'.

4.4.6.4.

If the installation does not meet the requirements of 4.4.6.2 and 4.4.6.3, compensation shall be required. However, the uncompensated position error shall not exceed the range of the ratio of measured static pressure to static pressure of 0.96 to 1.20.

Wording of the above paragraph was altered slightly for clarification.

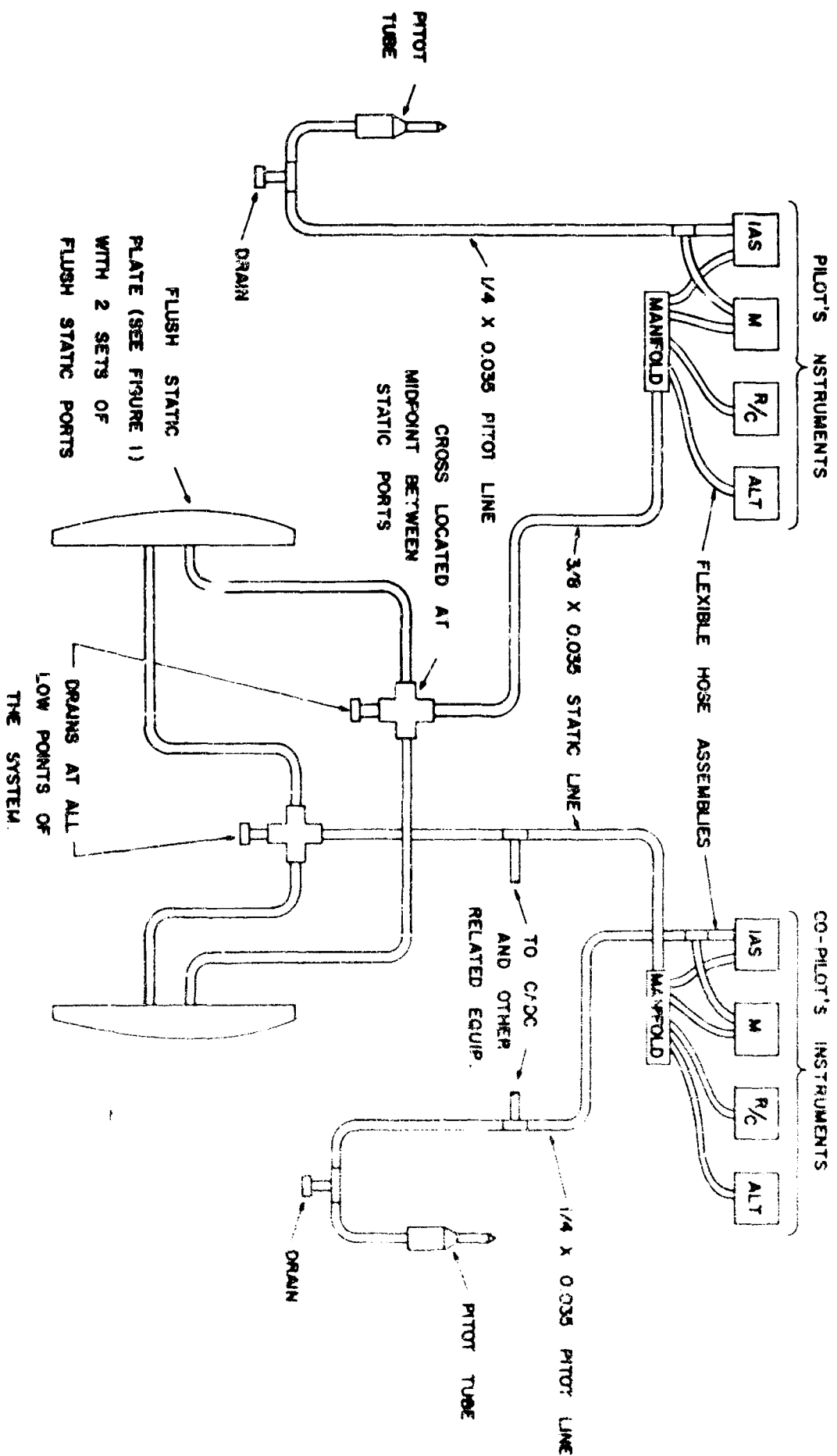


FIGURE 3. PITOT TUBE AND FLUSH STATIC PORT SYSTEM
(REVISED FIGURE 3, PAGE 8, OF MIL-F-26292)